

NASA  
TP  
1977  
c.1

TECH LIBRARY KAFB, NM



0068147

NASA  
Technical  
Paper  
1977

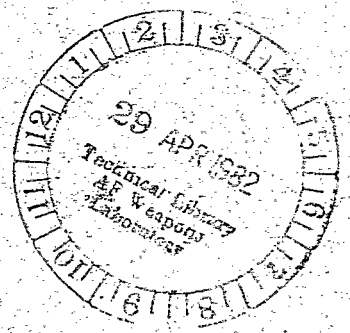
April 1982

# Long-Term Thermal Degradation and Alloying Constituent Effects on Five Boron/Aluminum Composites

George C. Olsen

LOAN COPY: RETURN TO  
AFWL TECHNICAL LIBRARY  
KIRTLAND AFB, N. M.

NASA



NASA  
Technical  
Paper  
1977

1982

TECH LIBRARY KAFB, NM



0068147

# Long-Term Thermal Degradation and Alloying Constituent Effects on Five Boron/Aluminum Composites

George C. Olsen  
*Langley Research Center  
Hampton, Virginia*



National Aeronautics  
and Space Administration

Scientific and Technical  
Information Branch

## SUMMARY

The effects of thermal exposures on the properties of five boron/aluminum composite systems were experimentally investigated. Composite specimens were fabricated with 49 volume percent boron fibers (203  $\mu\text{m}$  diameter) in aluminum-alloy matrices, 1100 Al, 2024 Al, 3003 Al, 5052 Al, and 6061 Al. In addition, specimens of matrix alloy only were identically fabricated. The specimens were tested as-fabricated, after isothermal exposures of up to 10 000 hours at 500 K and 590 K, up to 500 hours at 730 K, and after thermal cycling exposure of up to 2000 thermal cycles between 200 K and 590 K. Composite longitudinal and transverse tensile strengths, longitudinal compression strength, and in-plane shear strength were determined in each condition by mechanical testing. None of the systems was severely degraded by the long-term exposure at 590 K. The best performing system was B/2024 Al with no transverse tensile strength degradation due to interaction and less than 10 percent longitudinal tensile strength degradation due to interaction.

The effects of matrix alloys on the degradation mechanisms of the composite materials were experimentally investigated. Composite specimens and individual fibers were metallurgically analyzed with a scanning electron microscope and an electron microprobe to determine failure characteristics, chemical element distribution, and reaction layer morphology. Alloying constituents were found to affect the composite degradation mechanisms as follows: alloys containing iron, but without manganese as a stabilizer, caused increased low-temperature degradation; alloys containing magnesium, iron, or manganese caused increased degradation; and alloys containing copper caused increased fiber strength.

## INTRODUCTION

Technological advances in the aerospace industry continuously demand stronger, stiffer, lighter weight structural materials capable of long service life at elevated temperatures. Often these demands cannot be efficiently met by metal alloys. As one alternative, boron/aluminum composite technology began to develop 25 years ago. Improvements in the technology have included the evolution of 203- $\mu\text{m}$ -diameter boron fibers with less core-flaw sensitivity (ref. 1) and improved diffusion bonding techniques (ref. 2). Currently boron/aluminum composites have strength-to-weight and stiffness-to-weight ratios three times higher than aluminum and titanium alloys.

Initially, the accepted temperature for long-term use of boron/aluminum composites was 590 K (refs. 3 and 4). This limitation was imposed by the aluminum matrix properties and considered to be below the point of serious interaction problems (ref. 4). Most thermal degradation studies were therefore confined to temperatures typical of fabrication and secondary processing operations. However, a more recent study of boron/6061 aluminum degradation at exposure temperatures of 450 K, 560 K, and 700 K for up to 10 000 hours reported severe strength degradation and recommended a maximum use temperature of 450 K (ref. 5).

Fiber-matrix bonding and composite property degradation have been attributed to an aluminum-boron reaction forming  $\text{AlB}_2$  (ref. 6). Other constituents of aluminum alloys were said to be less reactive with boron than aluminum and were not considered significant contributors to composite degradation (ref. 2). As a result, aluminum

matrix alloys have been selected on the basis of bonding characteristics, fracture toughness, creep forming capability, strength, and corrosion resistance (ref. 2) without concern about the effect of their alloying constituents. However, recent work on boron/6061 aluminum composites (refs. 7 and 8) suggests magnesium, an alloying constituent in the matrix, is an active reactant with the fiber. If magnesium significantly contributes to thermal degradation of boron/aluminum composites, it could account for the extremely different degradation rates for composites with different alloys reported in the literature (refs. 9 and 10). In addition, this theory raises questions about the effect of other alloy constituents on composite degradation.

This investigation had two purposes. One was to determine the effects of long-term thermal exposure and cyclic thermal exposure on the mechanical properties of boron/aluminum composites. The other was to determine the effects of the aluminum-alloy constituents on the degradation mechanisms in boron/aluminum composites. To accomplish these purposes boron/aluminum composites made from five commercially available aluminum-alloy foils were studied. The composites were exposed for up to 10 000 hours at 500 K and 590 K to study behavior in the anticipated use range and for up to 500 hours at 730 K to study behavior at an over-temperature condition. Composites were thermally cycled for up to 2000 cycles between 200 K and 590 K to study effects of rapid temperature reversals.

Mechanical property tests including longitudinal and transverse tensile tests, longitudinal compression tests, and in-plane shear tests were conducted on the composite specimens. Composite specimens and individual fibers were metallurgically analyzed with a scanning electron microscope and an electron microprobe to determine failure characteristics, chemical element distributions, and reaction layer morphology.

## MATERIALS AND EXPOSURE CONDITIONS

### Materials and Test Specimens

Boron-aluminum composites made from five different aluminum alloys were investigated. The alloys, in the form of 115- $\mu\text{m}$ -thick foils, were 1100 Al (a commercially pure aluminum), 2024 Al (a heat-treatable aluminum-copper-magnesium alloy), 3003 Al (an aluminum-manganese alloy), 5052 Al (an aluminum-magnesium alloy), and 6061 Al (a heat-treatable aluminum-magnesium-silicon alloy). The nominal composition, tensile strength in the original temper condition, and tensile strength in the fully annealed condition of each of these alloys are listed in table I (ref. 11). The 203- $\mu\text{m}$ -diameter boron fibers are amorphous boron vapor deposited on a 12- $\mu\text{m}$ -diameter tungsten wire substrate. In the virgin state the fiber strength was 3.78 GPa (the mean of 25 measurements) and the elastic modulus was 400 GPa (vendor supplied data).

Composite panels, 500 mm by 300 mm by 2 mm thick, were fabricated with the component materials. Alternate layers of aluminum foil and boron fibers were laid up to form eight-ply laminates with 49 volume percent fibers (except for B/3003 Al which had 47 volume percent fibers). Separate panels were fabricated with fibers oriented either unidirectionally or at  $\pm 45^\circ$ . These panels were consolidated by a hot press diffusion bonding process. The bonding parameters for each alloy system are listed in table II. The alloys with more aluminum content have more coherent oxide layers which offer more resistance to diffusion. As a result, these alloys require higher processing temperatures and longer processing times to produce well-bonded

composites. In addition to the composite panels, panels of the aluminum alloys were fabricated in exactly the same manner as the composite panels except no boron reinforcing fibers were used.

Test specimens, in the configurations listed in table III, were cut from the panels with diamond cut-off wheels. Sets of three replicate specimens for each test and exposure condition were prepared. Each specimen was cleaned, inspected, and systematically numbered and measured. After thermal exposure, to be described later, strain gages were bonded to the specimens. An epoxy adhesive was used for specimens to be tested at room temperature and a ceramic base adhesive was used for specimens to be tested at elevated temperature. Four gages were bonded to each specimen, two back to back on the center line to measure longitudinal strain and two back to back on the center line to measure transverse strain. In addition, compression specimens were equipped with epoxy-bonded aluminum gripping tabs for room-temperature testing and ceramic-bonded titanium tabs for elevated temperature testing.

#### Thermal Exposures

Continuous isothermal exposures.— Continuous isothermal exposures were conducted in air-circulating electric ovens. Exposure temperatures were 500 K, 590 K, and 730 K. At 500 K, specimens were exposed for 5000 and 10 000 hours. At 590 K, specimens were exposed for 2500, 5000, 7500, and 10 000 hours. At 730 K, specimens were exposed for 100, 300, and 500 hours. After removal from the ovens, specimens were allowed to cool in ambient air.

Cyclic thermal exposures.— Cyclic exposures were conducted in a dual chamber apparatus. Specimens, mounted on a mechanically driven sliding tray, were alternately inserted in an air-circulating, electrically heated 590-K hot chamber and a liquid-nitrogen-cooled 200-K cold chamber. A full cycle was 29 minutes long with exposures of 21 minutes in the hot chamber and 8 minutes in the cold chamber required to approach the test temperatures. A schematic drawing of the apparatus and a typical specimen temperature profile for one cycle are shown in figure 1. Sets of specimens were exposed to 500 and 2000 cycles.

#### TEST PROCEDURES

##### Mechanical Property Tests

Longitudinal and transverse tensile tests were performed on all five of the composite materials. Longitudinal compression and in-plane shear tests were performed on the B/1100 Al, B/3003 Al, and B/6061 Al composite systems. Tensile tests were performed on the alloy specimens (specimens with no boron reinforcement). The test standards followed, the properties determined, and load rate used for each of the tests are shown in table IV. Room-temperature tests were conducted in a 245-kN hydraulic test frame equipped with hydraulic grips. The hydraulic grips were used for tension and shear tests. Minimum gripping pressure was applied, and acetate inserts protected the specimen surfaces from damage by the grips. An IITRI wedge grip fixture (fixture description in ref. 12) was used for compression tests. Elevated temperature tests were conducted in a 490-kN hydraulic test frame equipped with an electrically heated environmental test chamber. Longitudinal tensile specimens were tested with mechanical clevis grips, and transverse tensile and shear specimens were tested with wedge grips. Elevated temperature compression tests also

used the IITRI compression fixture. All load and strain data were processed through an on-line data acquisition system programmed to record, reduce, and plot the data.

Fibers were chemically removed from their aluminum matrix with a heated NaOH solution (ASTM Standard D 3553-76). Individual fiber breaking stresses were determined experimentally using the fiber bend-test fixture shown schematically in figure 2. Fibers approximately 100 mm long were bent around the successively smaller mandrels of the test fixture until they failed. The mandrel on which the fiber failed corresponds to a stress range determined by the equation for elastic bending stresses in a beam,  $\sigma_{\max} = E_f(r_f/R_m)$  (ref. 13), where  $\sigma_{\max}$  is the maximum stress,  $E_f$  is the fiber elastic modulus,  $r_f$  is the fiber radius, and  $R_m$  is the mandrel radius. A minimum of 40 fibers were tested from each specimen. Strength distributions were determined for fibers removed from as-fabricated specimens that were not mechanically tested and compared with the range and mean of the virgin fiber strength distribution (vendor-supplied data). In addition, residual fiber strength distributions were determined for all systems after mechanical testing of the composite. These fiber populations are biased by composite mechanical testing (i.e. weaker fibers are removed) but still show changes in upper bound strengths and variations in mean fiber strength and distribution.

#### Metallurgical Analysis

Representative specimens of each composite system in the as-fabricated condition, after isothermal exposures of up to 10 000 hours at 500 K, up to 10 000 hours at 590 K, up to 500 hours at 730 K, and after thermal cycling exposure of 2000 thermal cycles between 200 K and 590 K were metallurgically examined. Longitudinal and transverse tensile fracture surfaces of the composites were examined with a scanning electron microscope (SEM) to determine fracture modes. Polished and etched (Keller's reagent) cross-sections from longitudinal tensile specimens were analyzed with an electron microprobe to qualitatively determine chemical element distribution. Resolution of the microprobe is approximately 5  $\mu\text{m}$  so that reaction layers thinner than 5  $\mu\text{m}$  could not be investigated.

Fibers were chemically removed from the composite matrix (by digesting the aluminum in a heated NaOH solution) for further examination. Reaction layer morphology was examined by first etching one end of the fibers with Murakami's reagent to remove the reaction layer. Then the interfaces between the etched and unetched regions of the fibers were examined with an SEM and the chemical elements in the reaction layer determined with an energy dispersion analysis of X-rays (EDAX). Boron, a certain constituent of the reaction layer, cannot be detected by energy dispersion techniques (elements with atomic numbers less than 11 are transparent to X-rays, boron's atomic number is 5).

Reaction layers on chemically removed fibers were analyzed for crystalline structure using X-ray diffraction techniques. Fibers were laid up side by side to form a sample for analysis. Other fibers were ground and sieved to produce a powder sample higher in reaction product concentration. Some of the powder sample was further concentrated by chemically leaching away the boron fiber particles with Murakami's reagent. X-ray diffraction patterns were made from these samples using a copper  $\text{K}\alpha$  incident X-ray beam, a diffracted beam monochromator, a diffractometer, and a goniometer.

## RESULTS AND DISCUSSION

Results of all mechanical property tests are shown in tables V through X. Typical stress-strain curves for each condition are shown in appendixes A through E. Trends in these data are illustrated in the following sections of the report by graphic plots. These plots were prepared in the following manner: mean values of the data were plotted and fitted with straight line segments for the well-behaved data (alloy tensile data and the composite transverse tensile and in-plane shear data especially). Data that exhibited large scatter or deviated significantly from a straight line (composite longitudinal tensile and compression data, principally) were fitted with a first- or second-order polynomial in a least-squares regression analysis. Data points whose standardized residuals were more than two standard deviations from zero were dropped as out-lying points and the mean value calculation and regression analysis repeated for the remaining points. Those data dropped as out-lying points are identified in the tables by an asterisk.

### As-Fabricated Material

Fabrication effects on matrix strength.- The effect of the diffusion bonding process on the matrix material strength can be seen by comparing the strength of the diffusion bonded matrix-only specimens (table X) with the tempered and annealed strengths of the alloys (table I). Fabrication temperatures and times (table II) required to produce well-bonded composite materials were sufficient to fully anneal the non-heat-treatable strain-hardened 1100 Al and 3003 Al alloys. The remaining strain-hardened alloy, 5052 Al, consolidated at a slightly lower temperature and shorter time, approached the annealed condition (approximately 81 percent annealed). The heat-treatable alloys, 2024 Al and 6061 Al, were partially annealed (approximately 31 percent) during fabrication.

Fabrication effects on fiber strength.- Fiber strength distributions for fibers chemically removed from specimens after fabrication without performing mechanical property tests are shown in figure 3. Before fabrication, the virgin fiber mean strength was 3.78 GPa normally distributed over the range of 3.26 GPa to 4.14 GPa as indicated in the figure. After exposure to the fabrication process, fiber strength distributions ranged from similar to the virgin fibers to radically altered. Fibers from the 1100 Al system (fig. 3(a)) showed only minor degradation. Fibers from the 2024 Al system (fig. 3(b)) had a slightly higher mean value but the lower limit of strength was lower and the upper limit was significantly higher. This broadened range suggests that at least two mechanisms were functioning, one which weakened the fibers and another which strengthened them. Fibers from the 3003 Al system (fig. 3(c)) suffered a uniform degradation in strength of 15 to 20 percent as a result of the fabrication process. Fibers from the 5052 Al system (fig. 3(d)) were radically altered, their mean strength was lower, their upper limit was higher, and their lower limit was significantly lower. Again, as with the fibers from the 2024 Al system, dual mechanisms are suggested but in this alloy the degradation mechanism was more active and the strengthening mechanism was less active. The mean strength of fibers from the 6061 Al system (fig. 3(e)) increased approximately 10 percent without any significant change in the lower limit but a significant increase in the upper limit. This upward shift suggests that a strengthening mechanism was active.

Reaction layers on individual fibers were enhanced by partial etching. These fibers were studied in an SEM and the elemental composition of the reaction layers determined by EDAX (recall that boron, a certain constituent of the reaction layer cannot be detected by EDAX). SEM photomicrographs of the fiber reaction layers are shown in figure 4. Fibers from the 1100 Al system (fig. 4(a)) have a dendritic reaction layer composed of aluminum with a trace of silicon. Interspersed light-colored particles are iron rich. Fibers from the 2024 Al system (fig. 4(b)) have a reaction layer composed of approximately 1 part aluminum and 0.2 part magnesium with traces of silicon and copper. Interspersed light-colored particles are 1.4 parts magnesium to 1 part aluminum. Fibers from the 3003 Al system (fig. 4(c)) have a reaction layer of dark spherical particles composed of aluminum and manganese with a trace of silicon and light spherical particles rich in iron. Fibers from the 5052 Al system (fig. 4(d)) have a thick reaction layer of approximately 1.7 parts magnesium to 1 part aluminum with traces of silicon, chromium, iron, and copper. Interspersed light particles are iron rich. Fibers from the 6061 Al system (fig. 4(e)) have a thick reaction layer with equal aluminum and magnesium content and traces of silicon, chromium, iron, and copper.

Polished cross sections of as-fabricated specimens were scanned with an electron microprobe to determine elemental gradients. Traces across reaction zones did not indicate any increased elemental concentrations at the reaction zones. Gradients of boron and aluminum concentrations at the interfaces did not have plateaus indicating the reaction zone. The lack of these plateaus only indicates that the reaction zone was smaller than the resolution of the microprobe (5  $\mu\text{m}$ ).

If these observed effects of fabrication on the fiber strength distributions are compared with the alloying constituents shown in table I, several hypotheses can be proposed. First, only minor degradation in fiber strength occurred during fabrication as a result of reaction with commercially pure aluminum. Second, manganese as the only alloying element in 3003 Al contributed to a uniform degradation of fiber strength. Third, magnesium, usually present in the form of  $\text{Mg}_5\text{Al}_8$  or in solid solution in the 2024 Al and 5052 Al alloys, caused the fiber strength degradation and lower limit reduction noted in those systems. The order of increasing magnesium content of these alloys corresponds to the order of increased strength degradation observed. Isolation of the lower strength fibers, especially in the 5052 Al alloy, suggests the degradation was not uniform but a localized phenomena probably dependent on particle contact with the fiber. Magnesium is also an alloying constituent in 6061 Al, but there it is bound in  $\text{Mg}_2\text{Si}$  particles and not available for further reaction. Finally, increased mean fiber strength and upper limit of the fiber strength distributions were noted in the 2024 Al, 5052 Al, and 6061 Al alloys. These are copper bearing alloys with copper present in the form of  $\text{CuAl}_2$  or in solid solution. The order of increasing copper content of these alloys corresponds to the order of increased strength observed; this suggests that copper contributes to a fiber strengthening mechanism.

Room-temperature composite properties.- Typical room-temperature as-fabricated stress-strain curves for each composite and test type are shown in figure 5. The first-stage longitudinal elastic moduli (when both fiber and matrix are elastic) and the second-stage elastic moduli (when the matrix is plastic and contributes little to the composite strength) correspond to the rule-of-mixture (ROM) prediction for moduli. Longitudinal tensile strengths, however, do not agree with ROM calculations based on mean fiber strength. Transverse tensile strengths (fig. 5(b)) were similar to the matrix alloys but with much lower strains to failure because of fiber restriction. Strain hardening steps typical of strain hardenable aluminum alloys are present in the plastic region of the B/5052 Al transverse tensile curve and the B/6061 Al

system transverse tensile and in-plane shear curves (fig. 5(d)). This phenomenon, as well as early fiber failures, may have contributed to the perturbations seen in the latter stages of some of the longitudinal tensile curves. The B/6061 Al composite, a well characterized composite system, is used as a basis of comparison for the other systems. Mean values of room-temperature as-fabricated mechanical properties for each composite system as well as its percentage difference (in parentheses) compared with those for B/6061 Al are listed in table XI. The longitudinal tensile strength of the B/1100 Al system is only 11 percent less than the B/6061 Al system although the matrix-dominated transverse tensile strength, longitudinal compression strength, and in-plane shear strength are 63, 37, and 33 percent less, respectively. The longitudinal tensile strength of the B/2024 Al system is only 7 percent less than the B/6061 Al system and its transverse tensile strength is 27 percent greater. The B/3003 Al system longitudinal tensile strength, transverse tensile strength, longitudinal compression strength, and in-plane shear strength are 27, 53, 29, and 32 percent less than the B/6061 Al system, respectively. The longitudinal tensile strength of the B/5052 Al system is 29 percent less than the B/6061 Al system but its transverse tensile strength is only 2 percent less.

Longitudinal tensile fracture surfaces of all five systems were macroscopically irregular with matrix shear steps typically causing 5 mm variations in the failure planes. However, no fiber pullout is evident in the microscopic fractographs (fig. 6). The B/1100 Al system fracture surface (fig. 6(a)) has high necking tear ridges typical of the commercially pure highly ductile alloy. The B/3003 Al (fig. 6(c)), B/5052 Al (fig. 6(d)), and the B/6061 Al (fig. 6(e)) systems show less ductility and ultimate matrix failure by the dimpled rupture mode. The B/2024 Al system (fig. 6(b)) shows little ductility and a strong dimpled rupture mode resulting from its higher alloy content. All these fractographs show some evidence of incomplete matrix-matrix bonding.

Transverse tensile fracture surfaces, for all but the B/6061 Al system, were macroscopically flat for the most part but with some tendency toward a 45° failure plane; this indicates a mixed failure mode that was primarily tensile but with some local shear failure. The B/6061 Al systems failed on 45° planes; therefore, a matrix shear mode failure was indicated. Additional fracture surface details are shown in the microscopic fractographs in figure 7. The B/1100 Al system (fig. 7(a)) failed in tension through the matrix. Some bare fiber appears in the fracture surface, probably as a result of incomplete bonding. The B/2024 Al system (fig. 7(b)) failed entirely at the fiber-matrix interface. The B/3003 Al (fig. 7(c)) and the B/5052 Al (fig. 7(d)) systems failed in the mixed modes of matrix and interface tension failures. The B/6061 Al system (fig. 4(e)) failed in the matrix with elongated dimples; thus, a shear failure was indicated.

Residual fiber strength distributions (fibers removed from composite specimens after tensile testing) are shown in figure 8. The residual distributions are approximately the same as those obtained from untested specimens (fig. 3) except that the lower bounds have been modified by the failure of low strength fibers during composite tensile testing. Fiber stresses at the composite failure strain are indicated for each system and show that composite failure occurs when only a few percent of fibers have failed.

Effect of elevated test temperature.- As-fabricated specimens from each composite system were mechanically tested at room-temperature (295 K), 500 K, and 590 K. Typical stress-strain curves for each test condition and composite system are shown in appendix A. The effects of test temperature on the mean ultimate strengths of the composite systems are shown in figure 9. The matrix alloys alone (fig. 9(a)), though

varying from 70 MPa to 368 MPa at 295 K, tend toward the same strength as test temperature increases with the variation at 590 K only 20 MPa to 66 MPa. The composite transverse tensile strengths (fig. 9(b)) behaved in the same manner as the alloys. Fiber dominated longitudinal tensile strengths (fig. 9(c)) of the B/1100 Al, B/2024 Al, B/3003 Al, and B/6061 Al systems had only small losses in strength with increasing test temperature, whereas the B/5052 Al system had an anomalous increase in strength at 590 K. This increase probably resulted from improved diffusion bonding which occurs during the 2 hours required to bring the specimen and equipment to thermal equilibrium at 590 K. Longitudinal compression strengths (fig. 9(d)) for the B/1100 Al, B/3003 Al, and B/6061 Al systems at 590 K were 70 to 80 percent less than their room-temperature strengths. In-plane shear strengths for the same materials were only slightly decreased by the elevated temperatures (fig. 9(e)). These data show that matrix-dominated strength properties of the composite system tended to converge as test temperature increased, but in general the order of highest to lowest strength was maintained throughout the temperature range.

#### Effects of Isothermal Exposures

Exposure at 500 K.— The effects of isothermal exposure for up to 10 000 hours at 500 K on the tensile strengths of the matrix alloys and the longitudinal and transverse tensile strengths of the composites are shown in figure 10. In addition, typical stress-strain curves for each composite material and each test type are shown in appendix B. Matrix tensile strengths (fig. 10(a)) of the non-heat-treatable alloys indicate 1100 Al and 3003 Al were not affected by the 500 K exposure and 5052 Al reached its fully annealed condition early in the exposure period and remained constant thereafter. The heat-treatable alloys, 2024 Al and 6061 Al, approached their fully annealed strengths during the exposure period. Composite transverse tensile strengths (fig. 10(b)) behaved in the same manner as the matrix alloys alone and their strength losses may be attributed entirely to matrix annealing. Composite longitudinal tensile strengths (fig. 10(c)) show losses of 22 percent for the B/1100 Al system, 17 percent for the B/6061 Al system, and 10 percent for the B/2024 Al and B/3003 Al systems. Most of the losses occur in the first 5000 hours of exposure. The B/5052 Al system longitudinal tensile strength was not degraded by the 500 K exposure.

Residual fiber strength distributions for fibers removed from specimens after 10 000 hours exposure at 500 K and tensile testing are shown in figure 11. Fiber stress at the composite failure strain is indicated for each system. Comparison of these residual strengths with the as-fabricated residual strengths (fig. 8) shows uniform degradation of approximately 5 percent in the upper bound and mean strength of fibers from the B/1100 Al system and a 10-percent reduction in fiber stress at failure. Mean strength of fibers from the B/2024 Al system was degraded but the upper bound of the strength distribution and fiber stress at failure were unchanged. The mean and upper bound of B/3003 Al system fiber strength were unchanged but the fiber stress at failure was degraded approximately 6 percent. The upper bound of fiber strength from the B/5052 Al system was degraded but there were only small losses in mean strength and stress at failure. Mean fiber strength of the B/6061 Al system was degraded approximately 10 percent and stress at failure was degraded 18 percent.

Longitudinal tensile fracture surfaces were macroscopically and microscopically similar to the as-fabricated specimens. Transverse tensile fracture surfaces for the B/1100 Al, B/3003 Al, and B/5052 Al systems were macroscopically irregular indicating mixed mode failures as in the as-fabricated composites. The B/2024 Al and B/6061 Al

systems failed on 45° planes indicating a matrix shear mode failure. Additional fracture surface details are shown in the microscopic fractographs in figure 12. The B/1100 Al system (fig. 12(a)) failure occurred more at the interface than in the matrix as in the as-fabricated case (fig. 7(a)). The B/2024 Al system (fig. 12(b)) failed entirely by matrix shear, a change from the interface failure seen in the as-fabricated specimens. The remaining system failures were similar to the as-fabricated system failures.

Exposure at 590 K.— The effects of isothermal exposure for up to 10 000 hours at 590 K on the matrix alloys tensile strength and the composite system strengths are shown in figure 13. In addition, typical stress-strain curves for each composite material and each test type are shown in appendix C. The effect of 590 K thermal exposure on the matrix alloy strength (fig. 13(a)) was similar to the effect of 500 K exposure except the 2024 Al, 5052 Al, and 6061 Al alloys reached their fully annealed condition during the first 2500 hours of exposure and remained constant thereafter. Composite transverse tensile strength degradations (fig. 13(b)) were again similar to the matrix materials and may be attributed entirely to matrix annealing. The longitudinal tensile strengths of all the composite systems were degraded by the long term 590 K exposure (fig. 13(c)), with most of the losses occurring in the first 2500 hours of exposure. Strength losses over the 10 000 hours exposure for the B/1100 Al, B/2024 Al, B/3003 Al, B/5052 Al, and B/6061 Al systems were 10, 14, 10, 8, and 14 percent, respectively.

Longitudinal compression strengths (fig. 13(d)) of the 1100 Al, 3003 Al, and 6061 Al systems degraded in an approximately linear manner over the 10 000 hours exposure with a maximum loss of 38 percent. In-plane shear strengths (fig. 13(e)) of the B/1100 Al and B/3003 Al systems were unaffected by the 590 K exposure. The B/6061 Al system lost 22 percent of its in-plane strength in the first 2500-hour period, probably the result of annealing, but then increased linearly over the remaining 7500 hours for a net increase in strength of 8 percent.

Longitudinal tensile fracture surfaces for the 590 K exposure specimens were similar both macroscopically and microscopically to the as-fabricated specimens. Transverse tensile fracture surfaces of specimens exposed for 10 000 hours at 590 K (fig. 14) are unchanged from the as-fabricated specimens except for the B/2024 Al system (fig. 14(b)) which failed in matrix shear. The transition of the failure mode from interfacial to matrix shear occurred in the initial 2500-hour exposure period as a result of matrix annealing.

Residual fiber strength distributions for fibers removed from specimens after 10 000 hours exposure at 590 K and tensile testing are shown in figure 15. The mean strength and stress at composite failure strain of fibers from the B/1100 Al system were degraded approximately 5 percent when these distributions are compared with the residual distributions from as-fabricated specimens (fig. 8). Fiber stress at composite failure strain of fibers from the B/2024 Al system was degraded approximately 7 percent by the exposure even though the mean strength apparently increased. Mean strength of fibers from the B/3003 Al system was degraded approximately 15 percent but the stress at composite failure strain was degraded only 8 percent. Stress at composite failure strain of fibers from the B/6061 Al system was not degraded by the exposure but the mean strength dropped approximately 7 percent.

Reaction layers on individual fibers are shown in figure 16. Thermal exposure has increased the thickness and density of the reaction layer in the B/1100 Al system (fig. 16(a)) but the EDAX results indicate the makeup, aluminum with a trace of silicon and iron-rich particles, is the same as the as-fabricated specimens. Fibers from

the 2024 Al system (fig. 16(b)) have irregular reaction layers with large light-colored areas that have an acicular growth pattern. The reaction layer is composed of 1 part aluminum and 1.32 parts magnesium with traces of silicon, iron, and copper. Light-colored areas are 1 part aluminum and 0.8 part magnesium. Fibers from the 3003 Al system (fig. 16(c)) have a reaction layer of large spherical particles. EDAX shows the reaction layer is largely manganese and aluminum with traces of silicon and iron. Darker particles are richer in aluminum than the lighter particles. Fibers from the 5052 Al system (fig. 16(d)) have a thick acicular reaction layer composed of 1 part aluminum and 0.8 part magnesium with traces of silicon, chromium, and iron. Fibers from the 6061 Al system (fig. 16(e)) have a moderately thick reaction layer with light-colored nodes and an acicular growth pattern. The reaction layer is composed of 1 part aluminum, 0.4 part magnesium, and 0.1 part silicon and traces of chromium, iron, and copper. The light-colored nodes have a similar composition but with less aluminum.

The effect of exposure temperature on the longitudinal tensile strength of the composite systems exposed 10 000 hours, shown in figure 17, is divided into two groups. The first group of systems (B/2024 Al, B/3003 Al, and B/5052 Al) degrade in a linear manner with increasing exposure temperature (12, 12, and 6 percent, respectively). The second group (B/1100 Al and B/6061 Al), however, degraded approximately 22 percent at 500 K but only 9 percent at 590 K. These data indicate that there is a low-temperature degradation mechanism active at 500 K but not at 590 K and that there is some temperature between 295 K and 590 K that produces a maximum degradation. This phenomenon may be the result of a low-temperature boron reaction with the metastable phase  $\text{FeAl}_6$  in the matrix (iron is present as an impurity). The metastable phase is stabilized by manganese (ref. 14) which is present as an alloying constituent in the 2024 Al, 3003 Al, and 5052 Al alloys but not in the 1100 Al and 6061 Al alloys (table I). Also shown in figure 17 are data from reference 2 for 10 000 hours exposures of a B/6061 Al composite at 297 K, 450 K, 561 K, and 700 K. The composite was a six-ply unidirectional configuration with 49 volume percent of 142- $\mu\text{m}$ -diameter boron fibers. Strength degradation in this system was more severe than for the B/6061 Al system with 203- $\mu\text{m}$ -diameter fibers considered in this study. Much of the difference can be attributed to the smaller diameter fiber which has less strength initially, more surface area per unit volume for reaction, and more sensitivity to stress concentrations both at the surface and in the core.

The maximum mechanical property degradations of each system caused by up to 10 000 hours exposure at 500 K or 590 K are summarized in table XII. Transverse tensile strength degradations were caused entirely by matrix annealing. The systems ranked according to their minimum room-temperature transverse tensile strengths are as follows:

B/2024 Al	178 MPa
B/5052 Al	150 MPa
B/6061 Al	133 MPa
B/3003 Al	77 MPa
B/1100 Al	62 MPa

Longitudinal tensile strength degradations for the B/2024 Al, B/3003 Al, and B/5052 Al systems were 10 percent or less (disregarding matrix annealing). The

systems ranked according to their minimum room-temperature longitudinal tensile strengths are as follows:

B/6061 Al	1349 MPa
B/2024 Al	1343 MPa
B/1100 Al	1130 MPa
B/5052 Al	1089 MPa
B/3003 Al	1044 MPa

Longitudinal compression strengths of the three systems tested were degraded 38 percent by 10 000 hours exposure at 590 K. However, they are still 25 to 60 percent higher than the longitudinal tensile strengths. The systems ranked according to their minimum room-temperature longitudinal compression strengths are as follows:

B/6061 Al	2190 MPa
B/3003 Al	1574 MPa
B/1100 Al	1399 MPa

In-plane shear strengths of these systems were degraded 12 percent or less (disregarding matrix annealing). The systems ranked according to their minimum room-temperature in-plane shear strengths are as follows:

B/6061 Al	157 MPa
B/3003 Al	123 MPa
B/1100 Al	76 MPa

Design applications utilizing B/Al composites in elevated temperature environments must be based on their fully annealed strengths and/or their minimum thermally degraded strength and/or their elevated temperature strength. Ranking the five B/Al systems tested in this investigation for long term use at temperatures up to 590 K gives the following order of performance:

B/2024 Al	High strengths Low degradation
B/5052 Al	Moderate strengths Low degradation
B/6061 Al	High strengths Moderate degradation at 500 K
B/3003 Al	Low strengths Low degradation
B/1100 Al	Low strengths High degradation at 500 K

Exposure at 730 K.—The effects of isothermal exposure for up to 500 hours at 730 K on the matrix alloys tensile strength and the composite systems strength are shown in figure 18. In addition, typical stress-strain curves for each composite material and each test type are shown in appendix D. Tensile strengths of the non-heat-treatable alloys (fig. 18(a)) behaved in the same manner as noted in the lower temperature exposures, 1100 Al and 3003 Al were unaffected by the exposure and 5052 Al reached the fully annealed condition early in the exposure and then remained constant. The tensile strengths of the heat-treatable alloys 2024 Al and 6061 Al exposed at 730 K did not behave in the same manner as observed at 500 K and 590 K. The strength of the 2024 Al alloy was not degraded at all by the 730 K exposure. Strength degradation for the 6061 Al alloy at 730 K was one-third less than at the lower temperatures. Less strength loss occurred at the higher temperature because at 730 K these materials are in their solution heat treating regime. In this regime, the solubility limits for their strengthening phases are increased and less precipitation occurs.

Transverse tensile strengths of the composite systems (fig. 18(b)) again behaved in a manner similar to the nonreinforced matrix material except that the B/2024 Al system strength degraded linearly with exposure time. After 500 hours exposure at 730 K the transverse tensile strengths of the B/2024 Al, B/5052 Al, and B/6061 Al systems were degraded 12, 16, and 11 percent, respectively.

Composite longitudinal tensile strength degradations were more severe for the 730 K exposure (fig. 18(c)) than for the lower temperature exposures. The B/1100 Al, B/2024 Al, B/3003 Al, B/5052 Al, and B/6061 Al system strengths were degraded by 53, 58, 32, 37, and 45 percent, respectively. The B/1100 Al and B/6061 Al systems degraded in a linear manner with exposure time. The other systems degraded in a nonlinear manner with the rate of degradation decreasing with increasing exposure time. The B/3003 Al and B/5052 Al systems reached their minimum strength after 300 hours and remained constant through 500 hours. Because longitudinal tensile strength, a key property of these materials, was severely degraded, these materials are not suitable for long-life applications at 730 K.

Longitudinal compression strengths of the composite systems exposed at 730 K (fig. 18(d)) varied in a nonlinear manner with exposure time initially decreasing then increasing. During the initial exposure periods the B/1100 Al, B/3003 Al, and B/6061 Al system strengths degraded 13, 2, and 18 percent, respectively. During the later period the strength recovered 4, 13, and 12 percent, respectively. Compression strength relies on matrix support of the fiber to prevent buckling. One possible cause of the observed strength recovery is that the reaction zone formed at 730 K provides improved fiber support.

In-plane shear strength of the B/1100 Al, B/3003 Al, and B/6061 Al systems degraded linearly 25, 25, and 40 percent, respectively, during the 500 hours exposure.

Longitudinal tensile fracture surfaces of the specimens exposed 500 hours at 730 K were macroscopically flat and did not have the irregular shear steps noted for the as-fabricated specimens. Microscopically, however, the 730 K specimens and the as-fabricated specimens were similar. Transverse tensile fracture surfaces of specimens exposed 500 hours at 730 K are shown in figure 19. The B/1100 Al and B/3003 Al fracture surfaces (figs. 19(a) and 19(c), respectively) are not significantly different from the as-fabricated specimens (figs. 7(a) and 7(c)). The B/2024 Al specimen (fig. 19(b)), however, has several unique features. It failed primarily at the interface of the reaction layer and the matrix, leaving the heavy reaction layer

attached to the fiber. At discrete sites along the fiber, the failure surface penetrated the reaction layer and extended into the fiber, removing a chip of fiber. The chipped sites are visible on the fiber in the center of the fractograph and the chips that were removed from a fiber on the opposing fracture surface are visible in the adjacent valley. In addition, several fibers failed by splitting their entire length (left side of fractograph). The B/5052 Al system (fig. 19(d)) also failed at the interface leaving a heavy reaction layer on the fiber and it also shows evidence of fiber chipping. The B/6061 Al system (fig. 19(e)) failed in matrix shear as it did in the as-fabricated condition, but, areas near the fiber show evidence of a thick fragmented reaction layer.

Fiber strength distributions from specimens exposed for 500 hours at 730 K are shown in figure 20. Strength degradation of fibers from all matrix alloy systems was severe. The mean strength of fibers from 1100 Al, 3003 Al, and 6061 Al matrices were degraded approximately 35 percent (to 2.4 GPa) and the fibers from the 2024 Al and 5052 Al matrices were degraded approximately 50 percent (to 2.0 GPa) as a result of the exposure. The greater degradation of the latter two systems was probably the result of magnesium in the matrix as cited in the discussion on fabrication effects.

Reaction layers on individual fibers taken from the composite specimens exposed 500 hours at 730 K are shown in figure 21. Fibers from the 1100 Al matrix (fig. 21(a)) have thin compact reaction layers that are dark with light-colored fringes and particles. EDAX results again show the dark areas are aluminum with a trace of silicon and the light areas are iron-rich particles. Fibers from the 2024 Al matrix (fig. 21(b)) have a thick, fluffy, light-colored reaction layer. EDAX results indicate the composition is approximately 1 part aluminum and 1.6 parts magnesium with traces of silicon, iron, manganese, and copper. Electron microprobe traces across interfaces of a polished cross section of a B/2024 Al specimen indicate magnesium concentration in the reaction layer is 10 times higher than in the matrix. Thickness of the reaction layer, determined by measuring the magnesium peak width at one-half the maximum peak height, is approximately 5  $\mu\text{m}$ . Fibers from the 3003 Al matrix (fig. 21(c)) have a thin gray reaction layer covered by small light-colored spherical particles. EDAX results show the reaction products contain aluminum and iron with traces of manganese and silicon. Fibers from the 5052 Al matrix (fig. 21(d)) have a thick, fluffy, light-colored reaction layer with small white spherical particles imbedded. EDAX results show the fluffy area is 1 part aluminum and 1.6 parts magnesium with traces of silicon, chromium, and manganese, and the white particles are again iron rich. Fibers from the 6061 Al matrix (fig. 21(e)) have a two-layer reaction zone. The inner layer is the same in appearance and elemental content as the as-fabricated specimens. The outer layer is a thick, fluffy, light-colored reaction product with some small white particles imbedded. EDAX results of the outer layer show it is 1 part aluminum and 1.6 parts magnesium with a trace of iron, chromium, silicon, and copper.

Attempts to use X-ray diffraction techniques to identify the phases present in the reaction layers seen here (and the thinner ones presented in earlier sections) were unsuccessful. Specimens used in the attempts included beds of fibers, powder samples made by grinding and sieving fibers to increase the volume percent of reaction products, and powder samples leached with Murakami's reagent to remove boron and further concentrate the reaction products. In each case, the patterns generated contained only two indistinct peaks (broad and weak) typical of amorphous boron (ref. 15). This suggests that the compounds formed have no long-range crystallinity agreeing with doubts that true crystalline borides form below 773 K (ref. 16).

### Effects of Thermal Cycling

The effects of thermal cycling between 200 K and 590 K for up to 2000 cycles on the matrix alloys tensile strength and the composite systems strengths are shown in figure 22. In addition, typical stress-strain curves for each composite material and each test type are shown in appendix E. The effects of thermal cycling on the matrix alloy tensile strengths (fig. 22(a)) are the same as noted for the 500 K and 590 K isothermal exposures; i.e., the 1100 Al and 3003 Al alloys, annealed during fabrication, were unaffected and the 2024 Al, 5052 Al, and 6061 Al alloys, partially annealed during fabrication, reached their fully annealed condition within the first 500 cycles and then remained constant. Transverse tensile strengths of the B/1100 Al and B/3003 Al composite systems (fig. 22(b)) were unaffected by thermal cycling, but, transverse tensile strengths of the B/2024 Al, B/5052 Al, and B/6061 Al systems were degraded 38, 54, and 33 percent, respectively, as a result of 2000 thermal cycles. These losses are 21, 30, and 5 percent, respectively, more than the losses incurred as a result of isothermal exposure at 590 K. Longitudinal tensile strengths of the B/1100 Al and B/2024 Al systems (fig. 22(c)) degraded linearly with number of cycles for total losses of 23 and 16 percent, respectively, after 2000 cycles. The B/3003 Al, B/5052 Al, and B/6061 Al systems lost less than 5 percent of their longitudinal tensile strength as a result of 2000 thermal cycles. Longitudinal compression strengths of the B/1100 Al, B/3003 Al, and B/6061 Al systems (fig. 22(d)) degraded linearly with number of cycles for total losses of 22, 26, and 39 percent, respectively, after 2000 cycles. In-plane shear strengths of these systems (fig. 22(e)) were unaffected by thermal cycling.

Longitudinal tensile fracture surfaces of the thermally cycled specimens were macroscopically and microscopically similar to the as-fabricated specimens. Transverse tensile fracture specimens were macroscopically similar to the as-fabricated specimens but microscopic fractographs (fig. 23) show higher densities of large dimples and voids in the interfacial regions and spheroidized matrix material attached to the fibers. These phenomena occur as a result of thermal cycling because of the high shear stresses induced by the large differences in thermal expansion between the fiber and matrix (4:1). (See ref. 17.) Initially these stresses produce plastic deformation and nucleate dislocations in the matrix material. Further cycling condenses the dislocations into voids. The stronger the matrix material is the higher its stress field will be and the more dislocations it will generate. This phenomenon produced the larger transverse tensile strength degradations observed for the thermally cycled B/2024 Al, B/5052 Al, and B/6061 Al systems in comparison with the degradation caused by long-term thermal exposure.

Fiber strength distributions from thermally cycled specimens (fig. 24) compared with the as-fabricated fiber strength distributions (fig. 8) show there was no degradation as a result of the exposure.

Ranking the five B/Al systems tested in this investigation for use in a cyclic thermal environment gives the following order:

B/6061 Al  
B/2024 Al  
B/3003 Al  
B/5052 Al  
B/1100 Al

## Constituent Effects

The reactions occurring within the B/Al composite systems are functions of the constituents, concentrations, temperatures, and time. Identification of these reactions is complicated by their short-range structures, low concentrations, and boron transparency to X-rays. As a result, direct identification of the reaction products using the available equipment and techniques was not possible. However, the foregoing metallurgical analyses, elemental identifications, and mechanical property data together with data gleaned from the literature provide a basis from which the effects of the various elemental constituents can be deduced.

Boron.- The amorphous boron fibers retain the same basic icosahedral (12 atom) cluster structure found in crystalline borons. The icosahedral clusters, however, are randomly oriented in the amorphous form (ref. 18). In the crystalline form long-range order leaves large inter-icosahedral spaces. These spaces host the metal atoms in boron-rich metal borides (ref. 19). Random orientation leaves even larger inter-icosahedral spaces and higher energy sites to accept metal atoms.

Boron fibers are the primary source of strength in the composites. Failure of the fiber-dominated longitudinal tensile specimens occurred catastrophically without evidence of an accumulation of fiber failures (i.e., no change in elastic modulus near failure). The failures occurred when the fibers were loaded near the lower bound of their strength distribution ranges and were not a function of reaction layer thickness (for exposure up to 590 K). This behavior corresponds to the critical energy release rate theory of B/Al composites (ref. 20) where the critical rate is exceeded as soon as fibers in the main body of the distribution range begin to fail. Because the lower bound of fiber strength governs the composite failure, localized reactions between the fiber and matrix that cause stress concentrations and reduce the lower bound of fiber strength are more detrimental to ultimate composite strength than are uniform reactions which lower the entire strength distribution.

Aluminum.- Aluminum/boron reactions are inevitable in the B/Al composite system. However, at temperatures up to 590 K, the slow uniform noncrystalline reaction causes little degradation even after 10 000 hours. At the composite fabrication temperature (770 K to 840 K), the reactions occur more rapidly but short exposure times minimize the effects. Long-term exposure at 730 K caused severe degradation and clearly is beyond the useful temperature range of B/Al composites. Aluminum forms the boron-rich borides  $\text{AlB}_2$ ,  $\text{AlB}_4$ , and  $\text{AlB}_{12}$  with a wide range of stoichiometry (ref. 19). The diboride phase, the one usually expected, has a hexagonal crystalline form dominated by the metal structure. However, at the reaction temperatures in this study, the boron atoms probably take up random interstitial sites in the face-centered-cubic aluminum structure resulting in a distorted structure. This, compounded by a wide range of stoichiometry and the ability of the other diboride-forming constituent metals to enter into isostructural diborides with aluminum, prevent the phase from forming any long-range structure. The higher borides, if they are formed, have structures dominated by the icosahedral cluster structure of boron with the metal atoms taking positions in the relatively large inter-cluster spaces. Their formation would require diffusion of aluminum into the boron and would probably be restricted to the surface or near-surface of the boron fiber and would assume the amorphous boron structure.

Iron.- Iron is not an alloying constituent in any of the alloys tested but it is present as an impurity (<1 percent) in all commercial alloys. Iron-rich particles were found in the fiber reaction layers and probably formed where iron bearing particles in the matrix were next to the fibers. These highly localized reaction sites

cause stress concentrations that are detrimental to fiber strength. Two binary phases can form in the B-Fe system, FeB and Fe<sub>2</sub>B (ref. 19). Both phases have structures determined by the metal lattice. In addition, there are two metal-rich ternary phases that can form in the Al-B-Fe system, B<sub>3</sub>Fe<sub>3</sub>Al and B<sub>2</sub>Fe<sub>2</sub>Al (ref. 14).

Alloy systems not containing manganese, 1100 Al and 6061 Al, were degraded more at the lower exposure temperature (500 K) than at 590 K. Apparently, manganese, a known iron stabilizer which combines with the metastable FeAl<sub>6</sub> phase to form (FeMn)Al<sub>6</sub> (ref. 14), protects the fibers from iron attack at lower temperatures. Since removal of iron from aluminum alloys would be impractical, the addition of a small amount of manganese to the matrix alloys offers some control of the deleterious iron effect at lower temperatures.

Silicon.- Silicon is an alloying constituent in the 6061 Al system (0.6%) but it is present in all commercial aluminum alloys as an impurity. Silicon was a minor constituent in all the reaction layers. It was uniformly distributed in the reaction products except in the B/6061 Al system where it was bound in Mg<sub>2</sub>Si and reduced the detrimental magnesium reaction effect found in other systems. Boron and silicon do not form binary compounds below 1073 K but 0.81 atomic percent of silicon is soluble in boron at room temperature (ref. 21).

Copper.- Copper appears as an alloying constituent in three of the alloys tested, 2024 Al (4.5%), 5052 Al (0.1%), and 6061 Al (0.3%). Fiber reaction products from these systems contained only small amounts of copper uniformly distributed. However, the as-fabricated fiber strength distributions from these systems showed upper strength limits increased in proportion to their copper content. Copper forms only CuB<sub>22</sub> or higher boride phases with boron (the exact stoichiometry is a matter of contention in the literature). These phases would again be dominated by the boron structure and would have to form by diffusion of copper into the boron fiber where it would take up either an interstitial position or substitute for a boron atom (ref. 22). Copper strengthening of boron by this type of mechanism has been reported for crystalline boron at temperatures above 1200 K (refs. 23 and 24). A similar phenomena may occur in amorphous boron at the temperatures encountered in this study. Penetration into the fiber would probably be minimal but the strengthening would occur at the fiber surface and help negate the effect of the inherent surface flaws.

Magnesium.- Magnesium is an alloy constituent in three of the alloys tested, 2024 Al (1.5%), 5052 Al (2.5%), and 6061 Al (1.0%). Fiber reaction products from all these systems contained magnesium and in some instances it appeared as the predominant constituent. It appeared in the uniform reaction products as well as in concentrated particles. For 500 hours exposure at 730 K, the magnesium in the B/2024 Al composite diffused to the fiber surface and was uniformly concentrated there. Magnesium in the uniform reaction products probably comes from solid solution in the matrix and probably substitutes for aluminum to form (MgAl)B<sub>2</sub> (refs. 7 and 8). Particles with high concentrations of magnesium are probably from magnesium bearing particles in the matrix reacting with the fiber. Magnesium particles formed in the B/6061 Al system also contained silicon (from Mg<sub>2</sub>Si phase).

Manganese.- Manganese appears as a minor alloying constituent in the 2024 Al (0.6%) and 5052 Al (0.1%) systems and as the only alloying constituent in the 3003 Al (1.2%) system. Although a small amount of manganese is apparently desirable to stabilize iron at low temperatures, an excess caused increased fiber degradation (by comparison of 1100 Al and 3003 Al system fiber strengths) during fabrication. Together manganese and boron form six binary borides (Mn<sub>4</sub>B, Mn<sub>2</sub>B, MnB, Mn<sub>3</sub>B<sub>4</sub>, MnB<sub>2</sub>, and MnB<sub>4</sub> (ref. 19)) and with aluminum they form two ternary borides (Mn<sub>2</sub>AlB<sub>2</sub> and

$Mn_5AlB_{11}$  (ref. 25)). There was no indication in this investigation which of these phases formed under the various exposure conditions.

#### Improving Boron/Aluminum Composites for Elevated Temperature Use

One of the purposes of this investigation was to determine the active degradation mechanisms in five B/Al composite systems with the supposition that the information could aid in formulating an improved matrix alloy for elevated temperature use. In this context, an "improved matrix alloy" is one which minimizes the strength losses due to fiber-matrix reactions during fabrication and subsequent long term use at elevated temperature. Specific applications may require additional considerations such as corrosion resistance, impact resistance, and fatigue strength to define an improved matrix alloy. Also in this context, "elevated temperature use" is used for environments up to 590 K. This limit is set because test results showed moderate degradation of fiber strength at 590 K but severe degradation at 730 K. Further investigation at intermediate temperatures may prove the 590-K limit to be conservative.

Aluminum alloys begin to anneal at temperatures as low as 370 K (ref. 11). Therefore, when considering them for extended use at temperatures up to 590 K, only the fully annealed properties can be considered. In fact, it may be advantageous to anneal the aluminum foil prior to composite fabrication to assure maximum formability and improve bonding.

Boron fibers are a brittle material sensitive to surface flaws which cause stress concentrations. They inherently contain many surface flaws which cause them to have a wide range of tensile strengths. The composite longitudinal tensile failures observed in this investigation all occur near the lower bound of the fiber strength distributions. This indicates that, for these large 203- $\mu\text{m}$ -diameter fibers at least, the critical energy release criteria for composite failure are exceeded almost as soon as the first fibers fail. Therefore, any reaction which tends to introduce more flaws or worsen those already present, even though not significantly reducing the mean strength of the fibers as a whole, can significantly reduce composite strength.

By induction, from the discussion of alloying constituent effects in the previous section, several general conclusions about fiber-matrix interactions and composite strength degradation can be drawn as follows:

1. Localized reactions between matrix phases and the fiber which form metal-rich borides introduce new surface flaws or worsen existing ones. These reactions are the most detrimental to composite strength.
2. Uniform reactions of aluminum and boron produce boron-rich borides which cause nominal fiber degradation.
3. Uniform reactions forming very-boron-rich borides (i.e.,  $CuB_{22}$ ) may actually help to heal existing fiber surface flaws and strengthen them.

More specifically, when the alloying constituents included in this investigation are considered, an aluminum copper alloy with a small amount of manganese to aid in stabilizing iron impurities should reduce composite strength degradation in use environments up to 590 K.

There are three existing aluminum-copper alloys, none of which exactly conforms to the suggested composition. They are aluminum alloys 2011, 2025, and 2219 (ref. 11). Aluminum 2011 contains 5.5 percent copper but no manganese, it also contains 0.5 percent lead and 0.5 percent bismuth. Lead is reportedly insoluble in boron and forms no phases with it (ref. 21) and no confirmed bismuth phases appear in the literature (ref. 16). Aluminum 2025 contains 4.5 percent copper and 0.8 percent manganese but it also contains 0.8 percent silicon. However, the results of this study indicate that the effects of small concentrations of silicon are probably not significant in composite strength degradation. Aluminum 2219 contains 6.3 percent copper and 0.3 percent manganese, it also contains 0.15 percent zirconium and 0.1 percent vanadium. Both zirconium and vanadium form metal-rich borides (ref. 19) and are probably undesirable as alloying constituents.

The results also suggest another method for improving composite strength. If, as postulated, the formation of very-boron-rich borides such as CuB<sub>22</sub> does "heal" existing fiber flaws, then the vapor deposition of a small amount of copper on the surface of the fiber could improve its strength. This operation could be added as a final step to the vapor deposition process for fabricating the fibers.

#### CONCLUSIONS

Boron-aluminum composites were investigated to determine the effects of long-term thermal exposure on the composite mechanical properties and the effects of the matrix alloying constituents on the degradation mechanisms. Five aluminum alloys, 1100 Al, 2024 Al, 3003 Al, 5052 Al, and 6061 Al, were used as matrix materials. Eight-ply composite panels of each matrix material reinforced with 49 volume percent boron fibers were fabricated by diffusion bonding. The 203- $\mu\text{m}$ -diameter boron fibers were oriented unidirectionally or at  $\pm 45^\circ$ . The composites were investigated in the as-fabricated condition, after isothermal exposures of up to 10 000 hours at 500 K, up to 10 000 hours at 590 K, up to 500 hours at 730 K, and after thermal cycling exposure of up to 2000 cycles between 200 K and 590 K. Mechanical properties, including longitudinal, transverse, and  $\pm 45^\circ$  tensile, and longitudinal compression, were measured in each condition. Fibers, chemically removed from the matrices, were individually bend tested to determine their strength distributions. Composite specimens and individual fibers were metallurgically analyzed with a scanning electron microscope and an electron microprobe to determine failure characteristics, chemical element distributions, and reaction layer morphology.

The following conclusions are made from the results of this investigation:

1. The five B/Al composite systems had good mechanical strength retention after long-term exposures of up to 10 000 hours at 500 K and 590 K. Specific findings were as follows:

Transverse tensile strengths of all the composite systems were unaffected by the exposures (except for matrix annealing).

Longitudinal tensile strengths of the B/2024 Al, B/3003 Al, and B/6061 Al systems were degraded by 10 percent or less by the exposures.

Longitudinal tensile strengths of the B/1100 Al and B/6061 Al systems were degraded more (22 and 13 percent, respectively) by exposure at 500 K than at 590 K.

Longitudinal compression strength of the systems tested were degraded by 38 percent. However, their compression strengths were still 25 to 60 percent higher than their tensile strengths.

The order of best performance of the composite systems based on initial strength, strength at temperature, and amount of degradation is

B/2024 Al  
B/5052 Al  
B/6061 Al  
B/3003 Al  
B/1100 Al

2. Thermal cycling the composite materials for 2000 cycles between 200 K and 590 K caused more transverse tensile strength degradation in the stronger matrix alloys than long-term thermal exposure.

3. Matrix alloying constituents do affect the degradation mechanisms of B/Al composites. Therefore, by tailoring the matrix alloy, property degradation caused by long-term thermal exposure could be reduced. Some of the specific observations were:

Low-temperature degradation caused by iron impurities can be reduced by selecting a matrix alloy containing a small amount of iron stabilizing manganese.

Boron aluminum composite property degradation is increased when magnesium, iron, and/or manganese are available to participate in the reaction.

The presence of copper in the matrix alloy increases fiber strength.

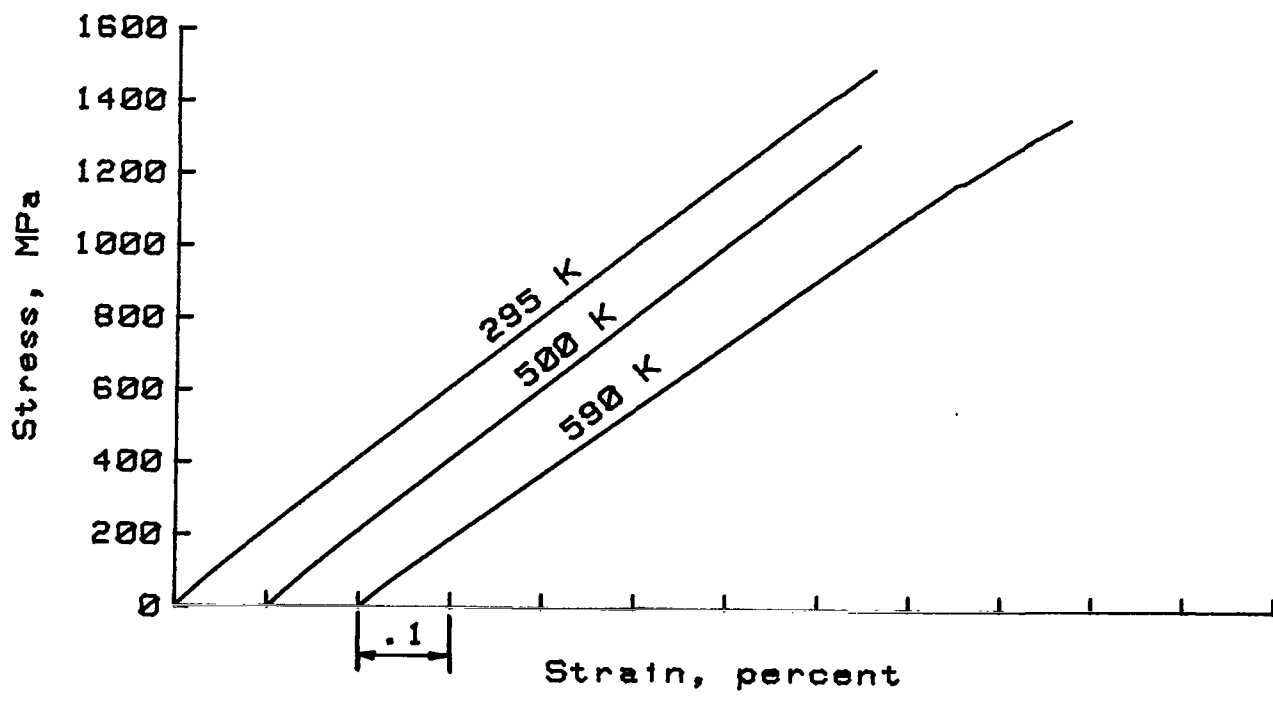
Langley Research Center  
National Aeronautics and Space Administration  
Hampton, VA 23665  
February 12, 1982

## APPENDIX A

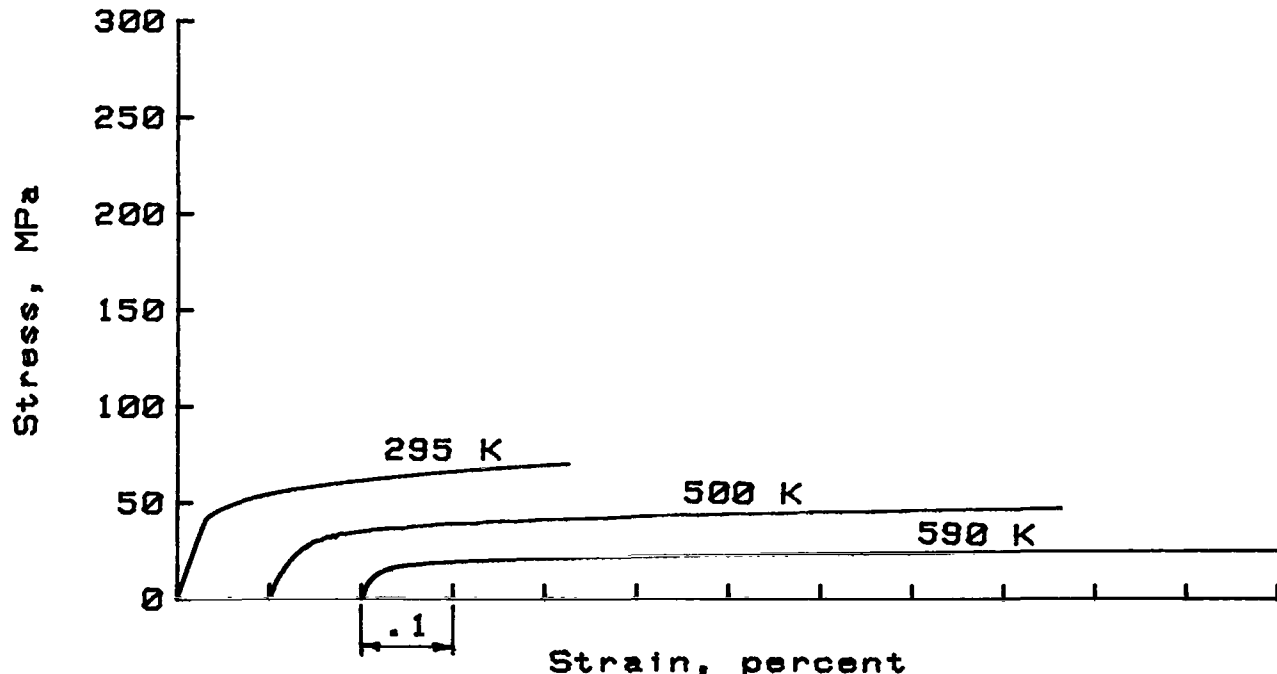
### AS-FABRICATED SPECIMENS TESTED AT 295 K, 500 K, and 590 K

The mechanical property data for all the B/Al composite tests conducted in this investigation are given in tables V through IX. Typical stress-strain curves for the as-fabricated specimens tested at 295 K, 500 K, and 590 K are presented in appendix A.

APPENDIX A



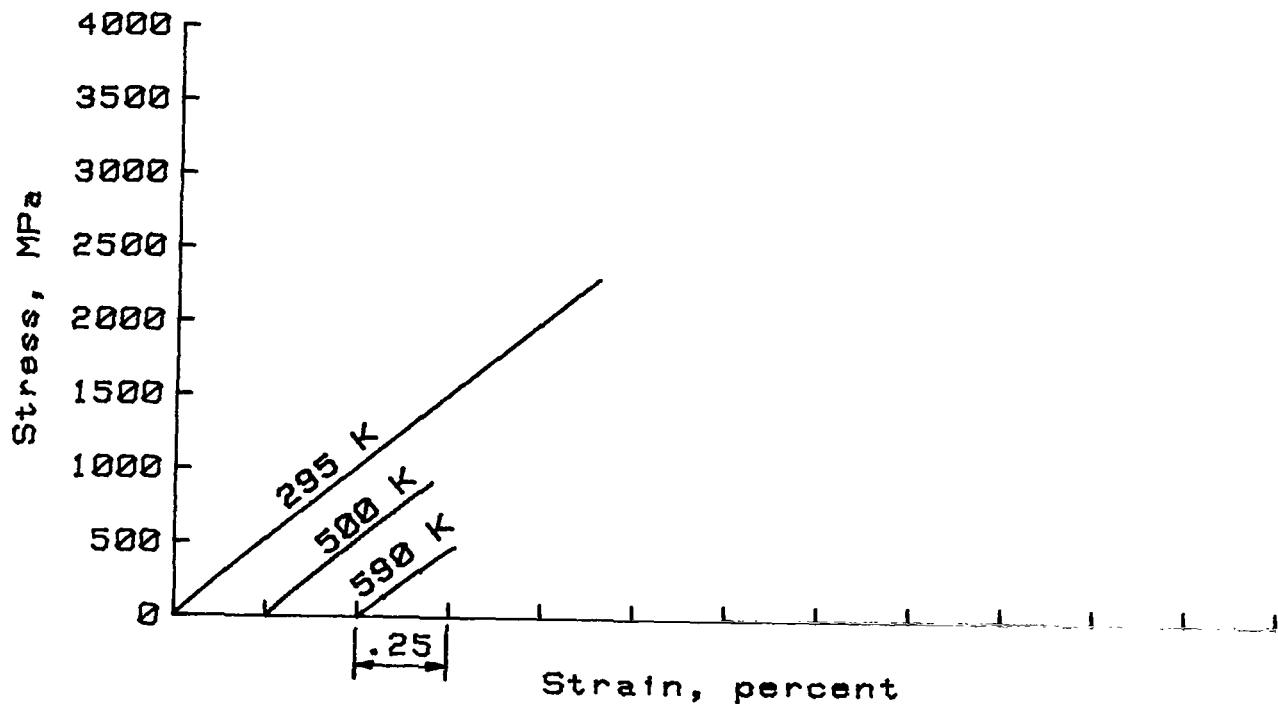
(a) Longitudinal tensile.



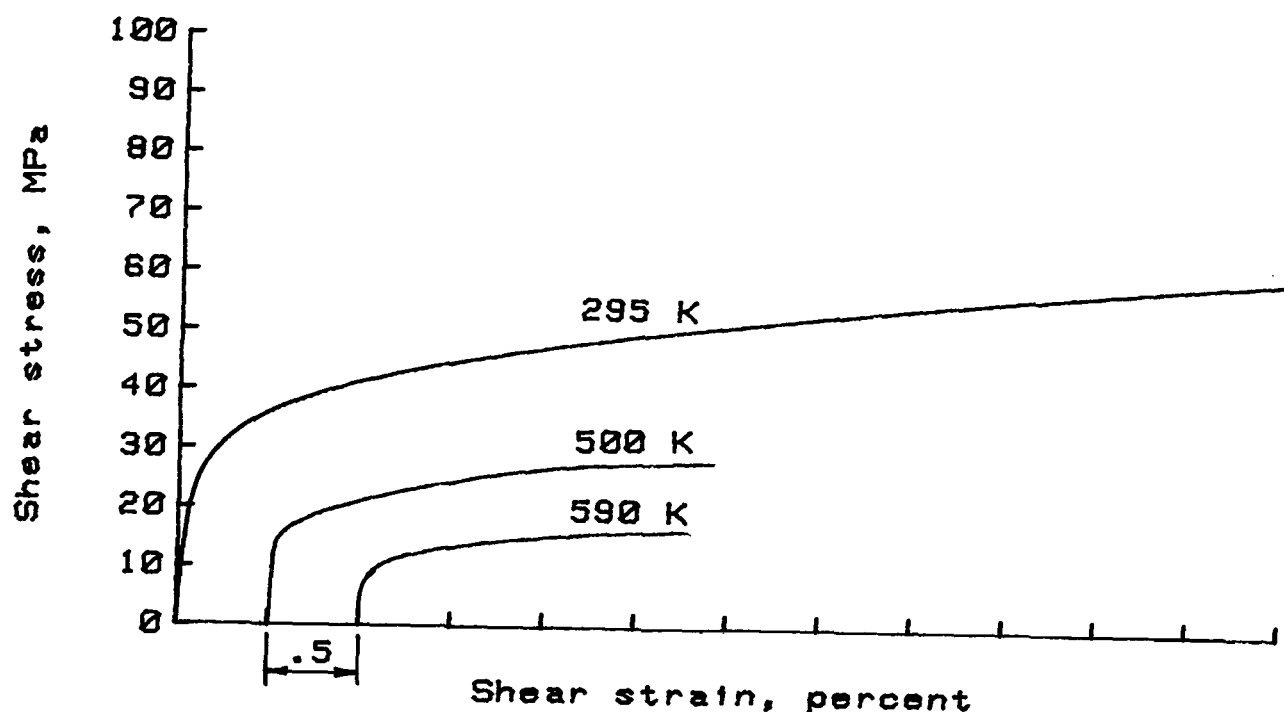
(b) Transverse tensile.

Figure A1.- Typical elevated test temperature stress-strain curves for B/1100 Al composite.

APPENDIX A



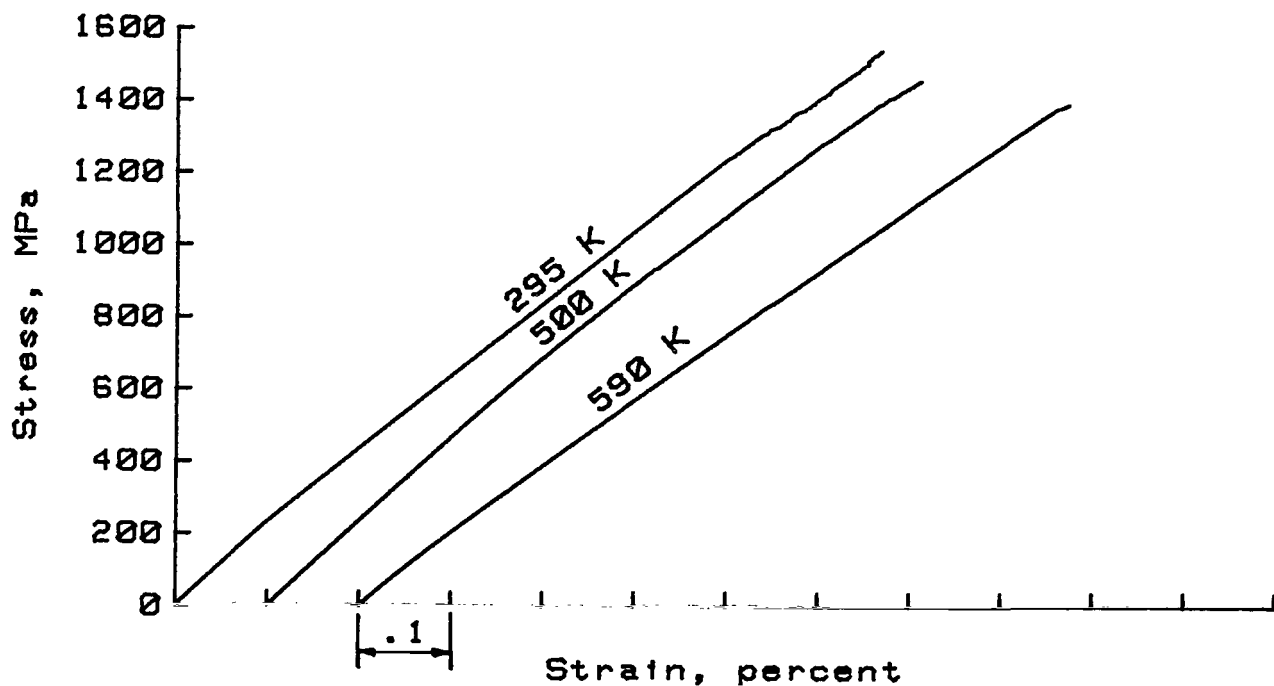
(c) Longitudinal compression.



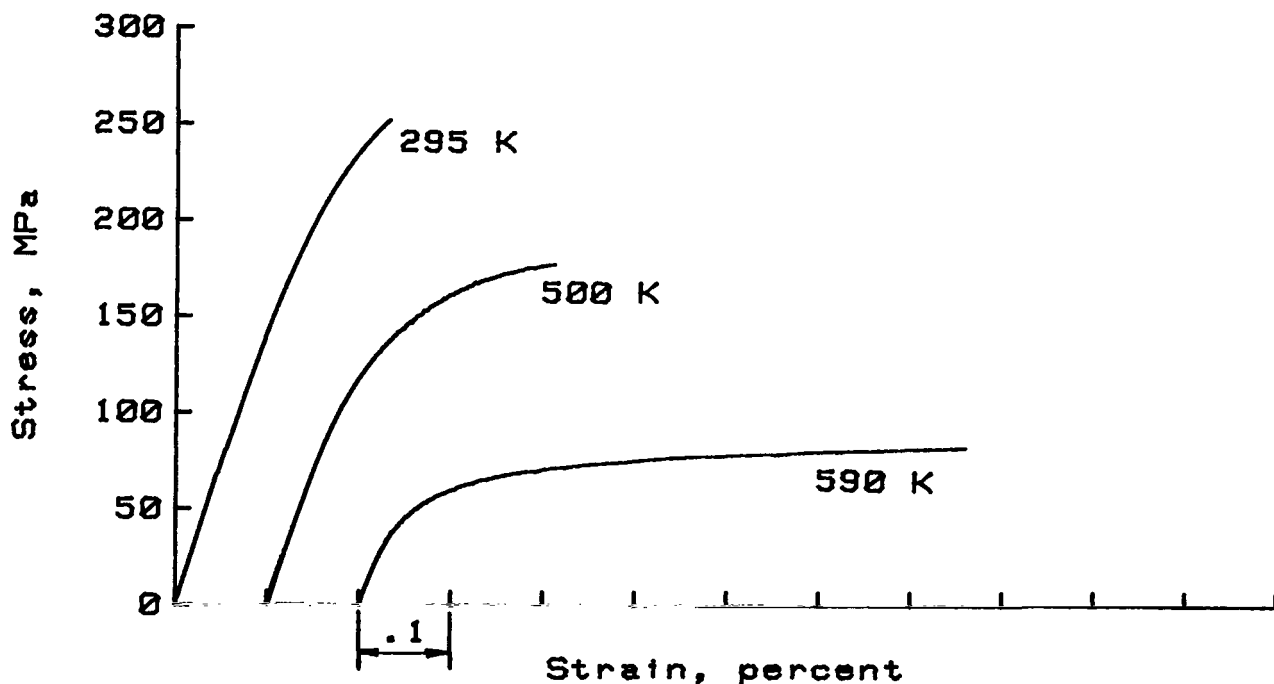
(d) In-plane shear.

Figure A1.-- Concluded.

APPENDIX A



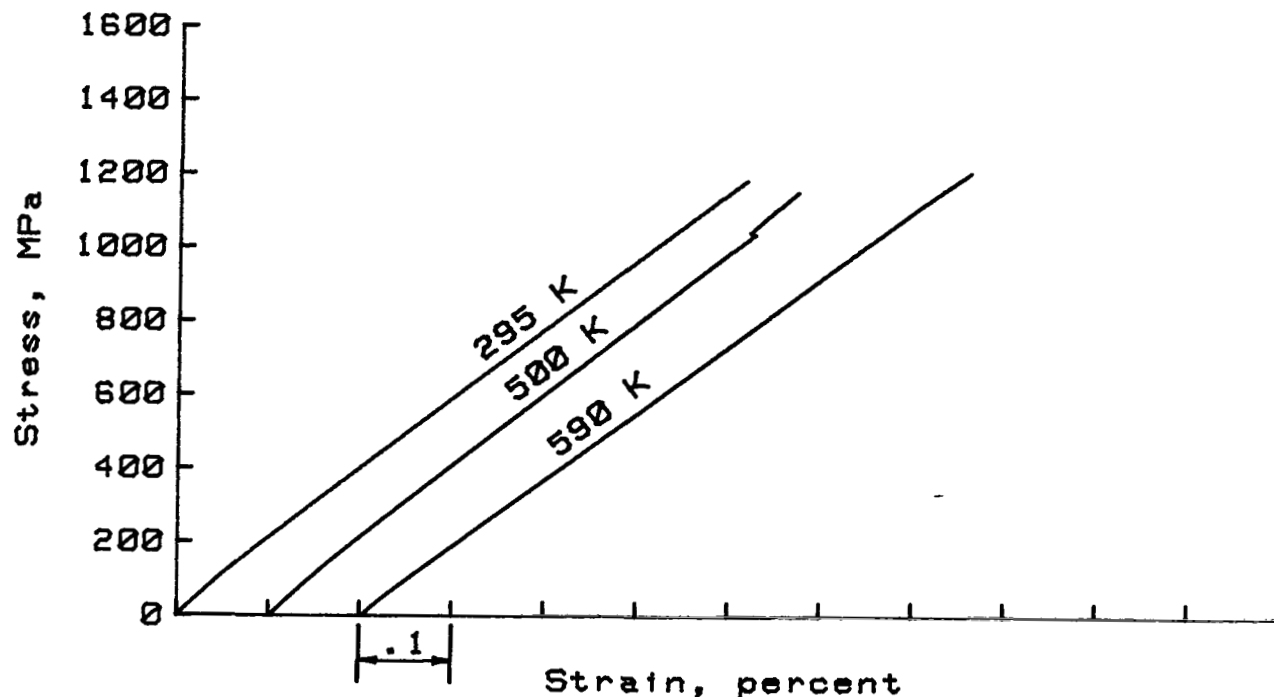
(a) Longitudinal tensile.



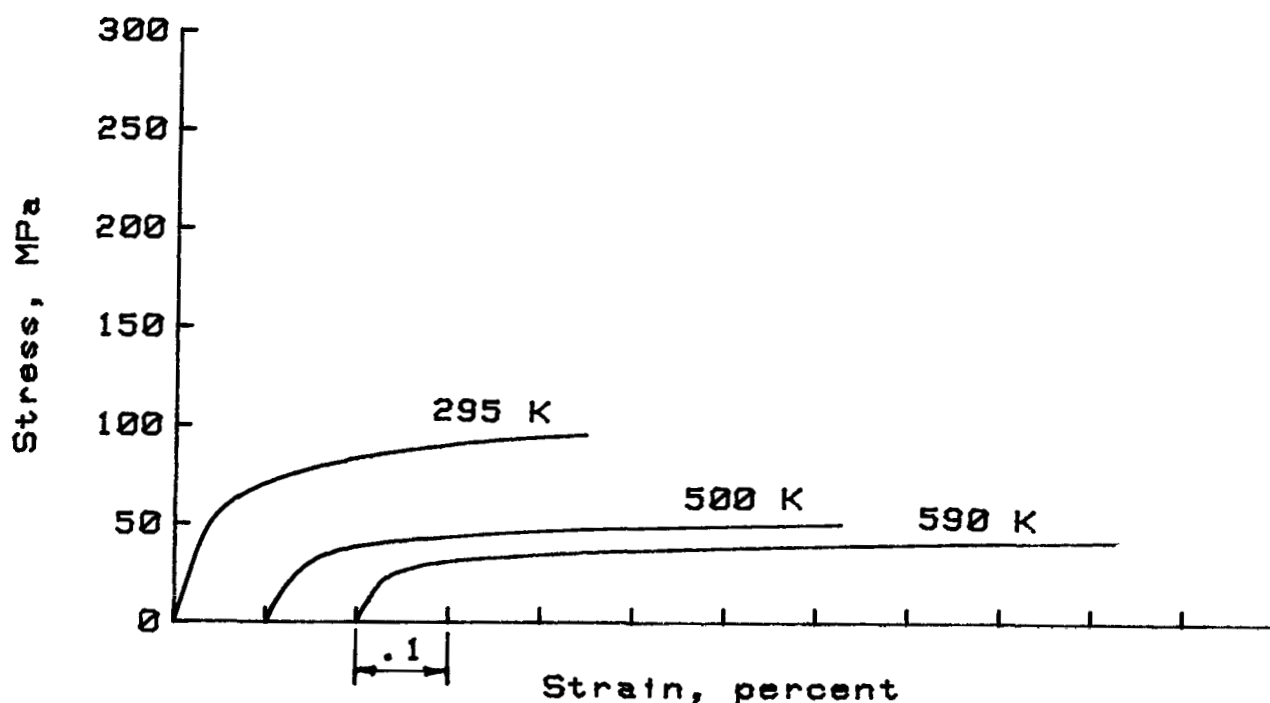
(b) Transverse tensile.

Figure A2.- Typical elevated test temperature stress-strain curves for B/2024 Al composite.

APPENDIX A



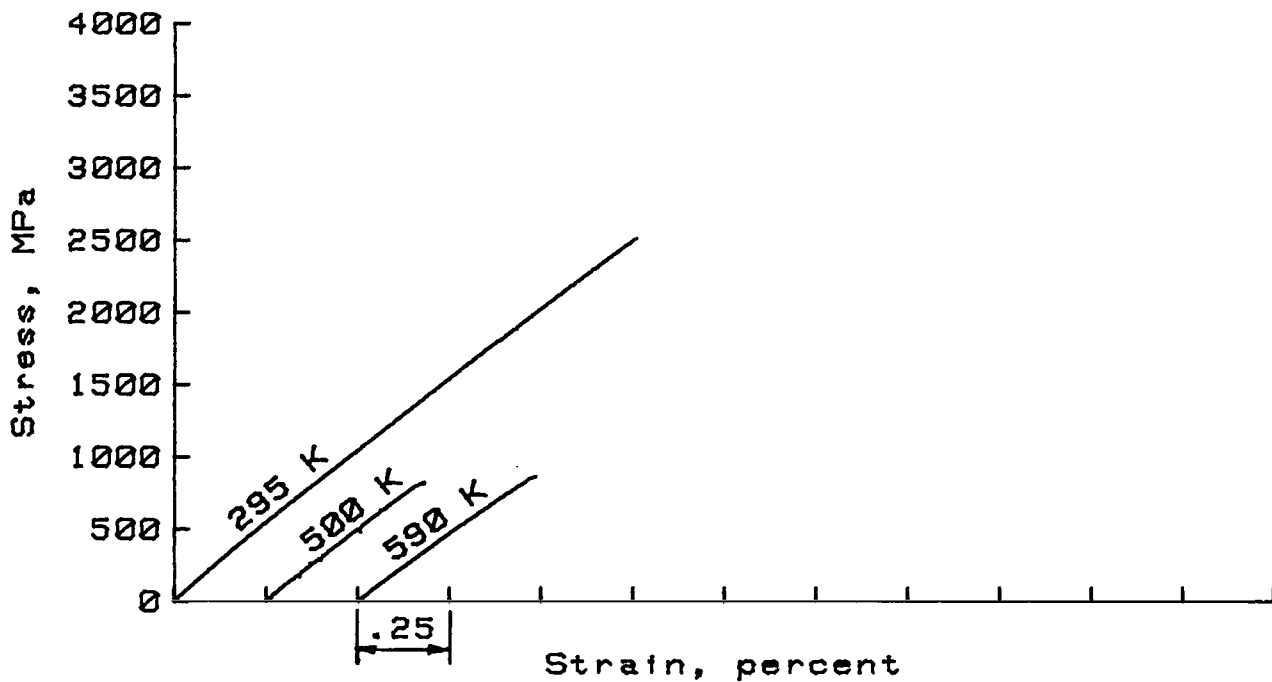
(a) Longitudinal tensile.



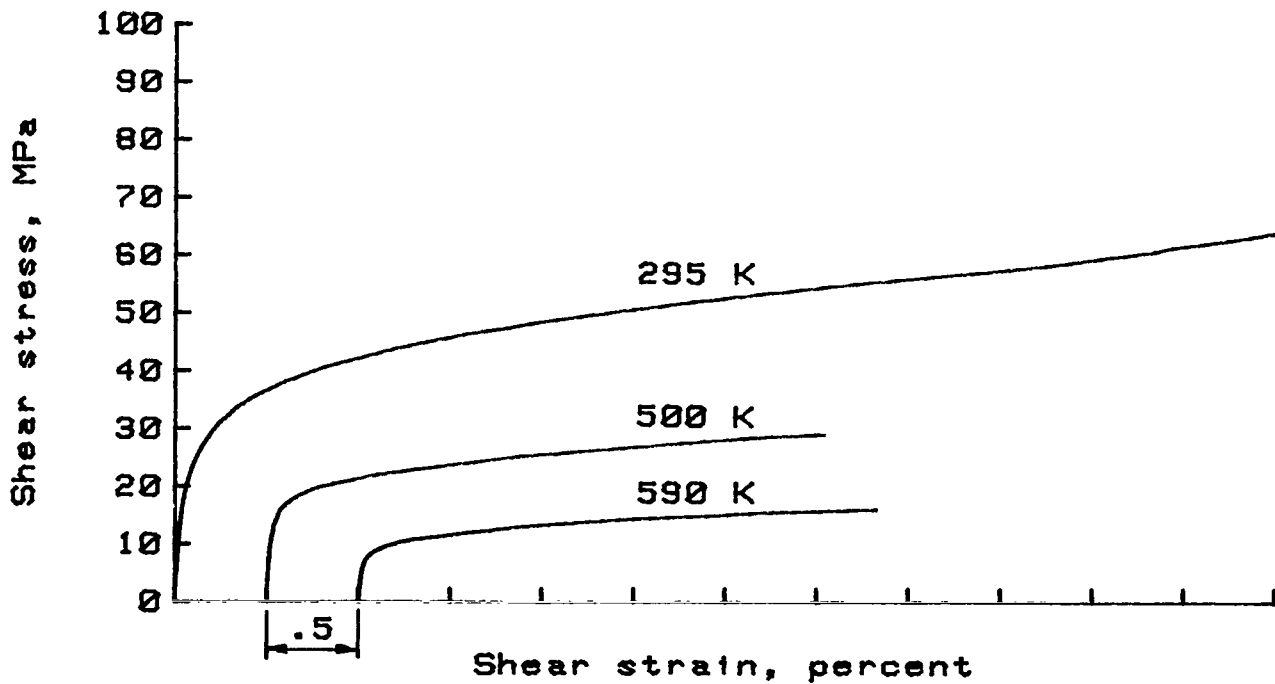
(b) Transverse tensile.

Figure A3.- Typical elevated test temperature stress-strain curves for B/3003 Al composite.

APPENDIX A



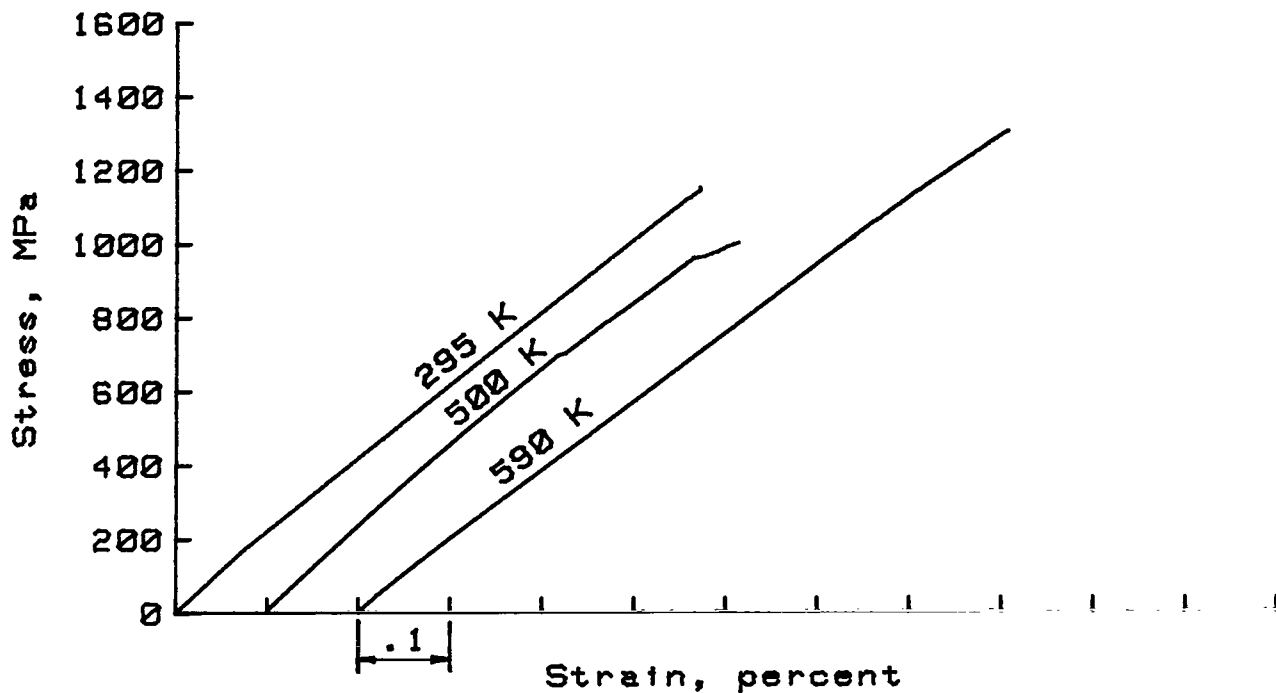
(c) Longitudinal compression.



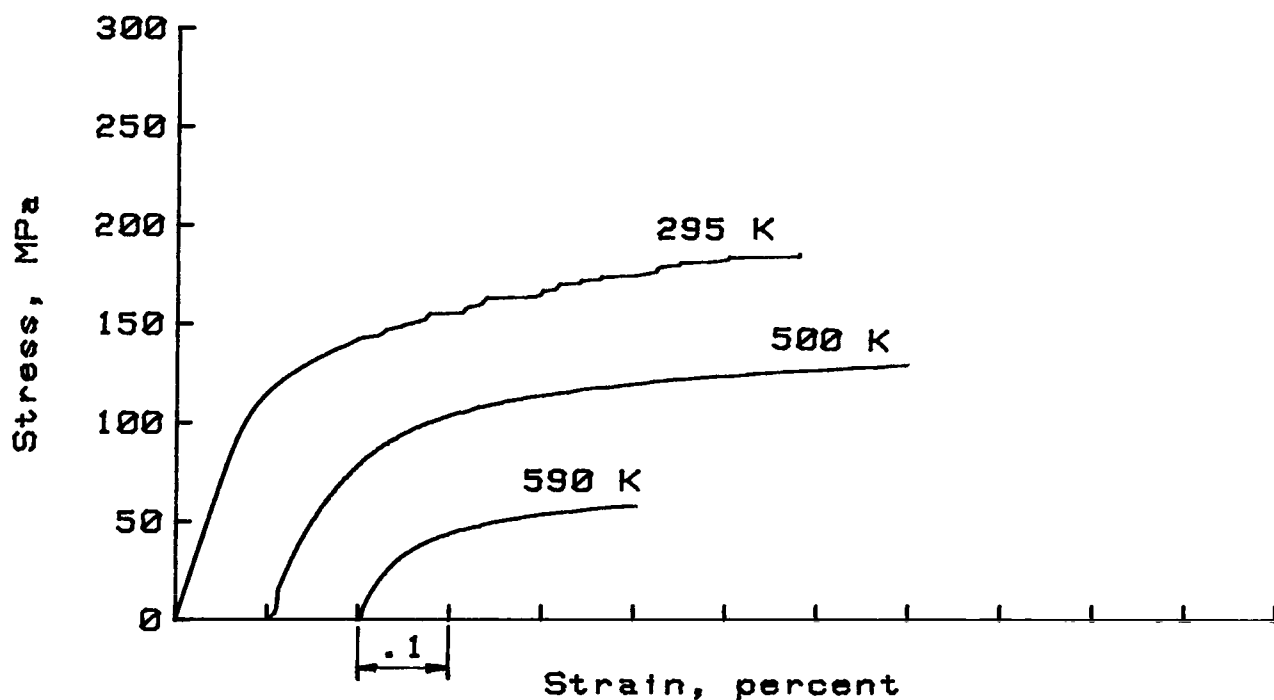
(d) In-plane shear.

Figure A3.- Concluded.

APPENDIX A



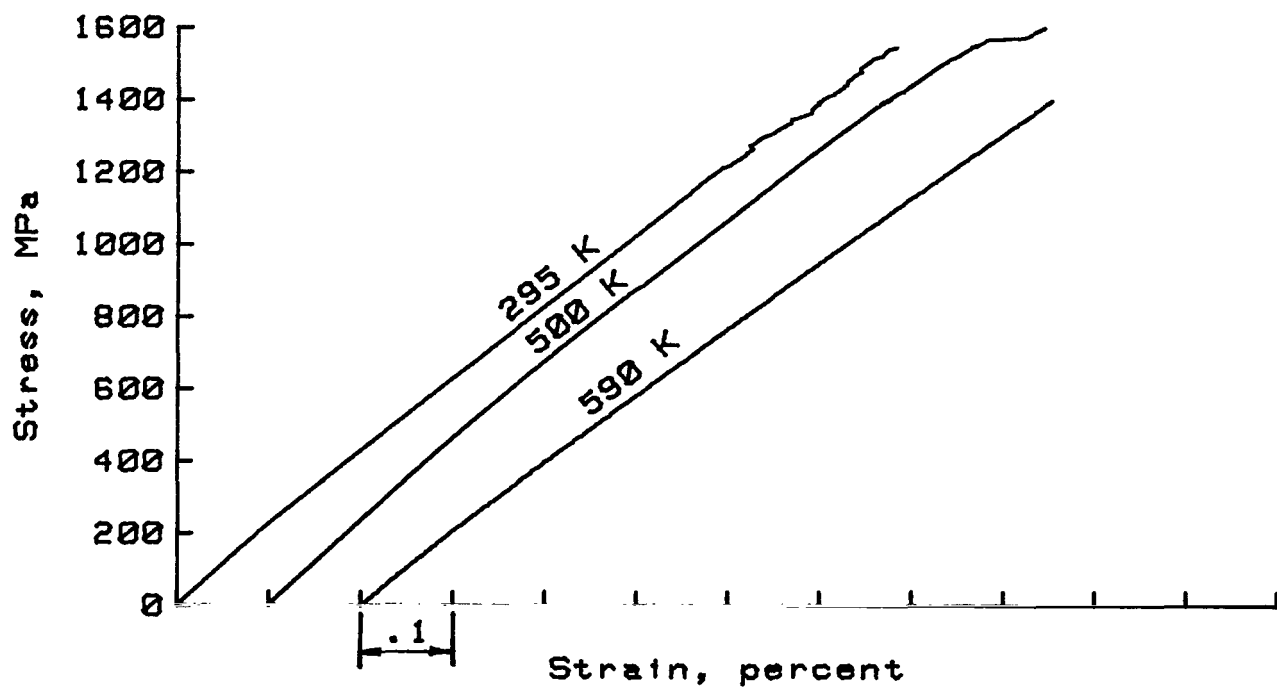
(a) Longitudinal tensile.



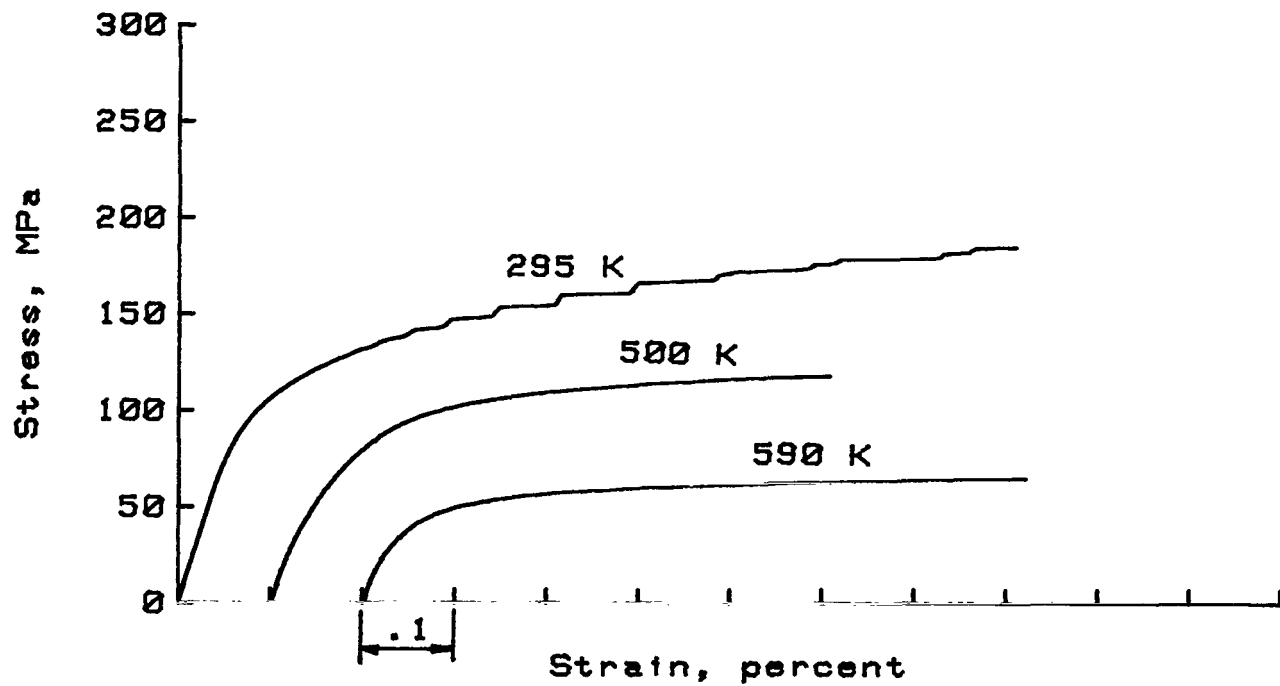
(b) Transverse tensile.

Figure A4.- Typical elevated test temperature stress-strain curves for B/5052 Al composite.

APPENDIX A



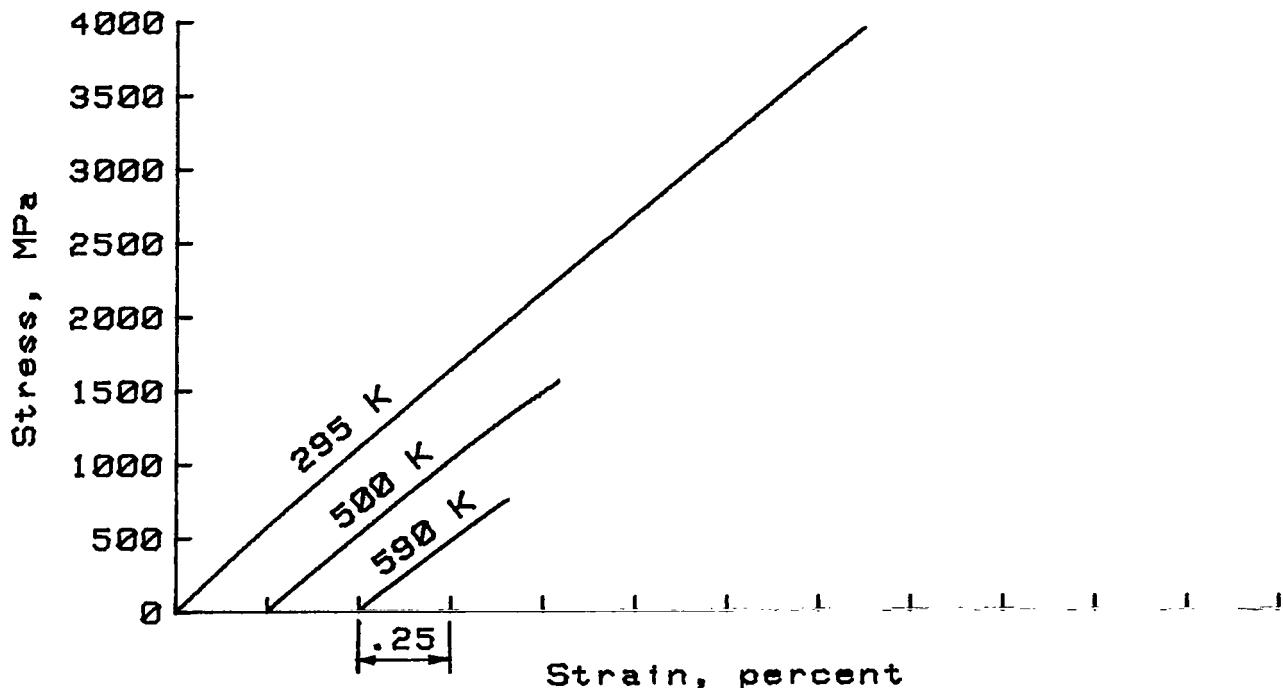
(a) Longitudinal tensile.



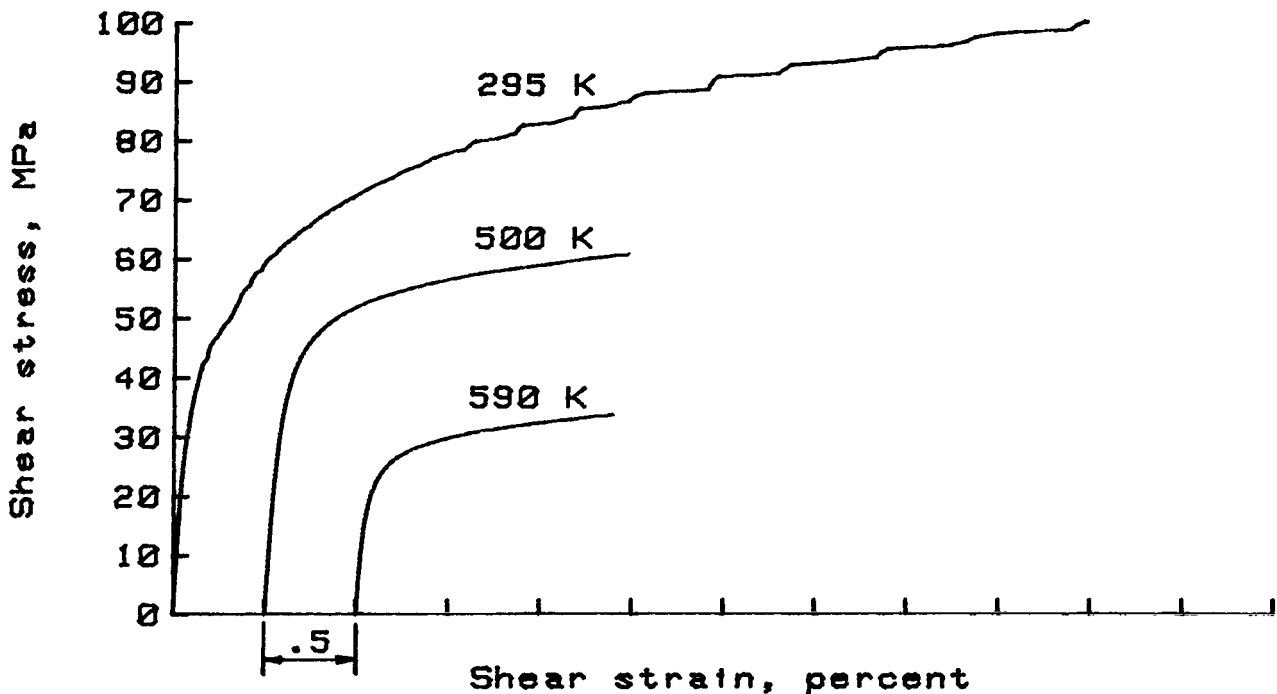
(b) Transverse tensile.

Figure A5.- Typical elevated test temperature stress-strain curves for B/6061 Al composite.

APPENDIX A



(c) Longitudinal compression.



(d) In-plane shear.

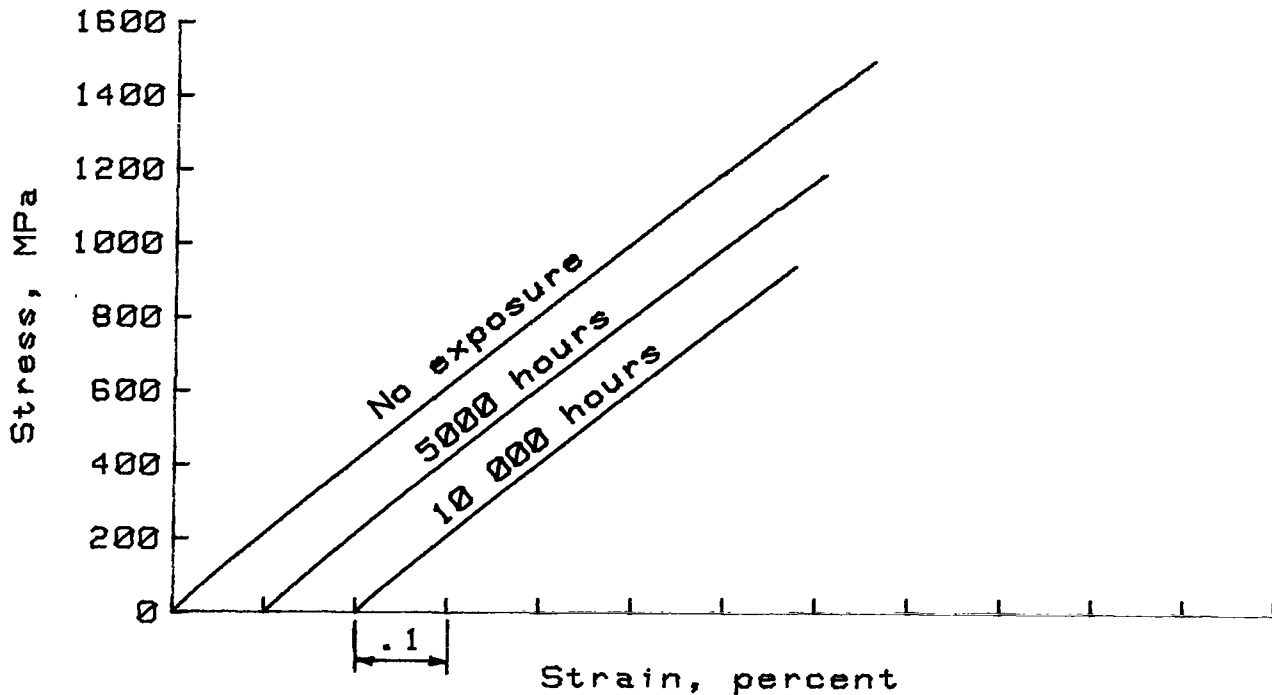
Figure A5.- Concluded.

## APPENDIX B

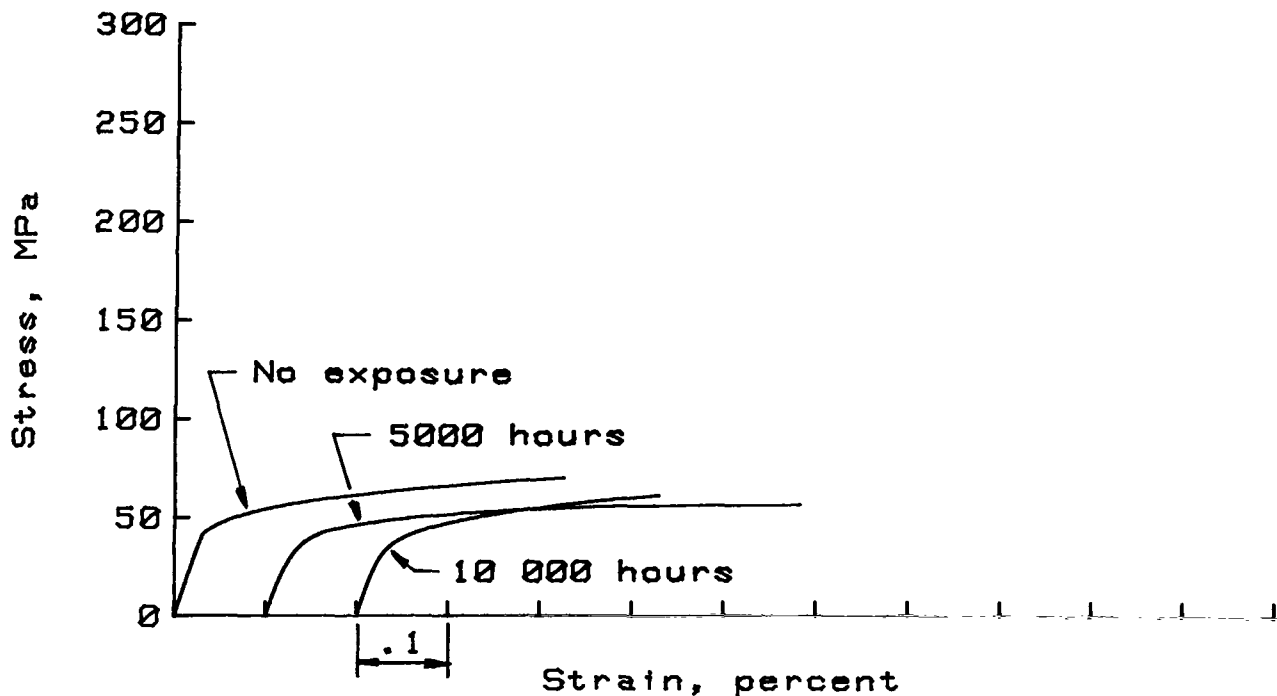
### SPECIMENS EXPOSED UP TO 10 000 HOURS AND 500 K

The mechanical property data for all the B/Al composite tests conducted in this investigation are given in tables V through IX. Typical stress-strain curves for the specimens exposed up to 10 000 hours at 500 K and tested at room temperature are presented in appendix B.

APPENDIX B



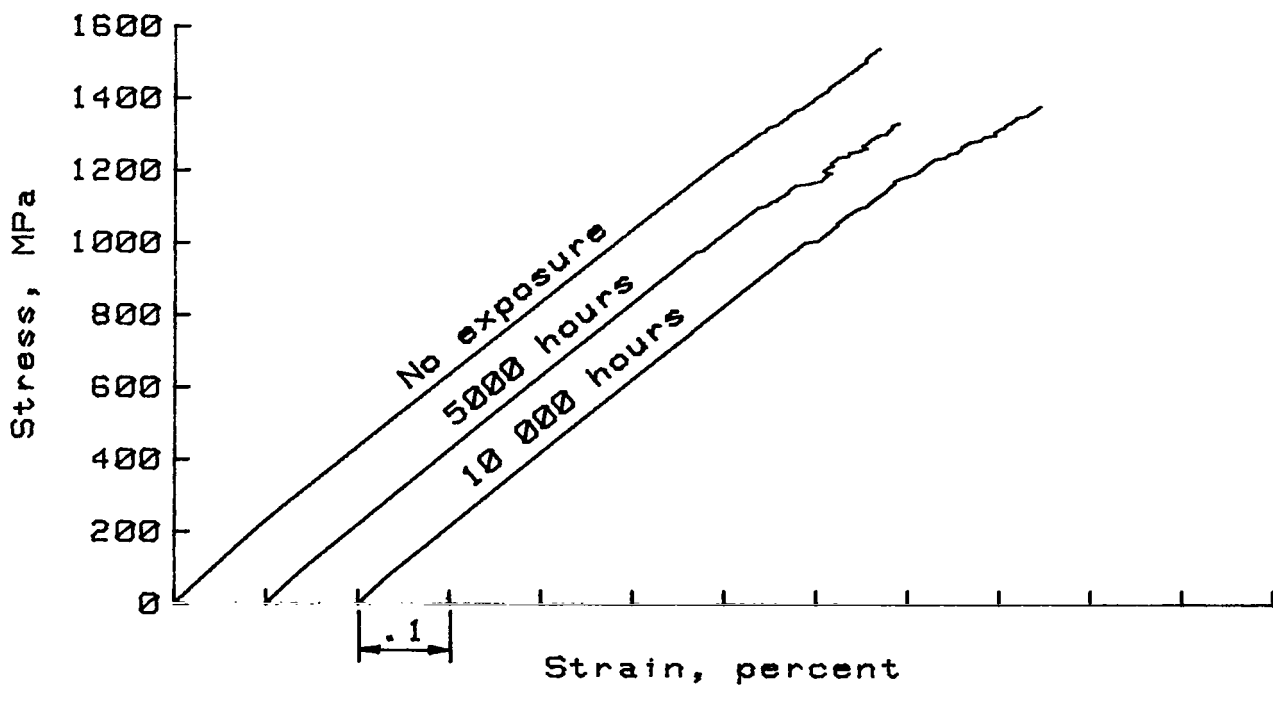
(a) Longitudinal tensile.



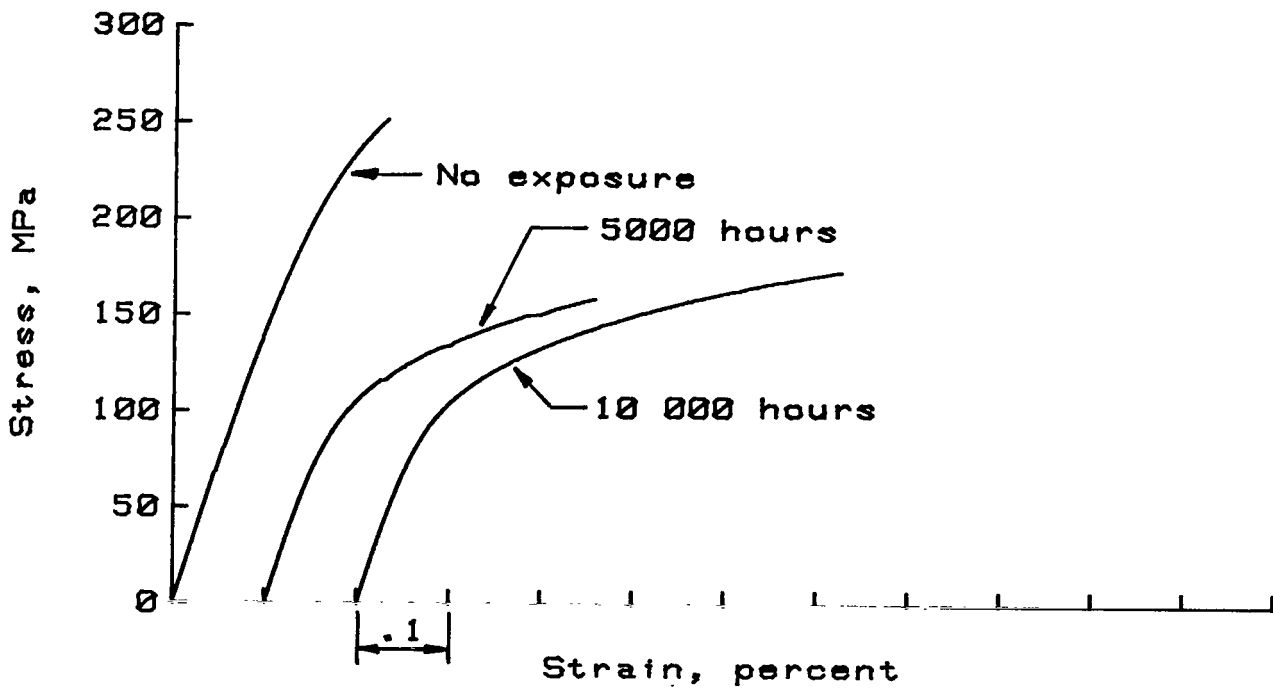
(b) Transverse tensile.

Figure B1.- Typical room-temperature stress-strain curves for B/1100 Al composite material exposed at 500 K.

APPENDIX B



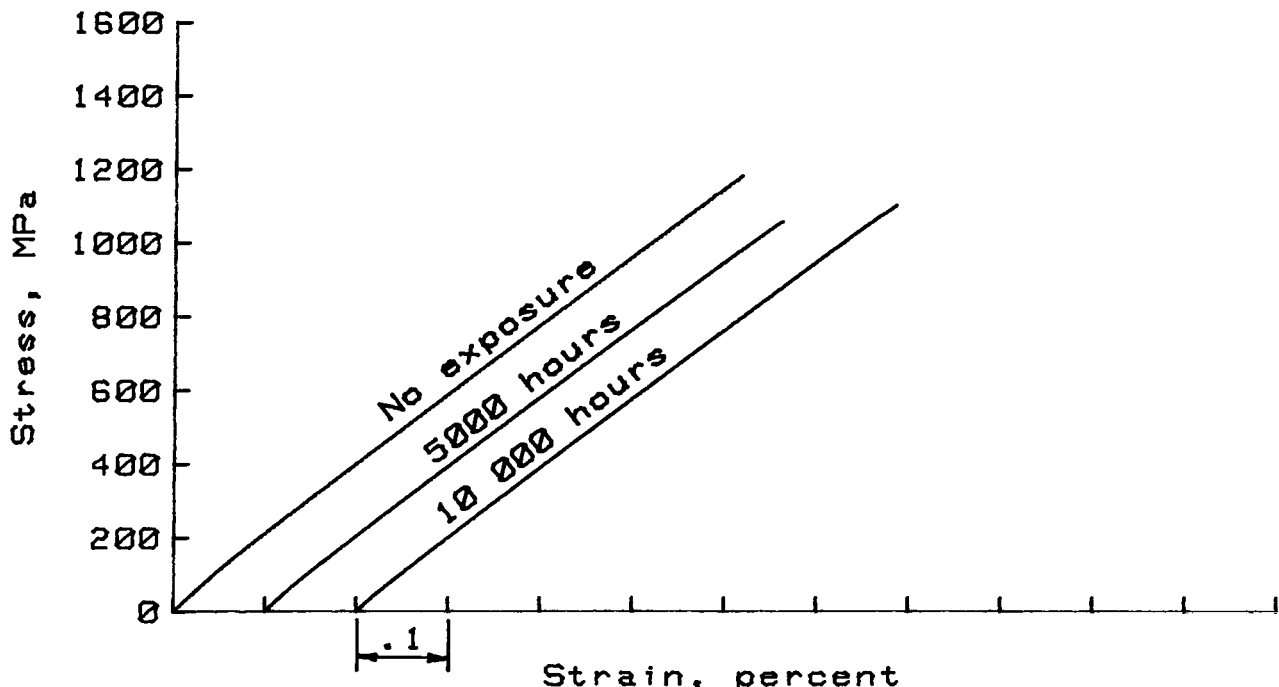
(a) Longitudinal tensile.



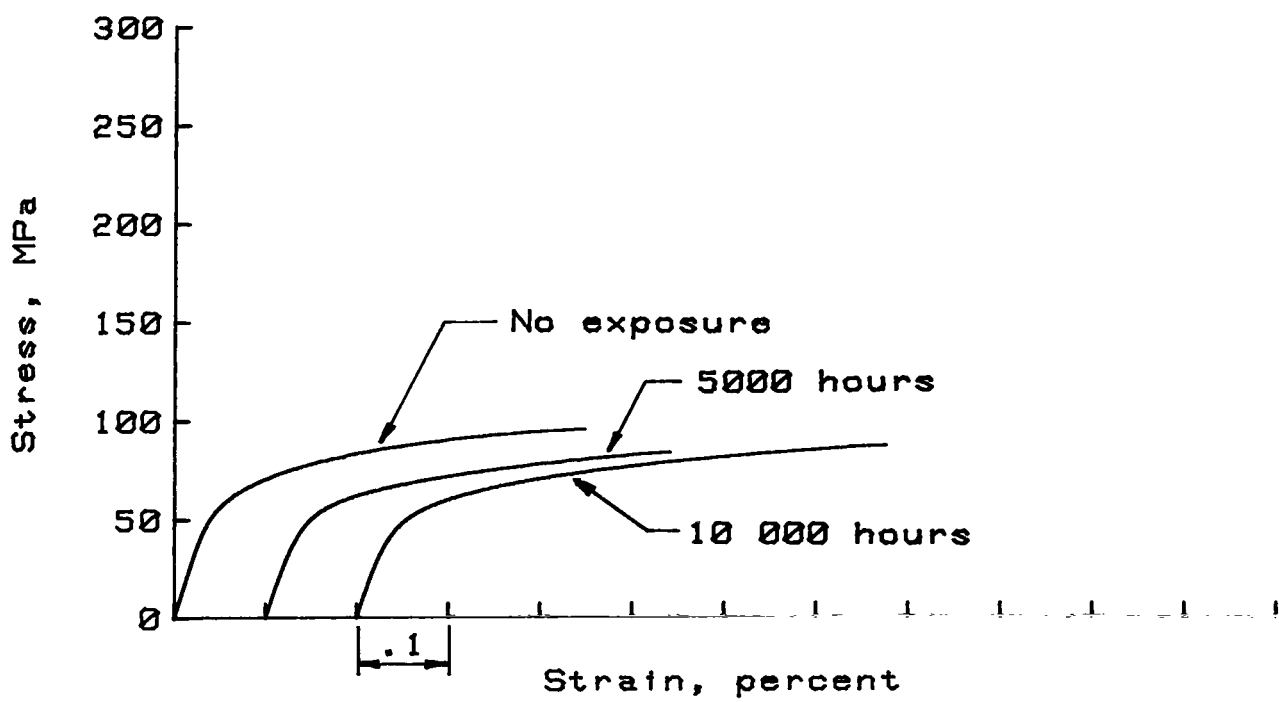
(b) Transverse tensile.

Figure B2.- Typical room-temperature stress-strain curves for B/2024 Al composite material exposed at 500 K.

APPENDIX B



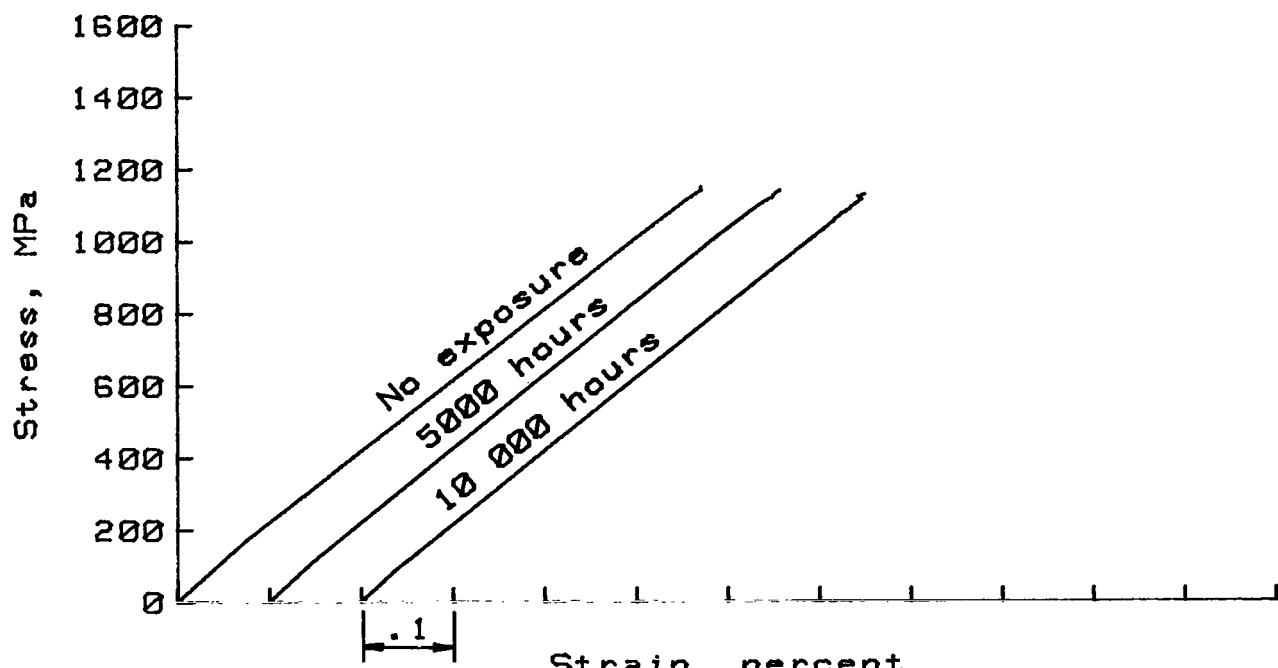
(a) Longitudinal tensile.



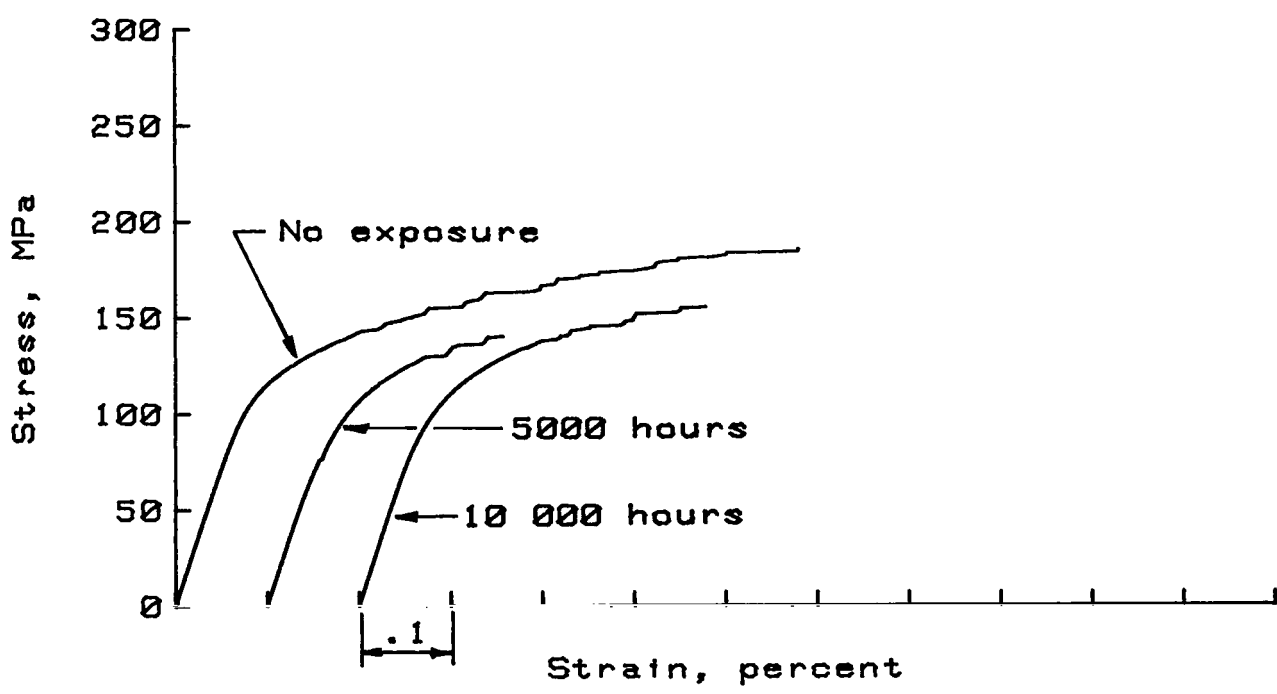
(b) Transverse tensile.

Figure B3.- Typical room-temperature stress-strain curves for B/3003 Al composite material exposed at 500 K.

APPENDIX B



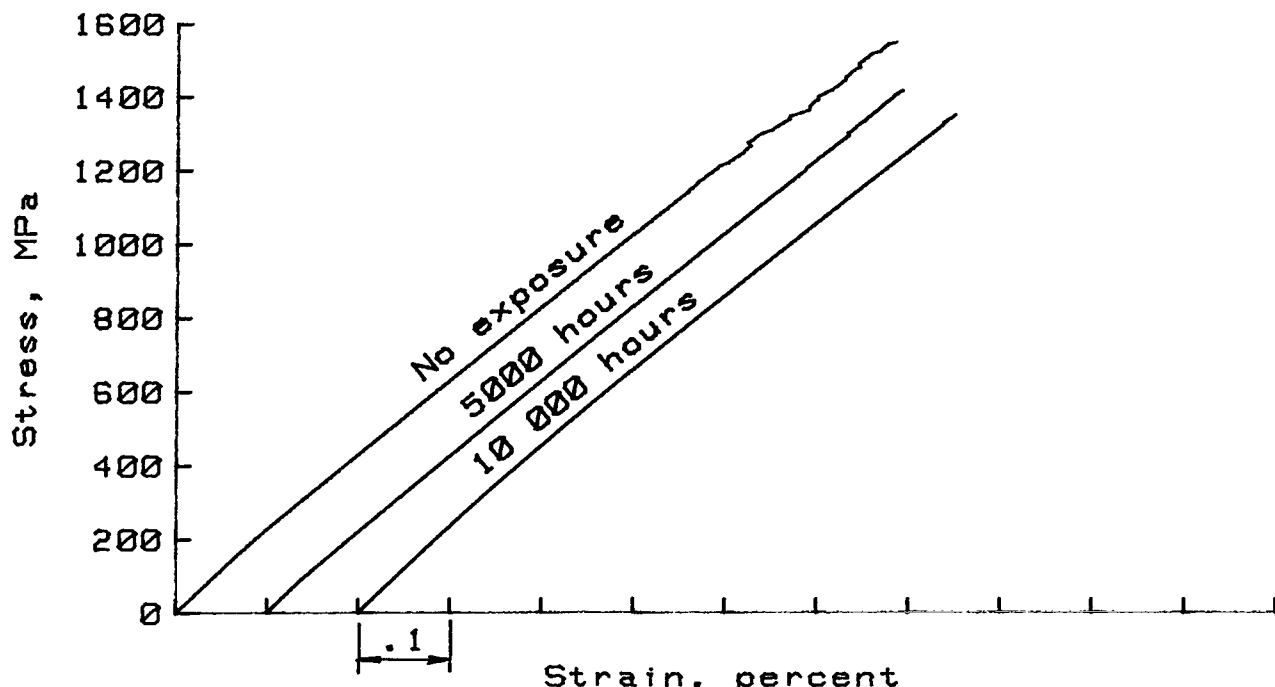
(a) Longitudinal tensile.



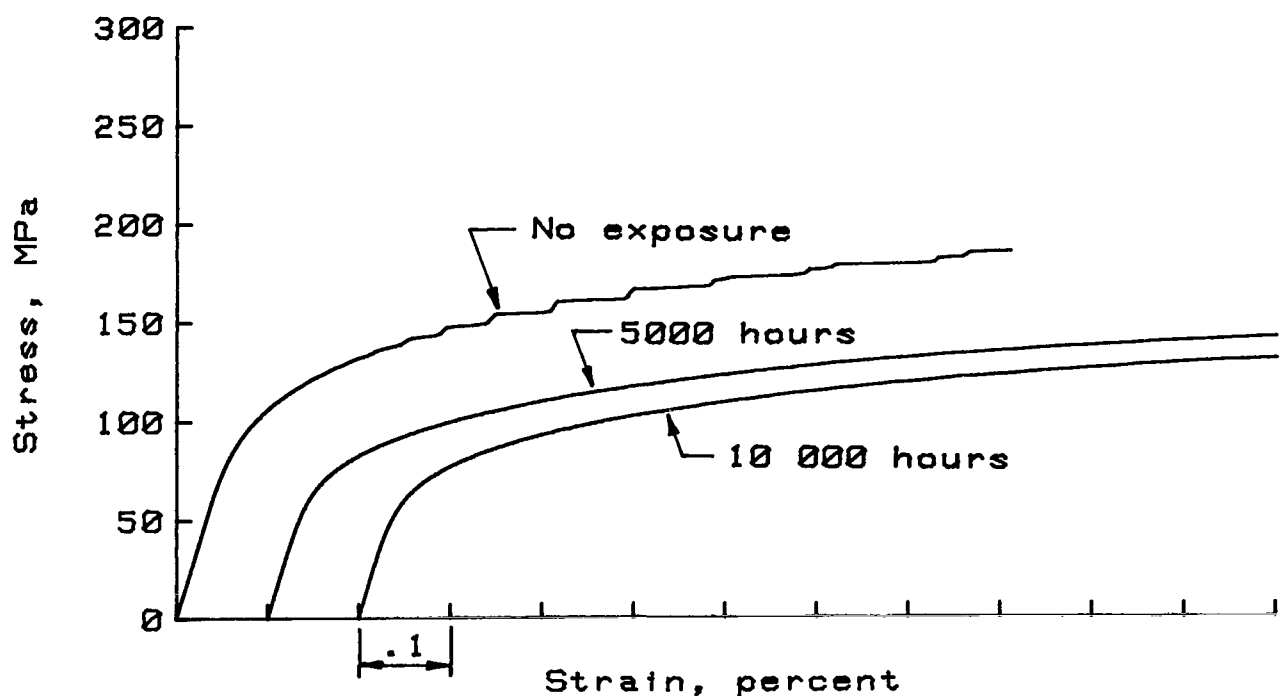
(b) Transverse tensile.

Figure B4.- Typical room-temperature stress-strain curves for B/5052 Al composite material exposed at 500 K.

APPENDIX B



(a) Longitudinal tensile.



(b) Transverse tensile.

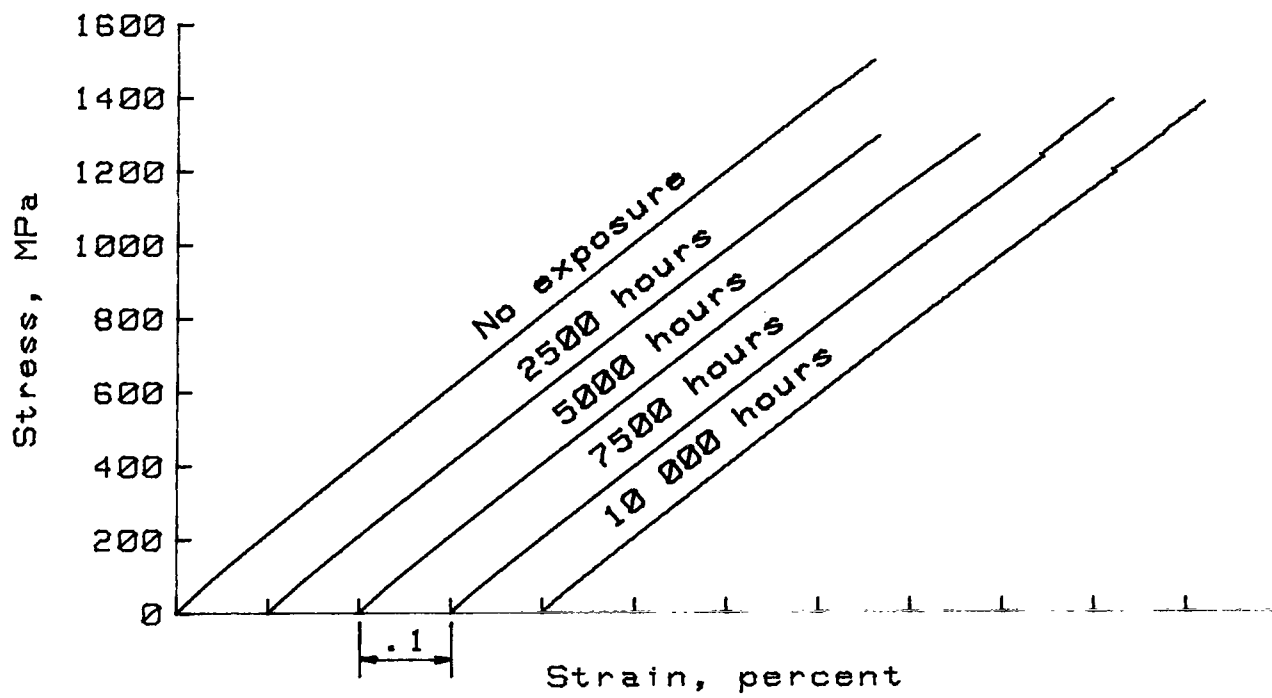
Figure B5.- Typical room-temperature stress-strain curves for B/6061 Al composite material exposed at 500 K.

## APPENDIX C

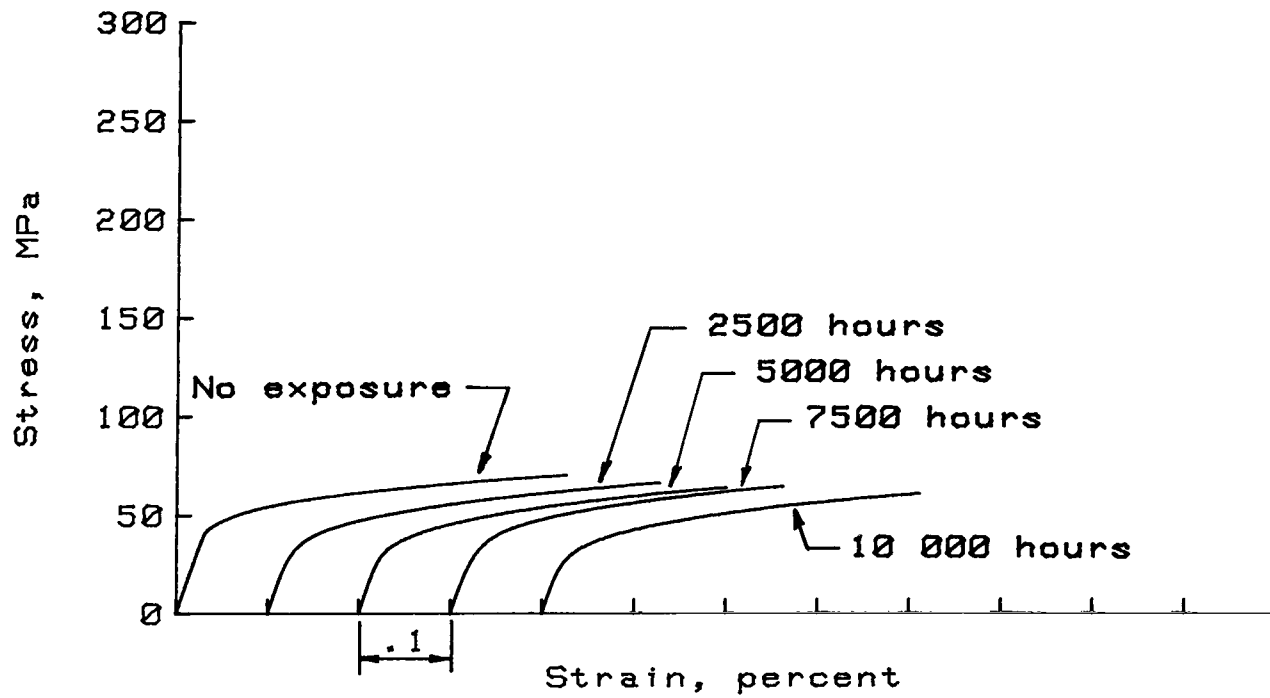
### SPECIMENS EXPOSED UP TO 10 000 HOURS AT 590 K

The mechanical property data for all the B/Al composite tests conducted in this investigation are given in tables V through IX. Typical stress-strain curves for the specimens exposed up to 10 000 hours at 590 K and tested at room temperature are presented in appendix C.

APPENDIX C



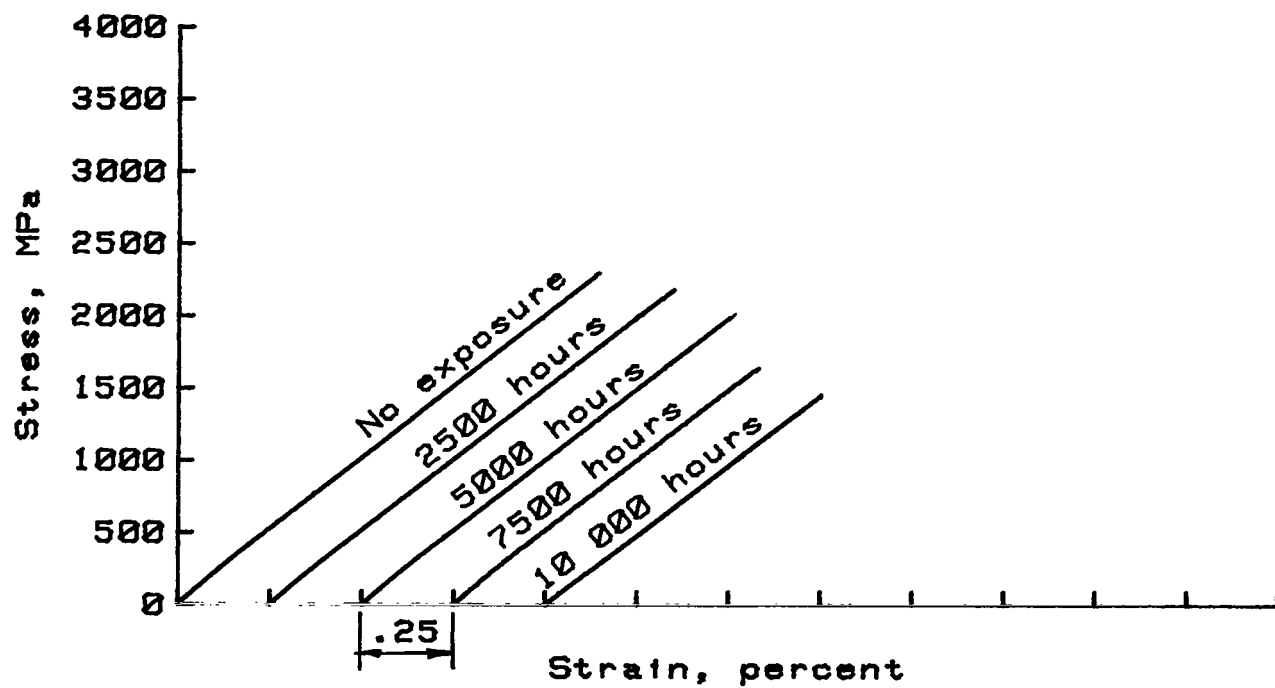
(a) Longitudinal tensile.



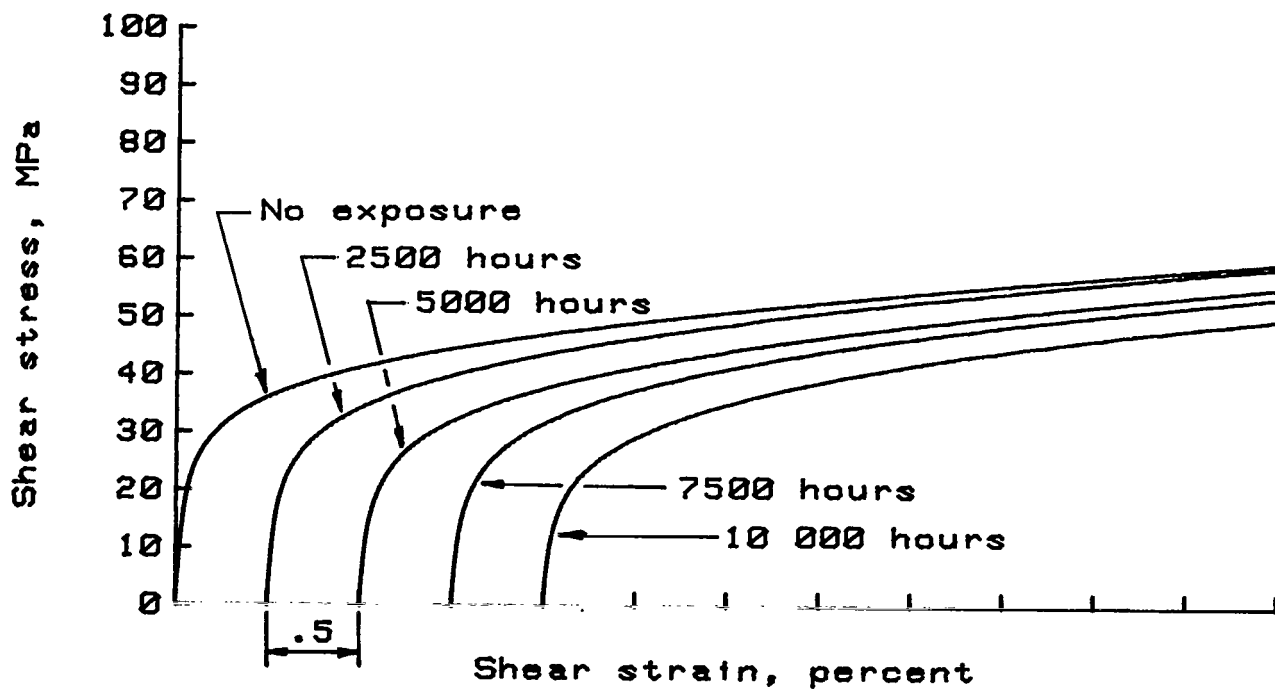
(b) Transverse tensile.

Figure C1.- Typical room-temperature stress-strain curves for B/1100 Al composite material exposed at 590 K.

APPENDIX C



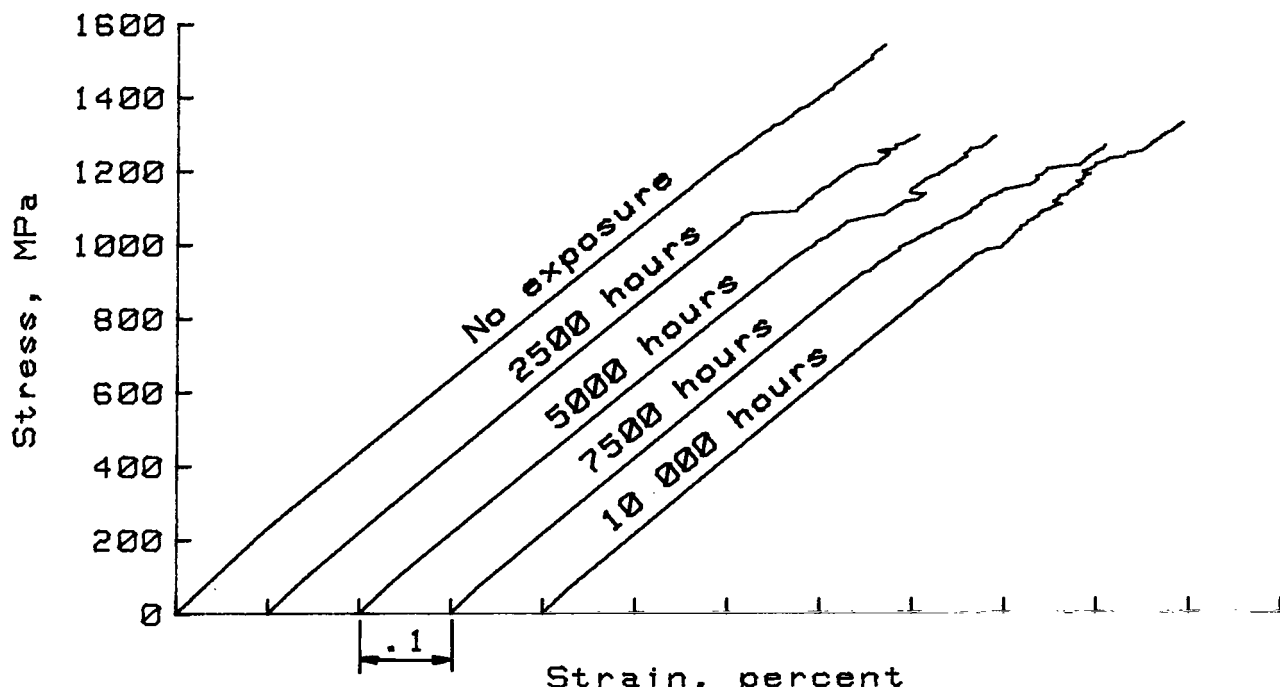
(c) Longitudinal compression.



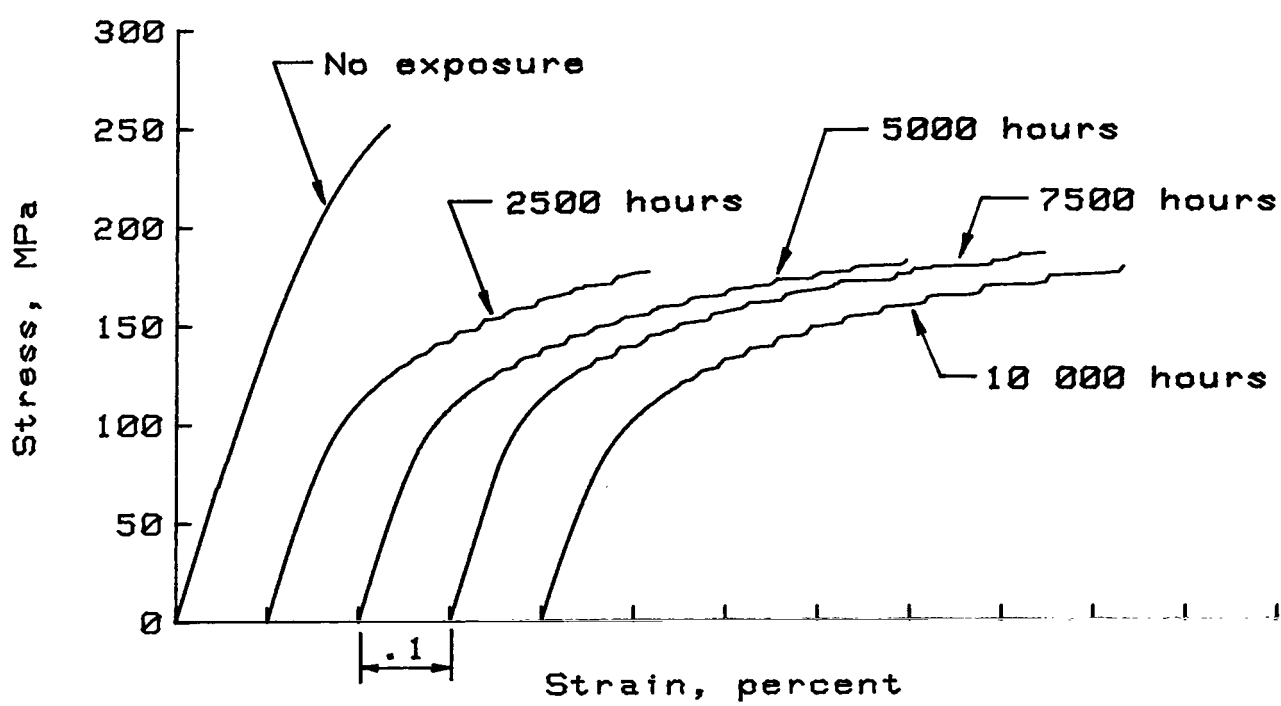
(d) In-plane shear.

Figure C1.- Concluded.

APPENDIX C

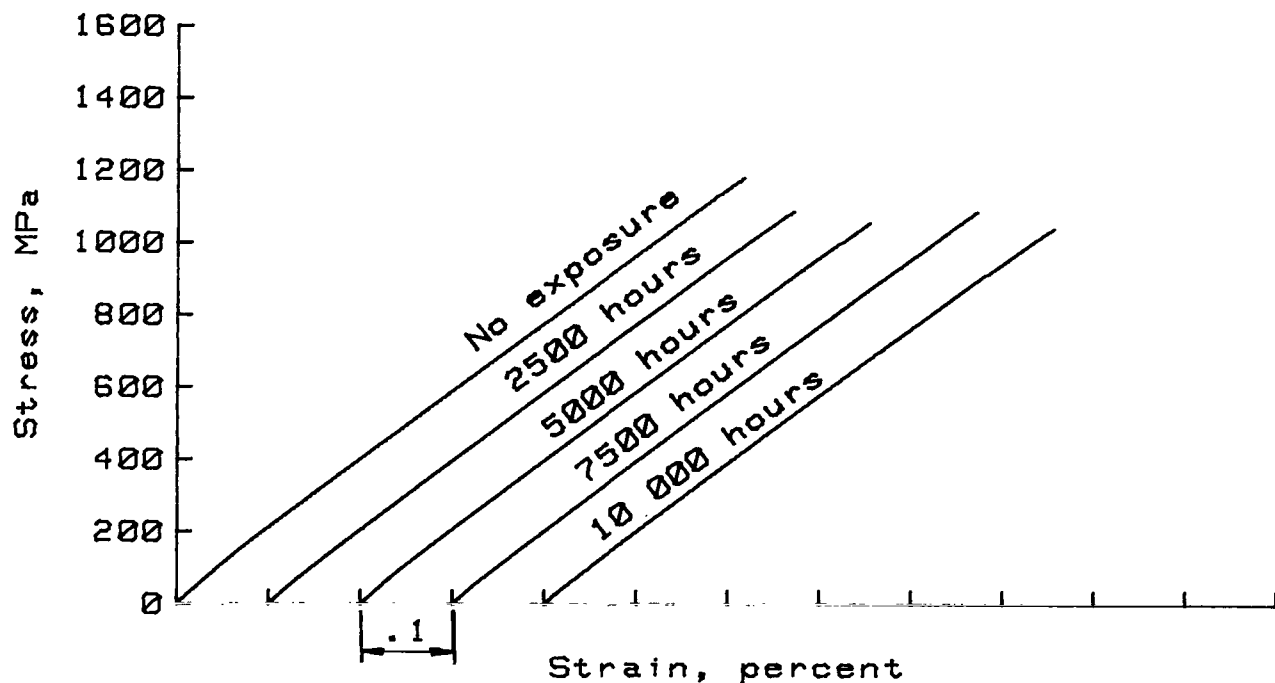


(a) Longitudinal tensile.

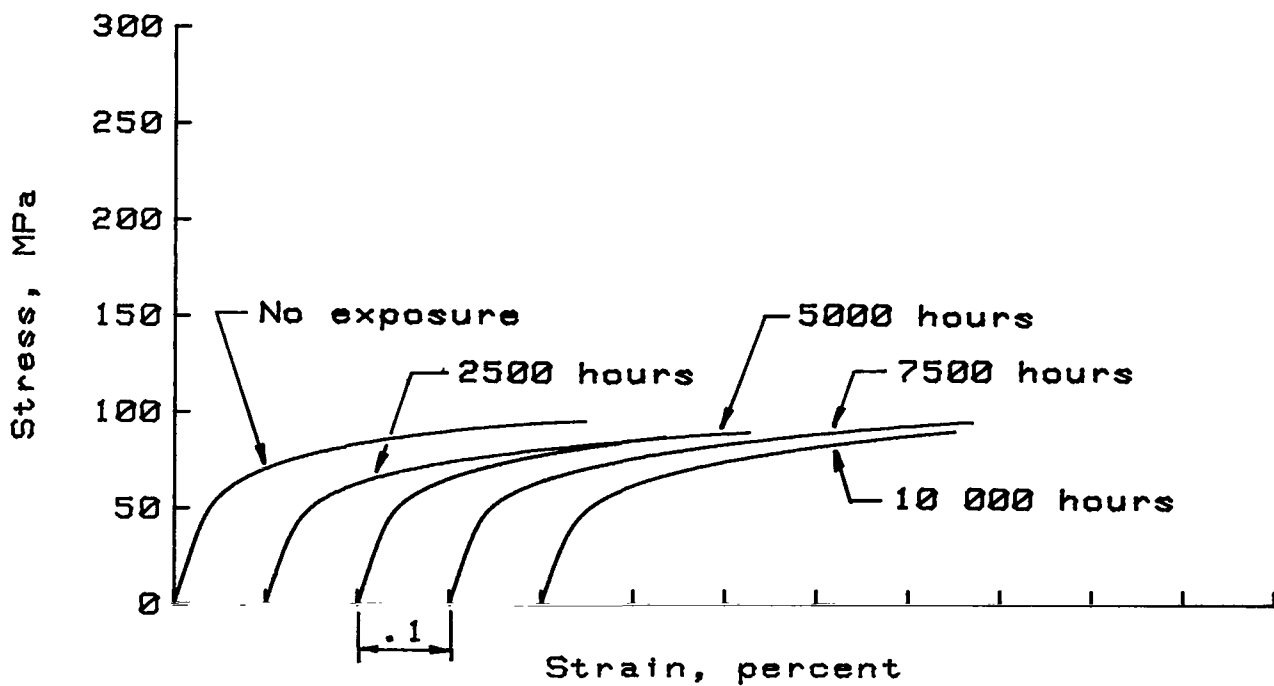


(b) Transverse tensile.

Figure C2.- Typical room-temperature stress-strain curves for B/2024 Al composite material exposed at 590 K.



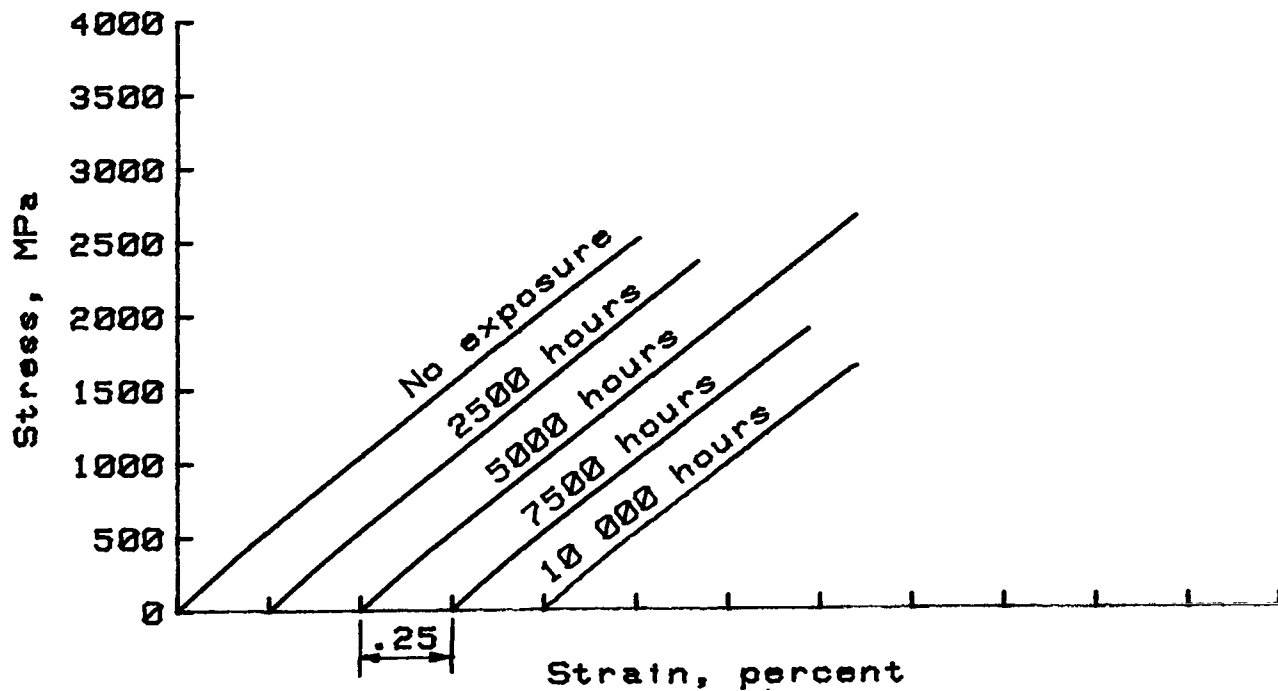
(a) Longitudinal tensile.



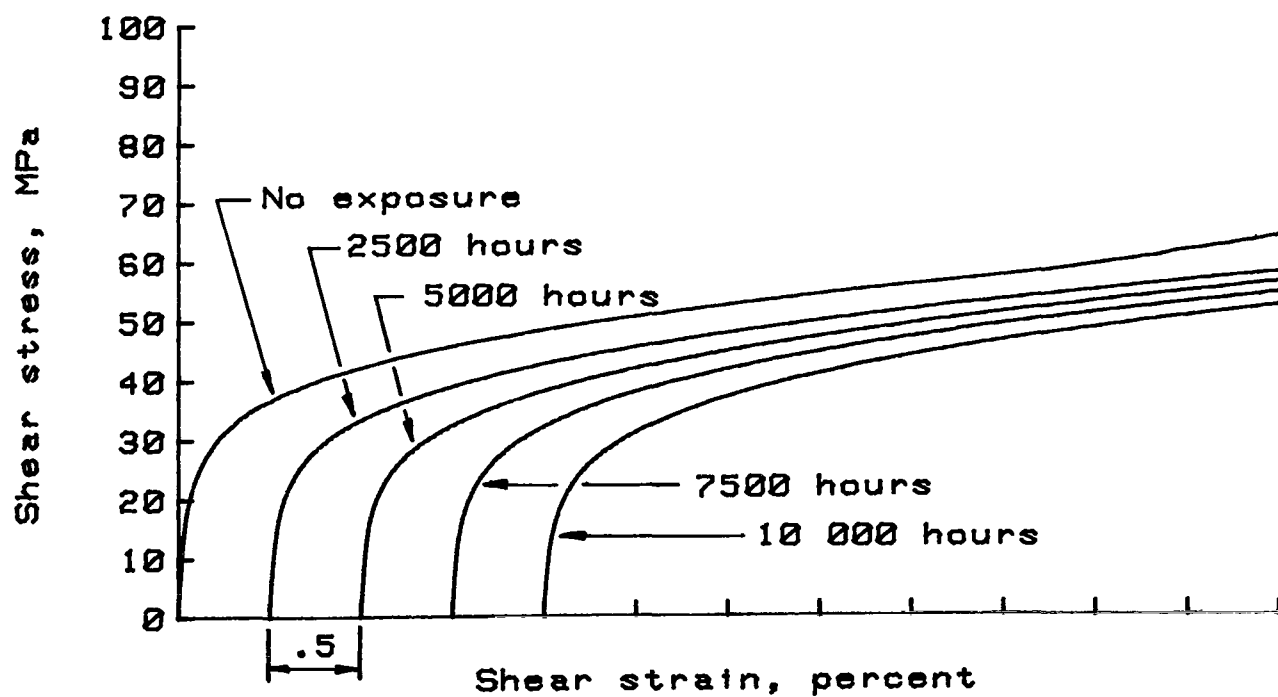
(b) Transverse tensile.

Figure C3.- Typical room-temperature stress-strain curves for B/3003 Al composite material exposed at 590 K.

APPENDIX C



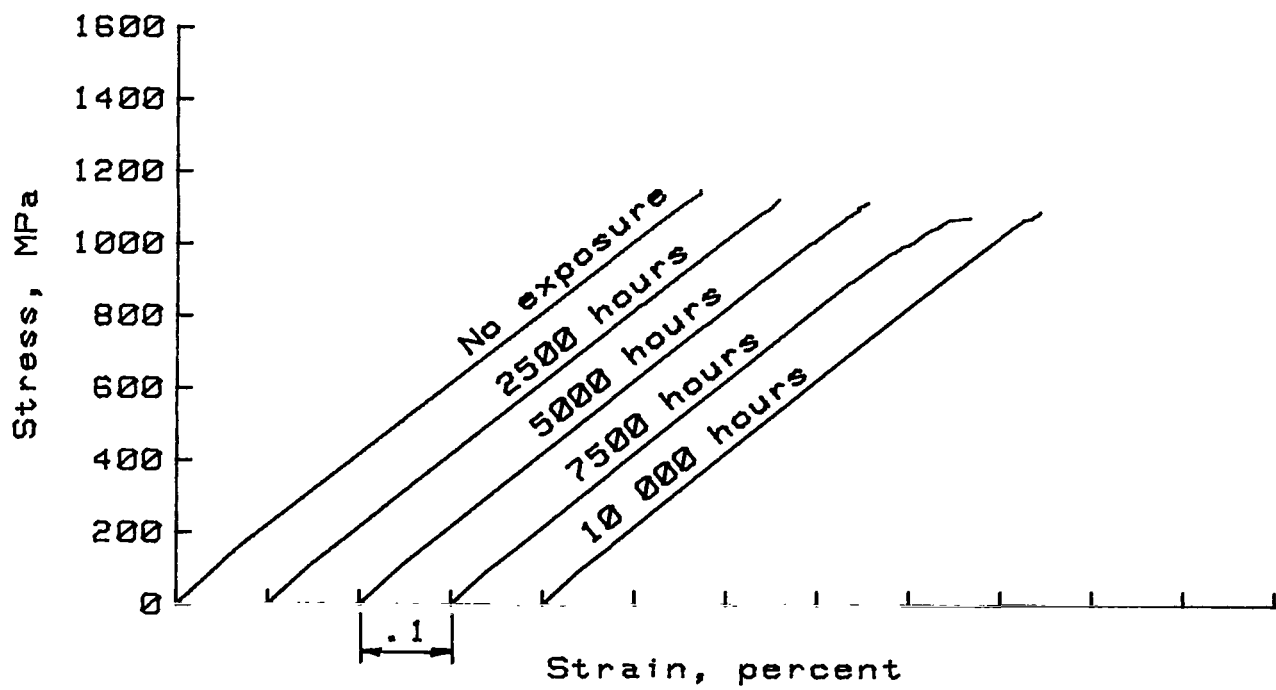
(c) Longitudinal compression.



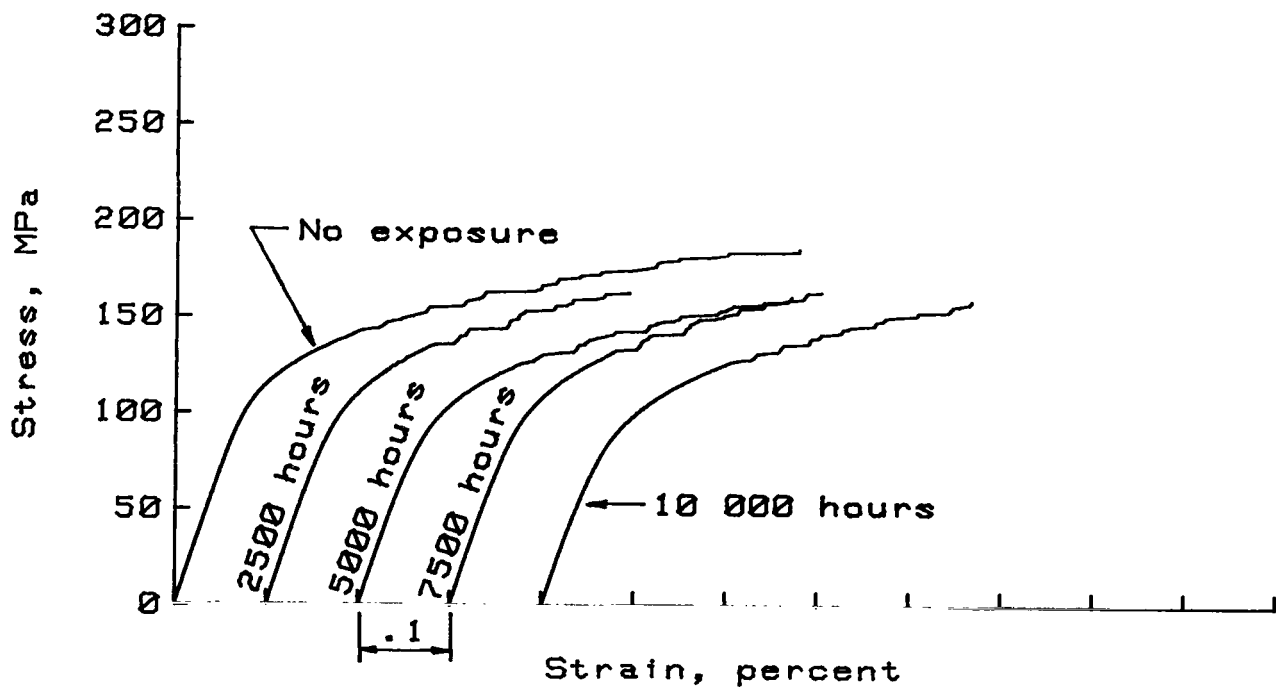
(d) In-plane shear.

Figure C3.- Concluded.

APPENDIX C



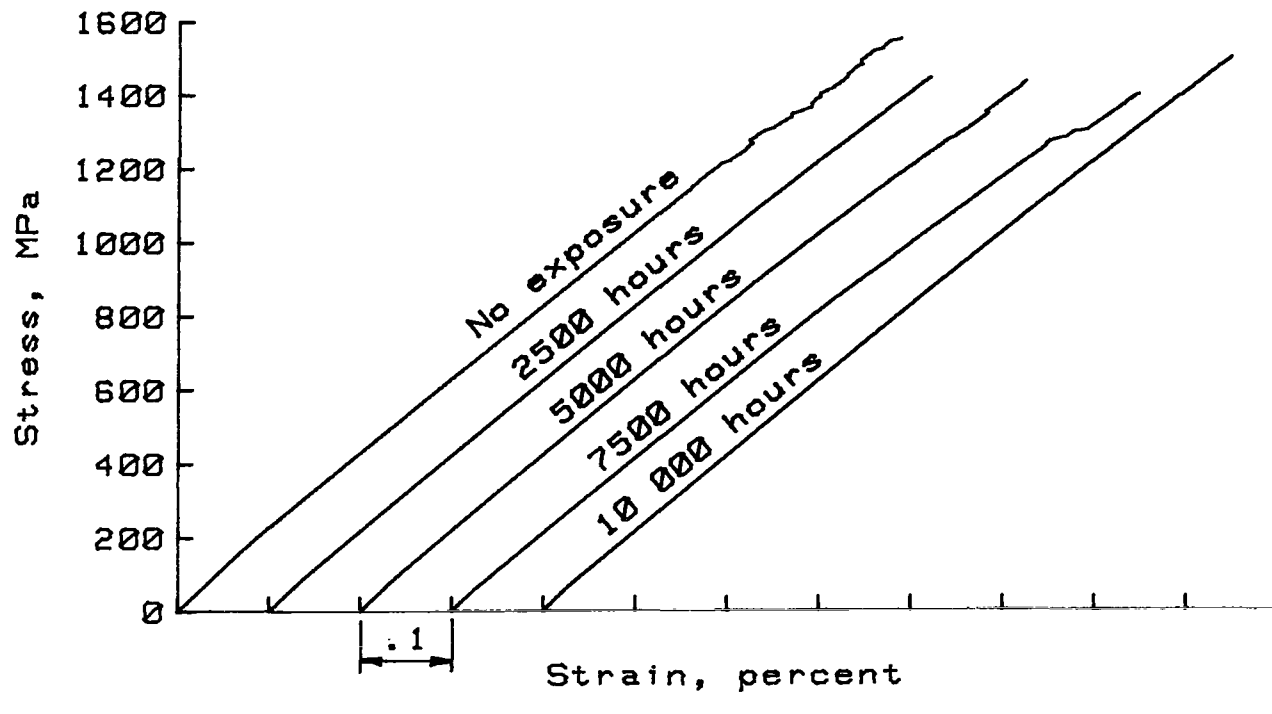
(a) Longitudinal tensile.



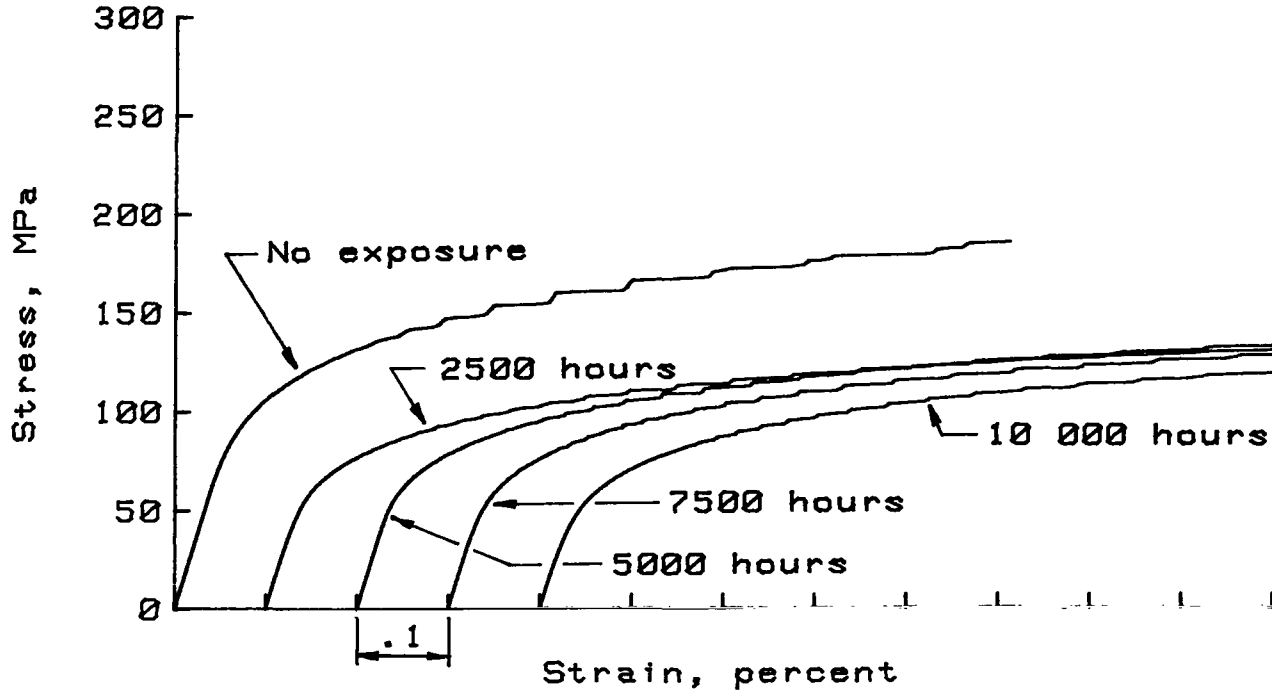
(b) Transverse tensile.

Figure C4.- Typical room-temperature stress-strain curves for B/5052 Al composite material exposed at 590 K.

APPENDIX C



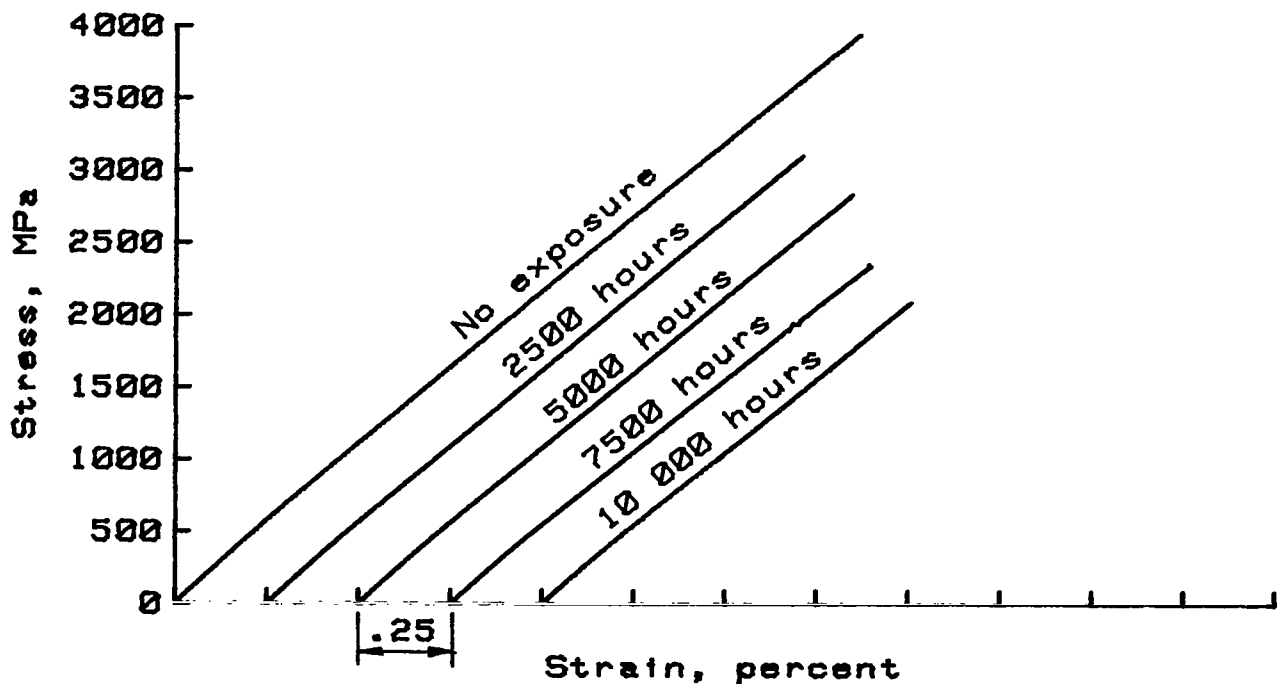
(a) Longitudinal tensile.



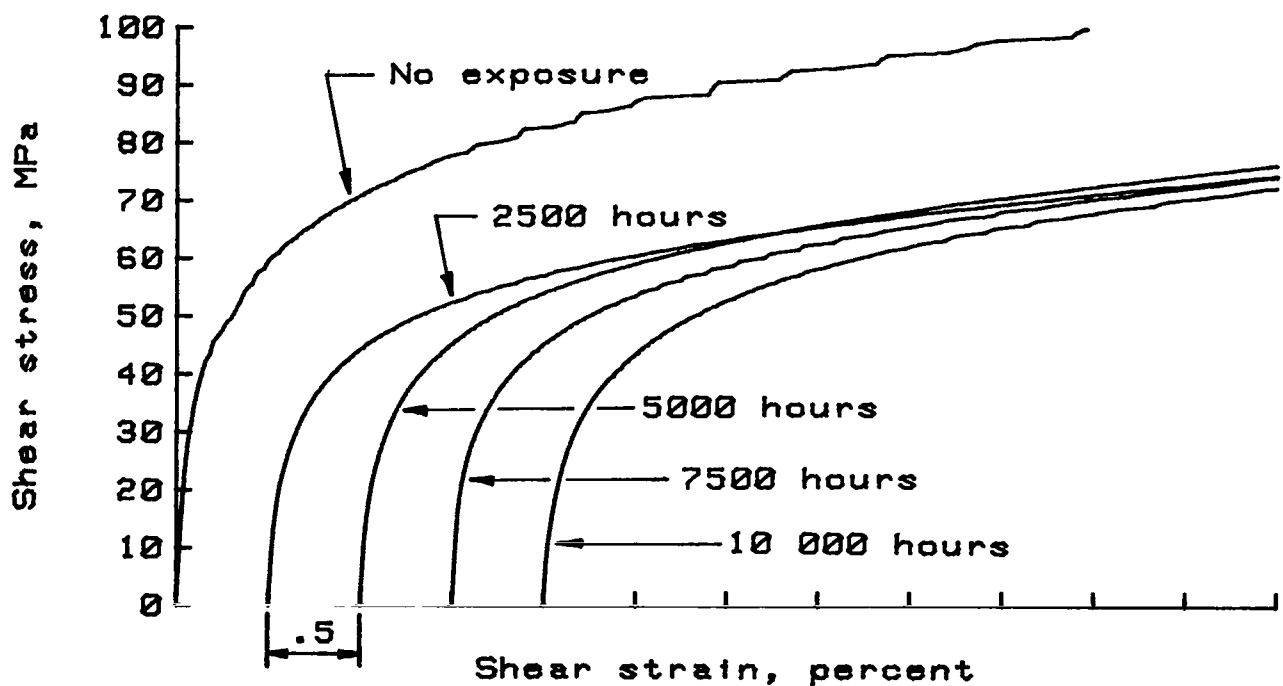
(b) Transverse tensile.

Figure C5.- Typical room-temperature stress-strain curves for B/6061 Al composite material exposed at 590 K.

APPENDIX C



(c) Longitudinal compression.



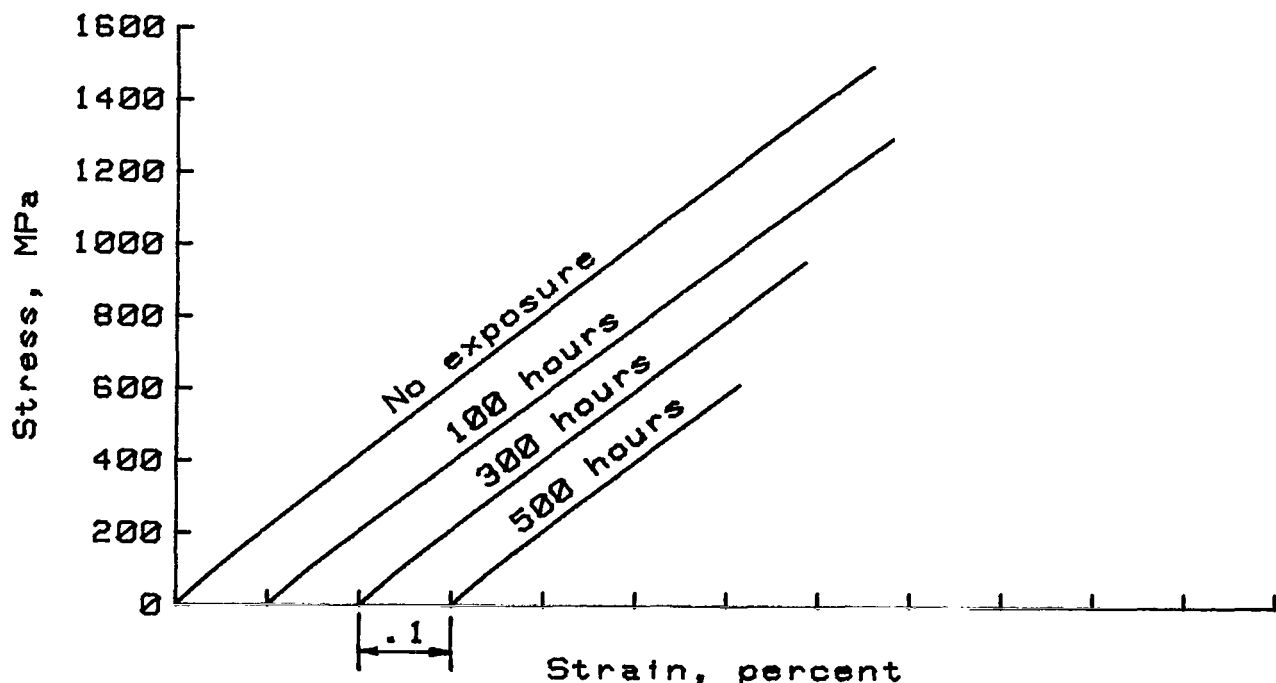
(d) In-plane shear.

Figure C5.- Concluded.

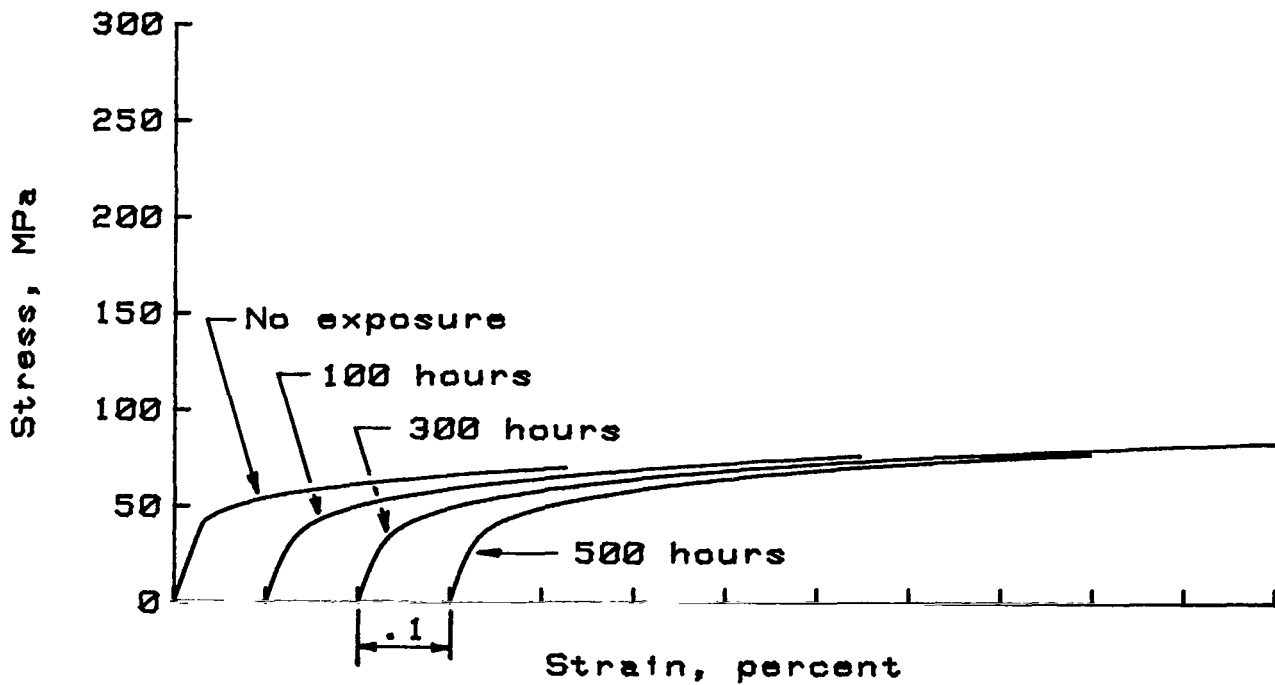
## APPENDIX D

### SPECIMENS EXPOSED UP TO 500 HOURS AT 730 K

The mechanical property data for all the B/Al composite tests conducted in this investigation are given in tables V through IX. Typical stress-strain curves for the specimens exposed up to 500 hours at 730 K and tested at room temperature are presented in appendix D.



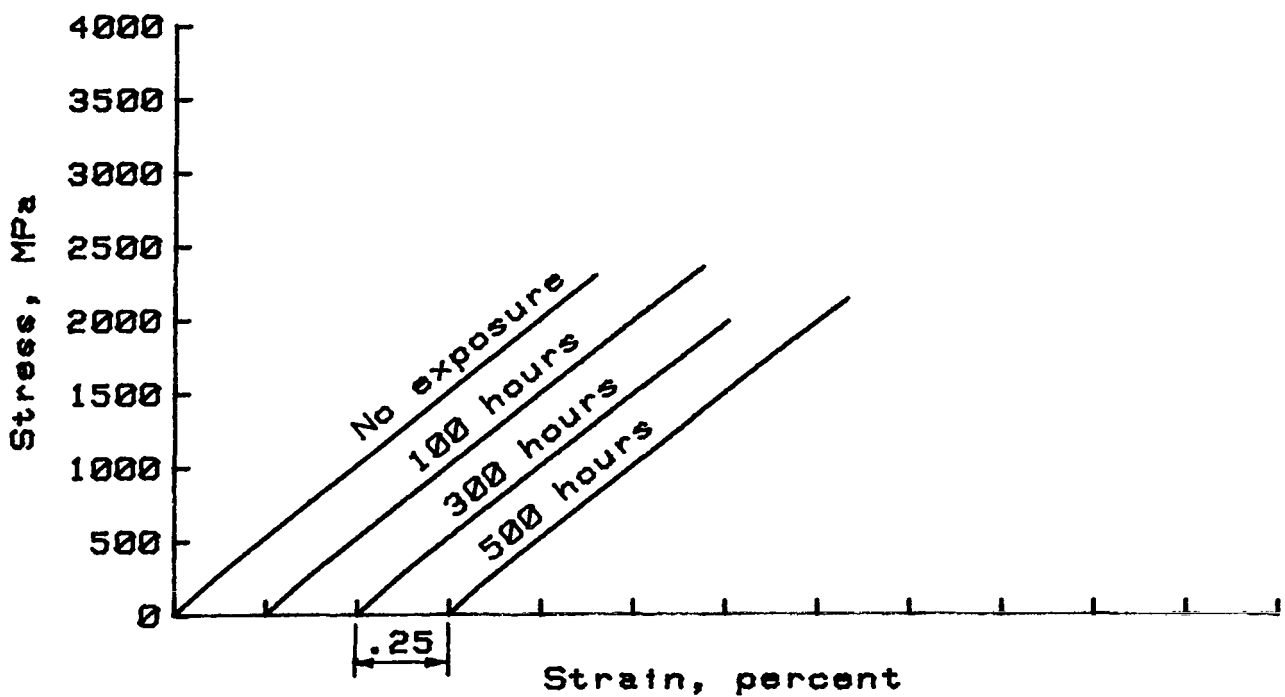
(a) Longitudinal tensile.



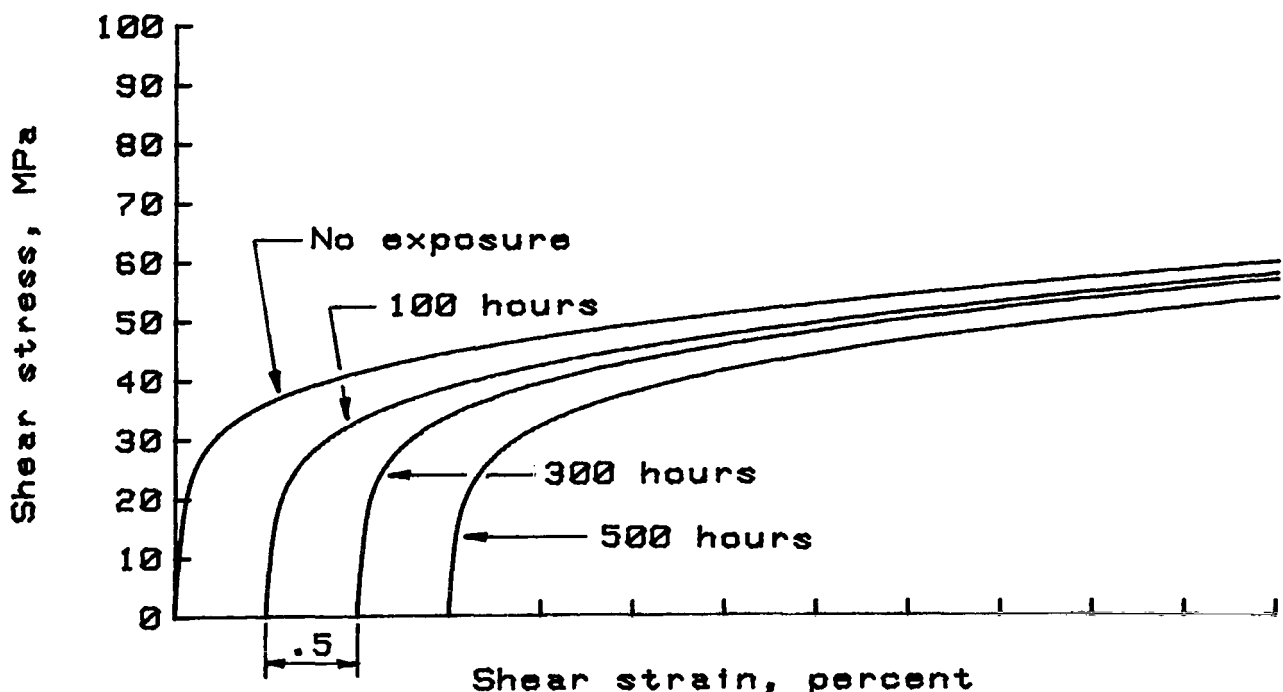
(b) Transverse tensile.

Figure D1.- Typical room-temperature stress-strain curves for B/1100 Al composite material exposed at 730 K.

APPENDIX D

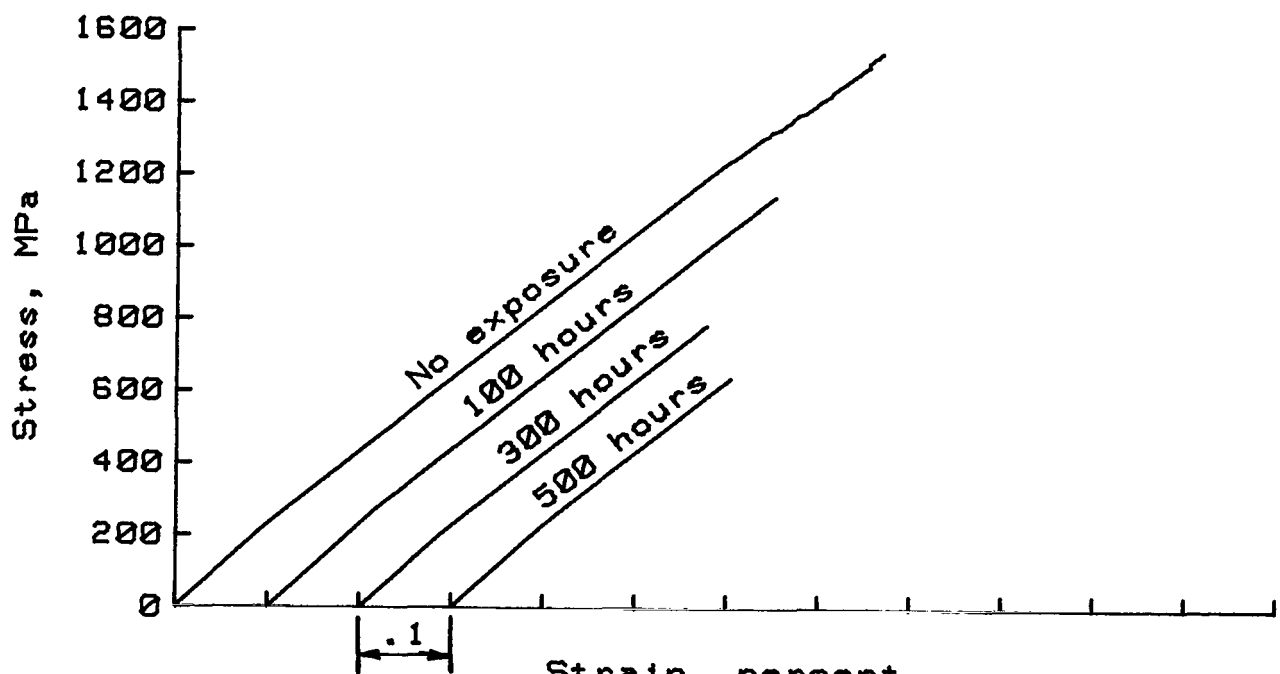


(c) Longitudinal compression.

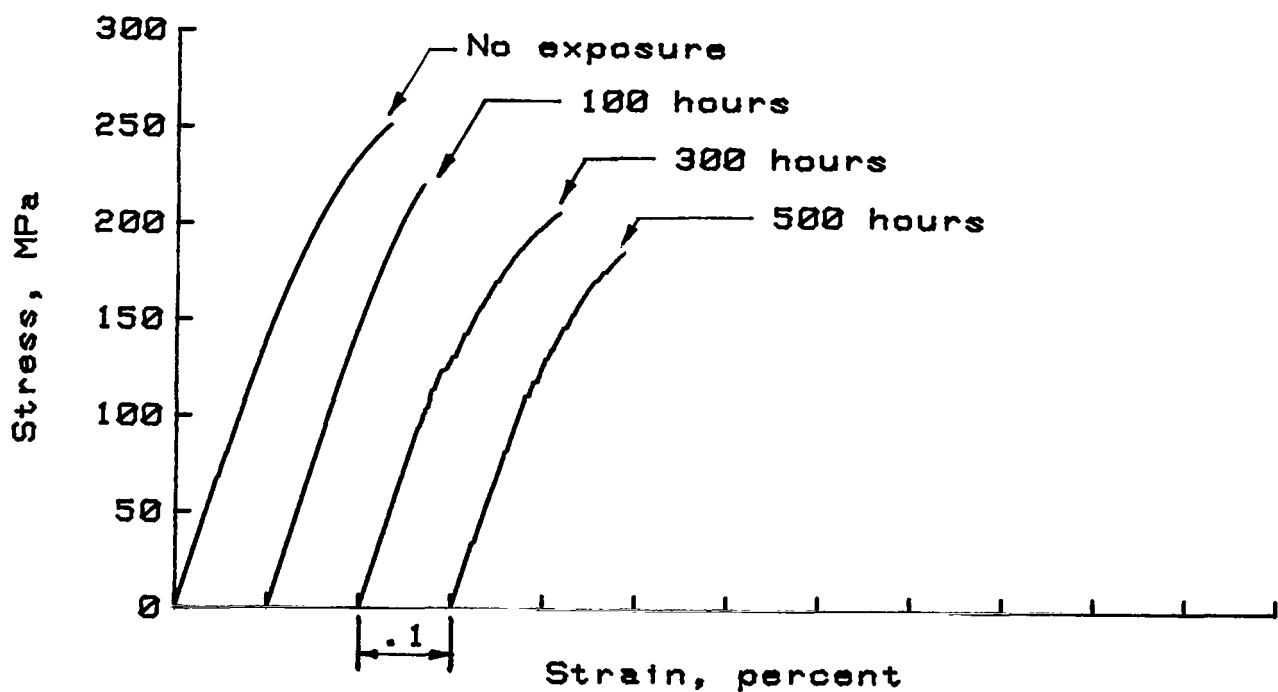


(d) In-plane shear.

Figure D1.- Concluded.



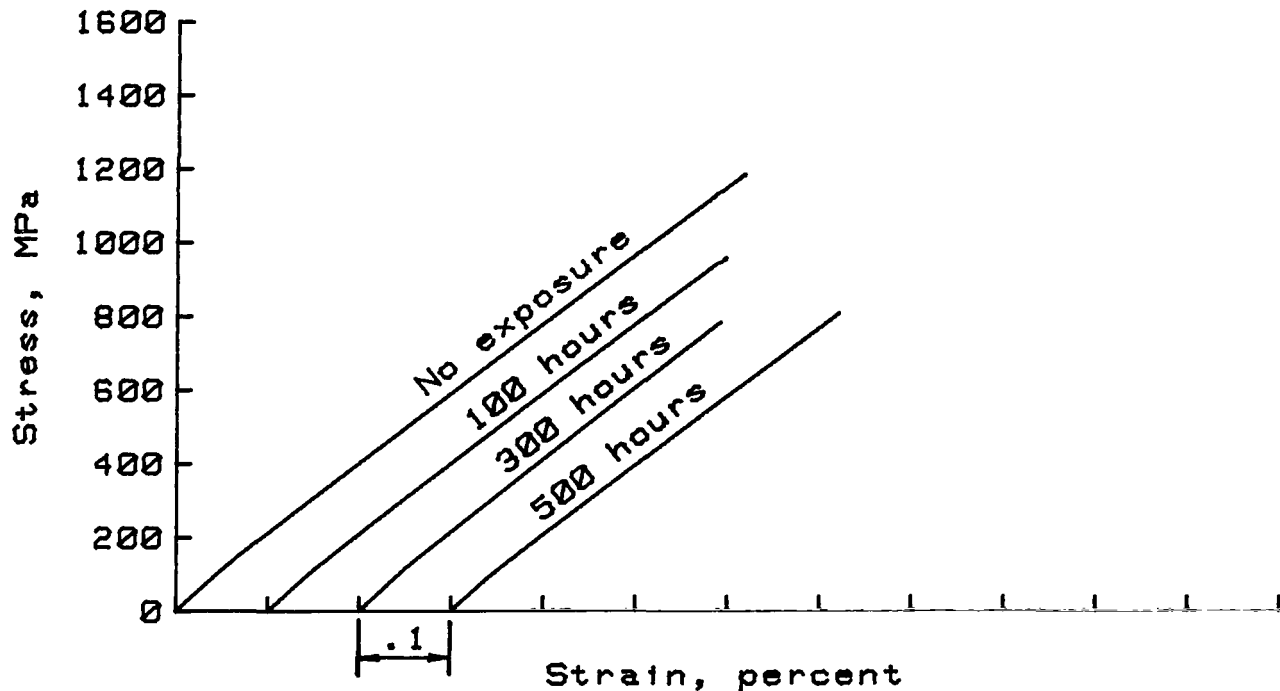
(a) Longitudinal tensile.



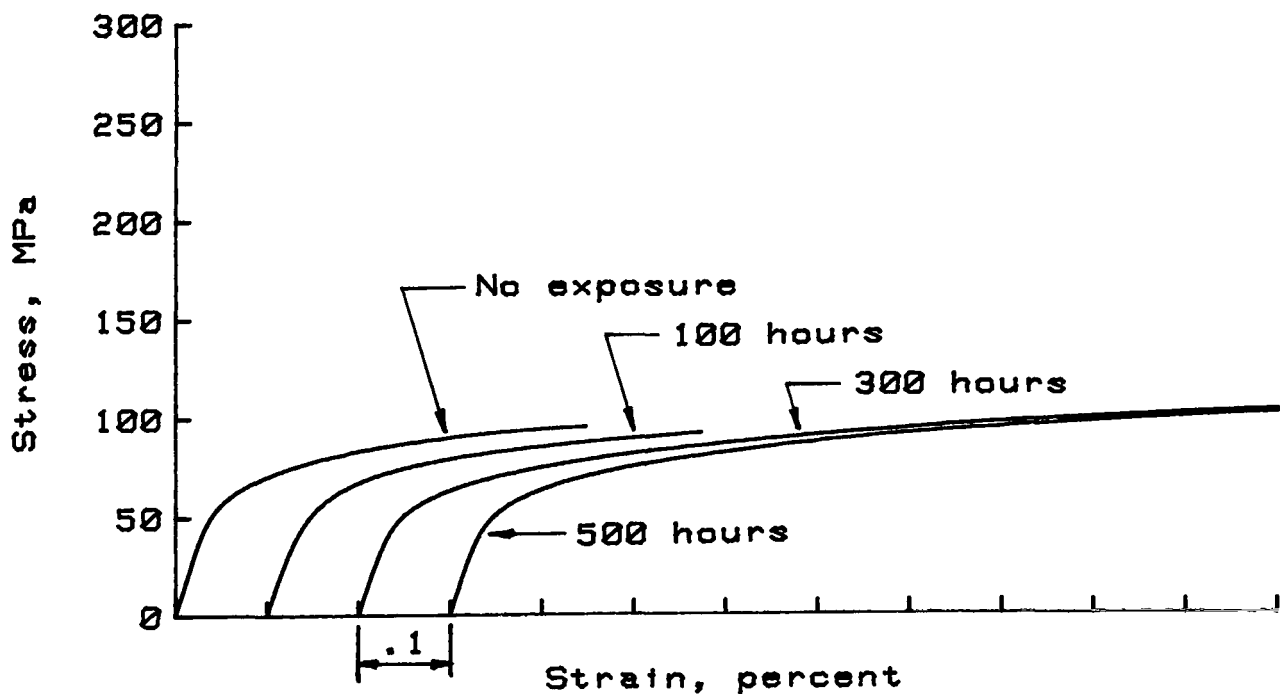
(b) Transverse tensile.

Figure D2.- Typical room-temperature stress-strain curves for B/2024 Al composite material exposed at 730 K.

APPENDIX D

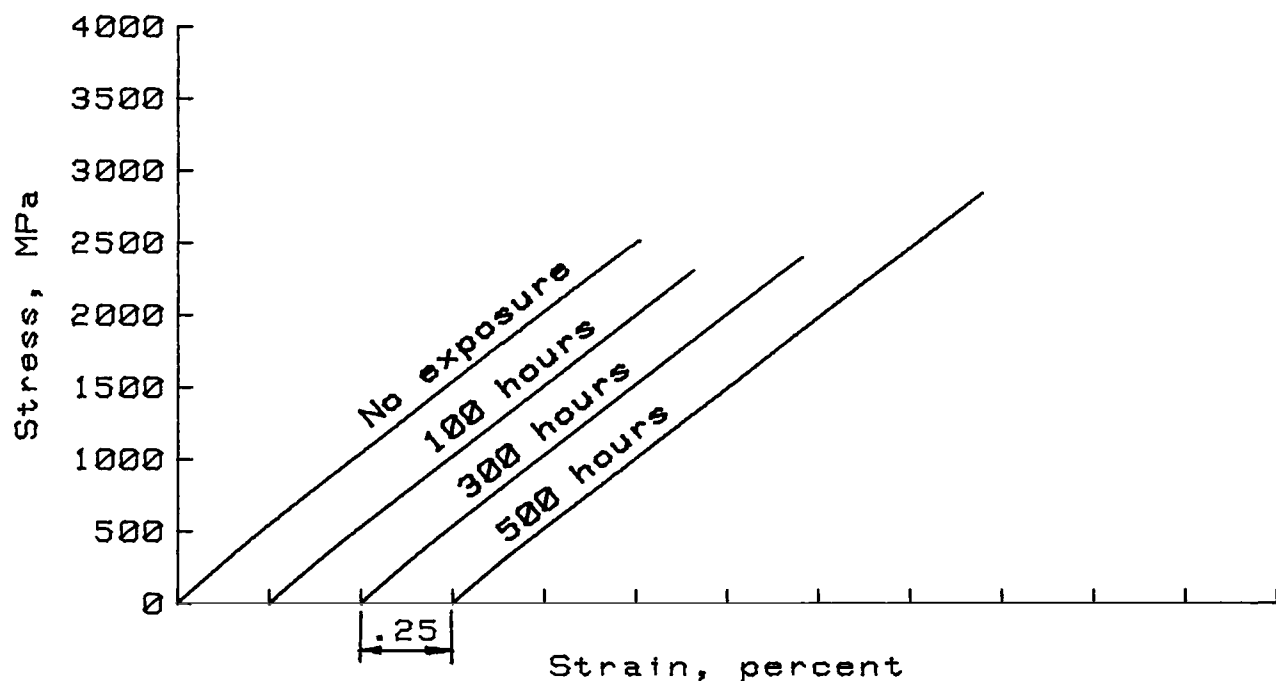


(a) Longitudinal tensile.

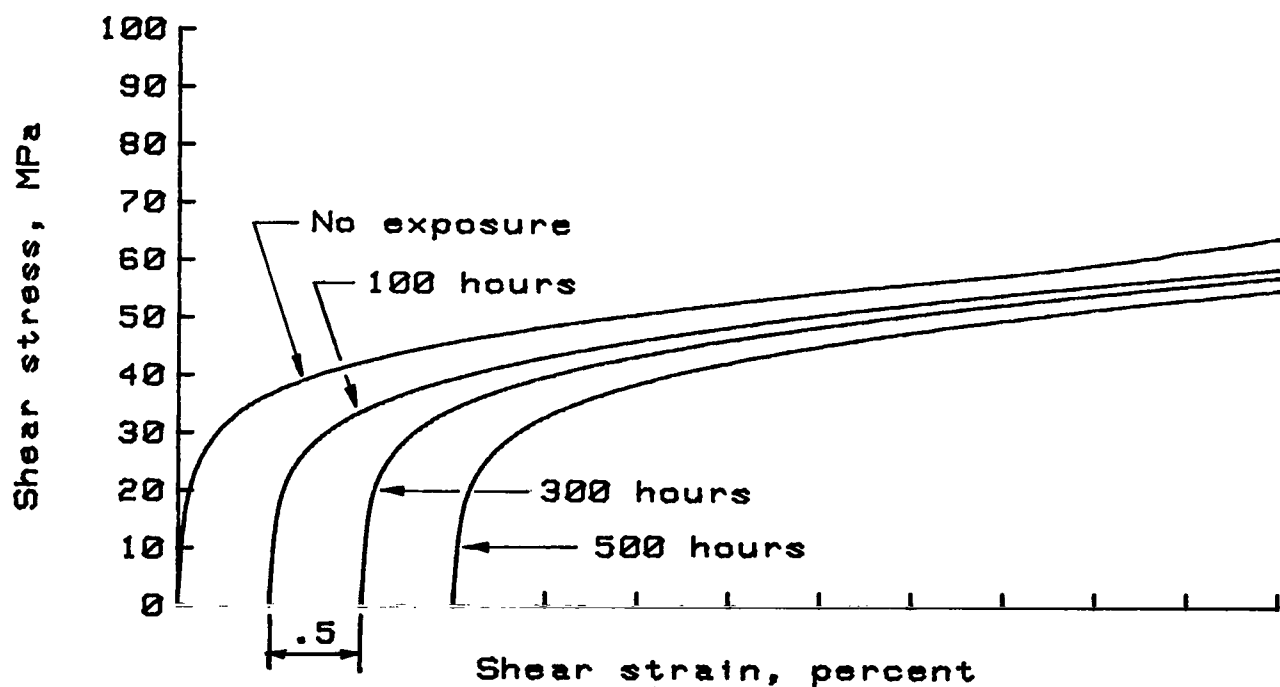


(b) Transverse tensile.

Figure D3.- Typical room-temperature stress-strain curves for B/3003 Al composite material exposed at 730 K.

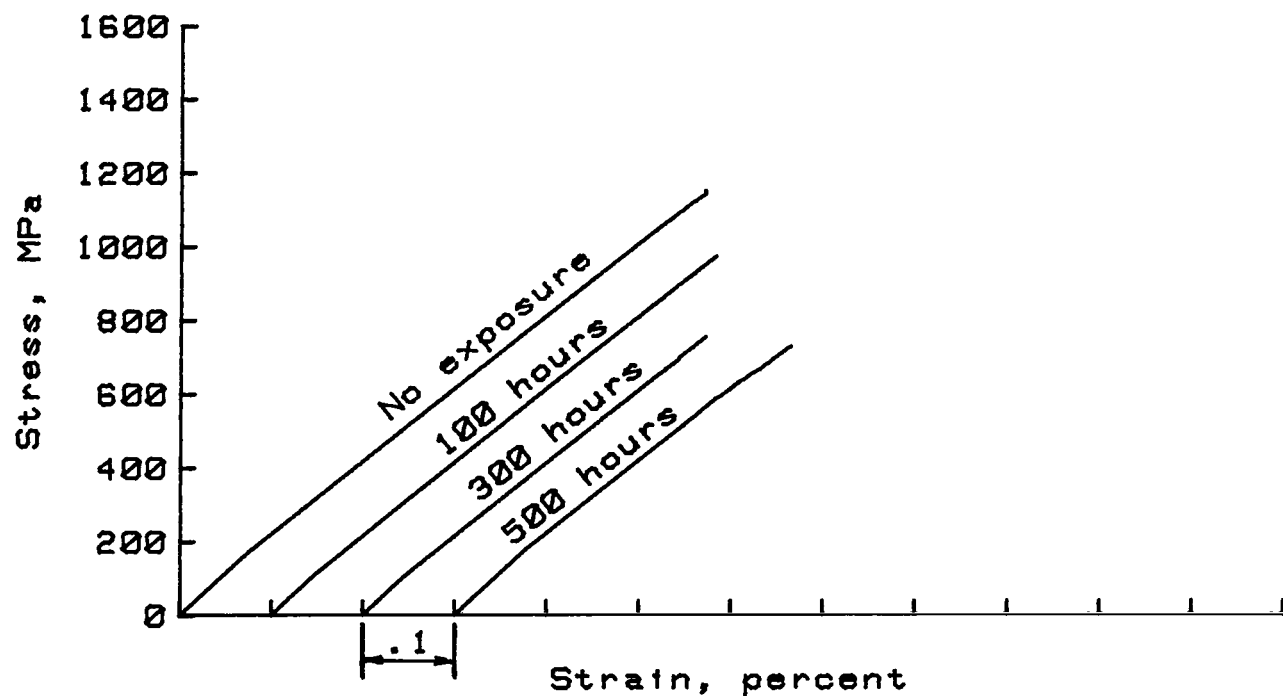


(c) Longitudinal compression.

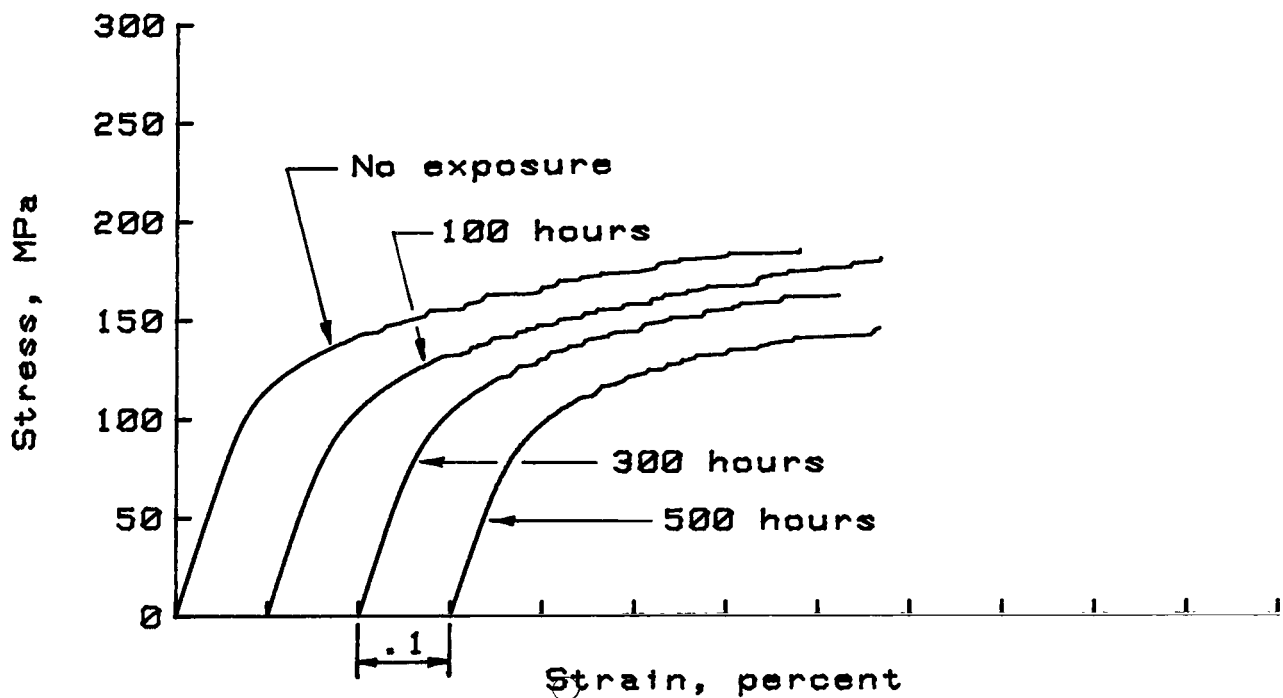


(d) In-plane shear.

Figure D3.- Concluded.

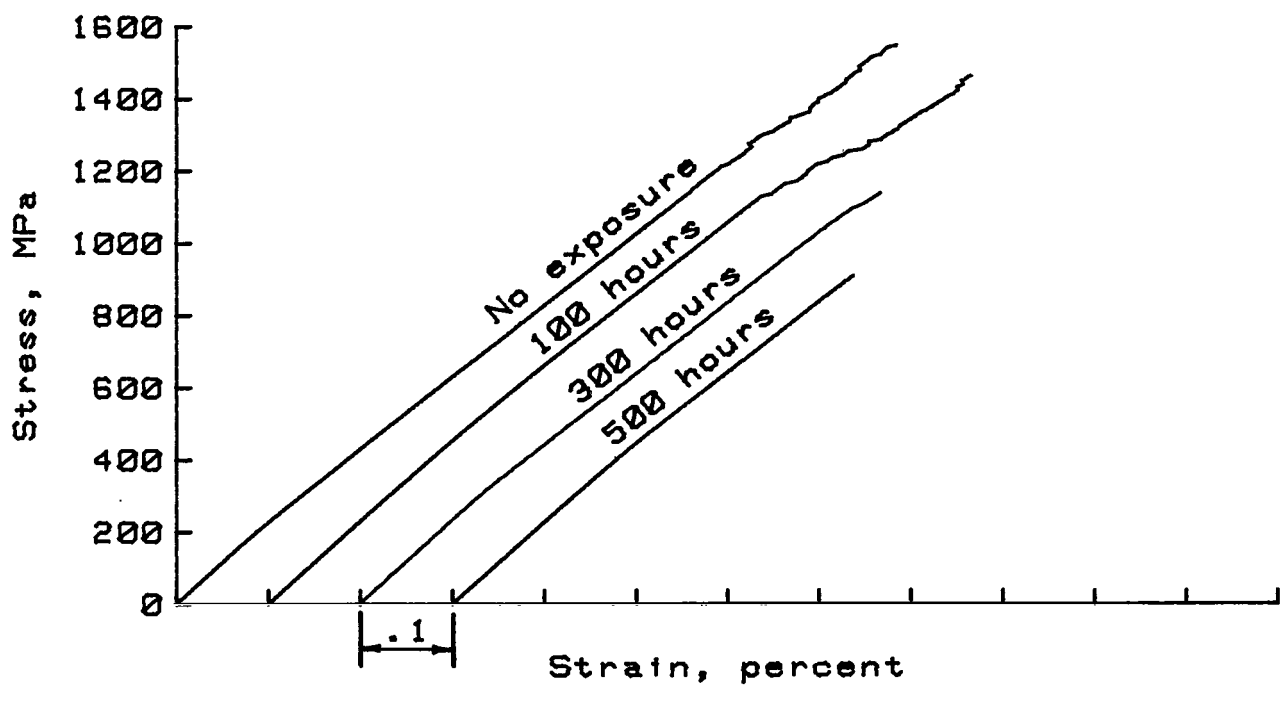


(a) Longitudinal tensile.

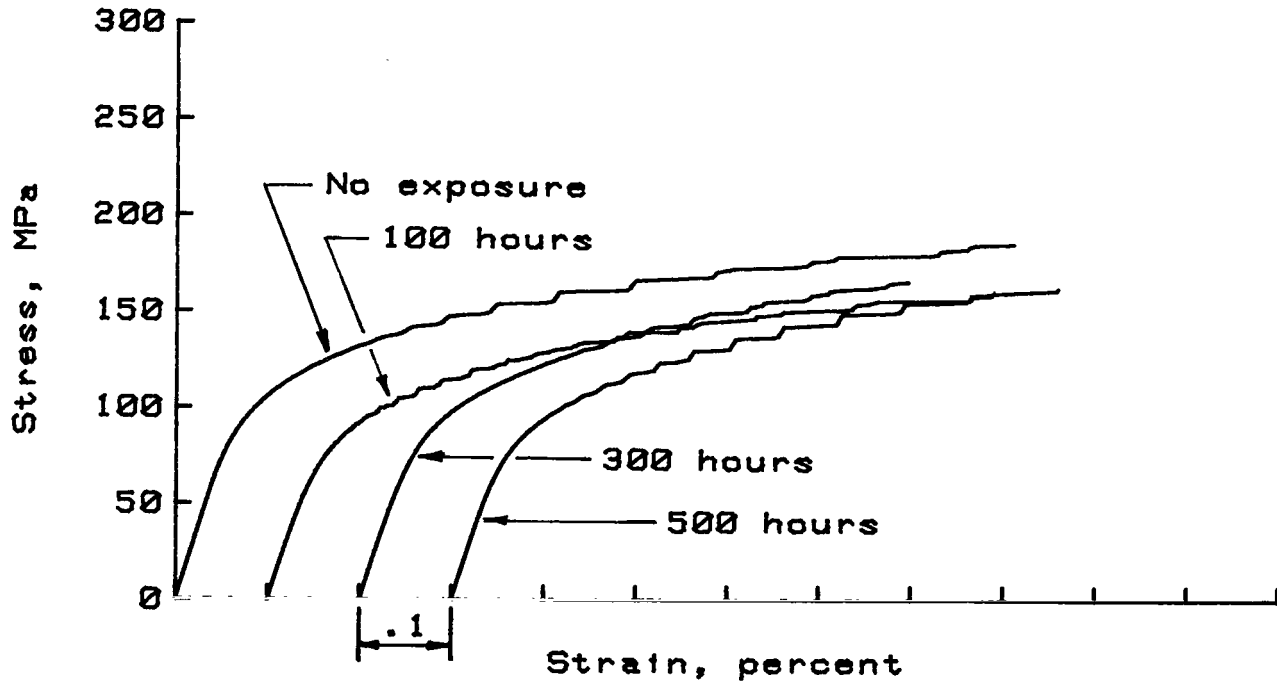


(b) Transverse tensile.

Figure D4.- Typical room-temperature stress-strain curves for B/5052 Al composite material exposed at 730 K.



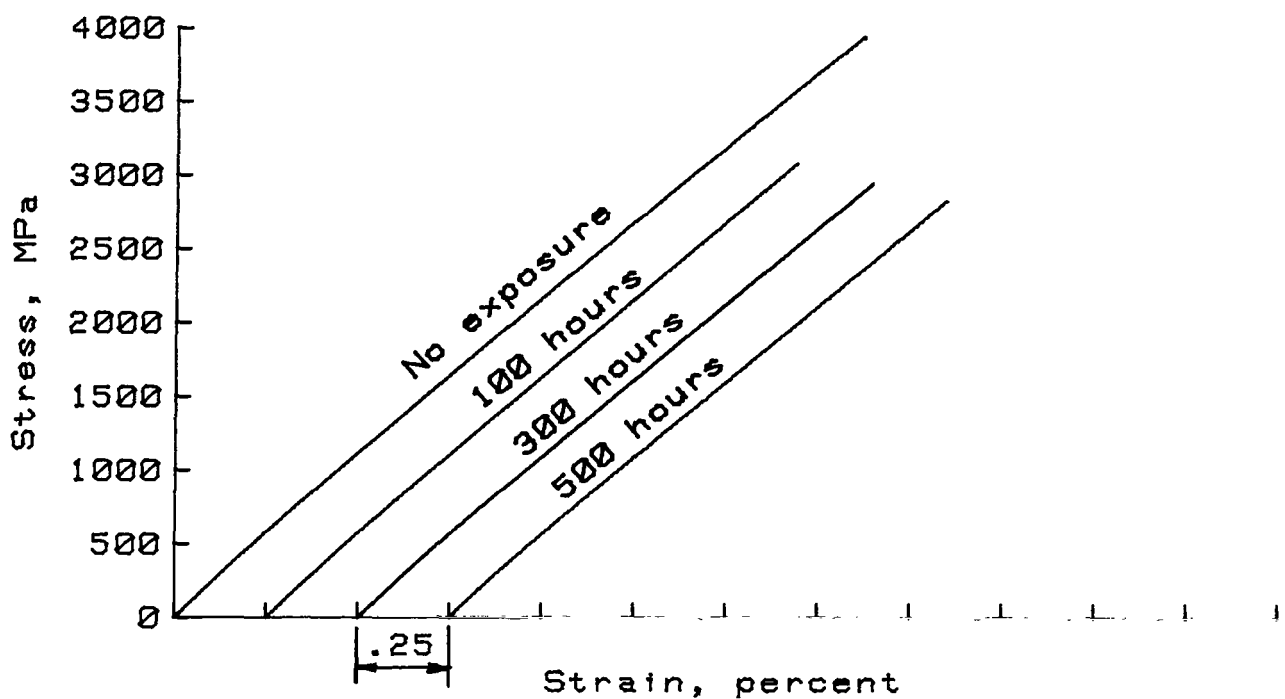
(a) Longitudinal tensile.



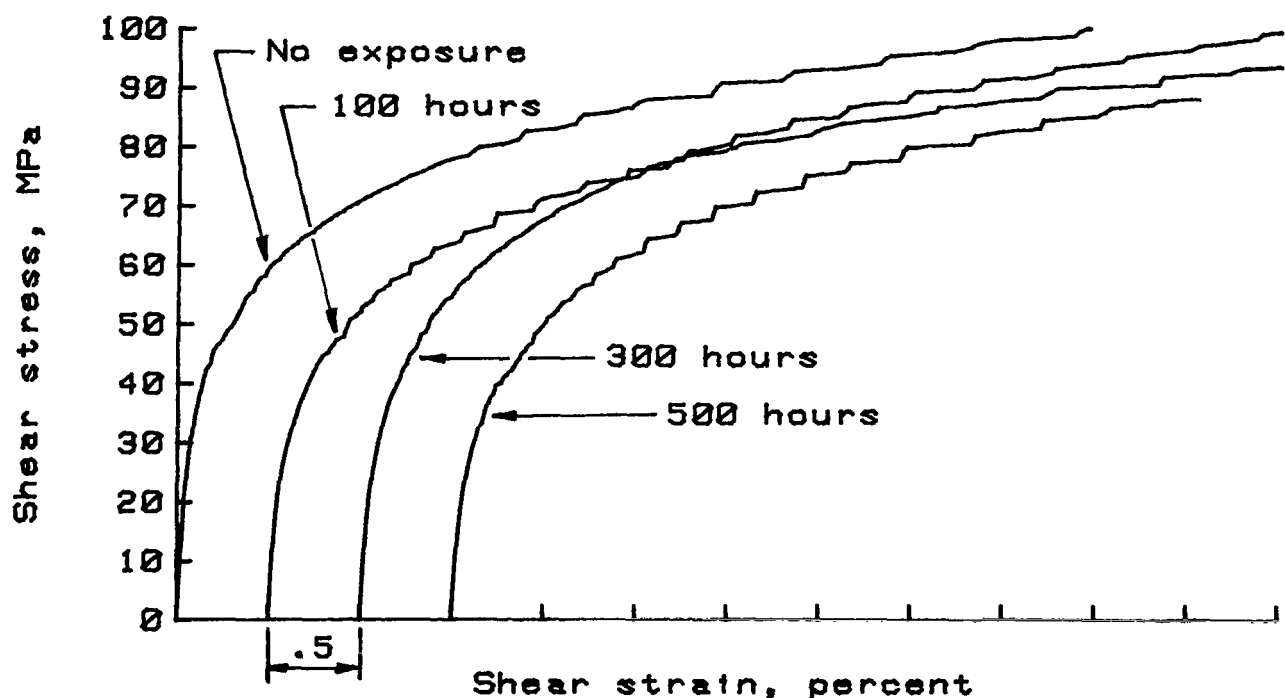
(b) Transverse tensile.

Figure D5.- Typical room-temperature stress-strain curves for B/6061 Al composite material exposed at 730 K.

## APPENDIX D



(c) Longitudinal compression.



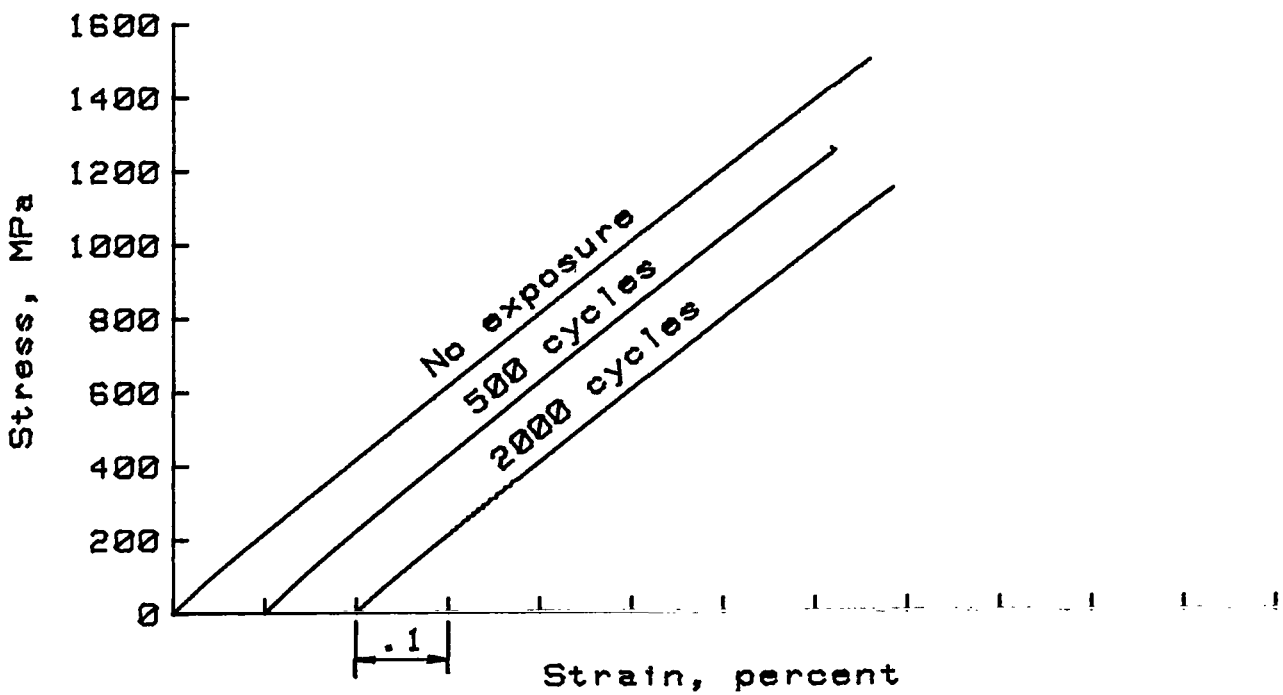
(d) In-plane shear.

Figure D5.- Concluded.

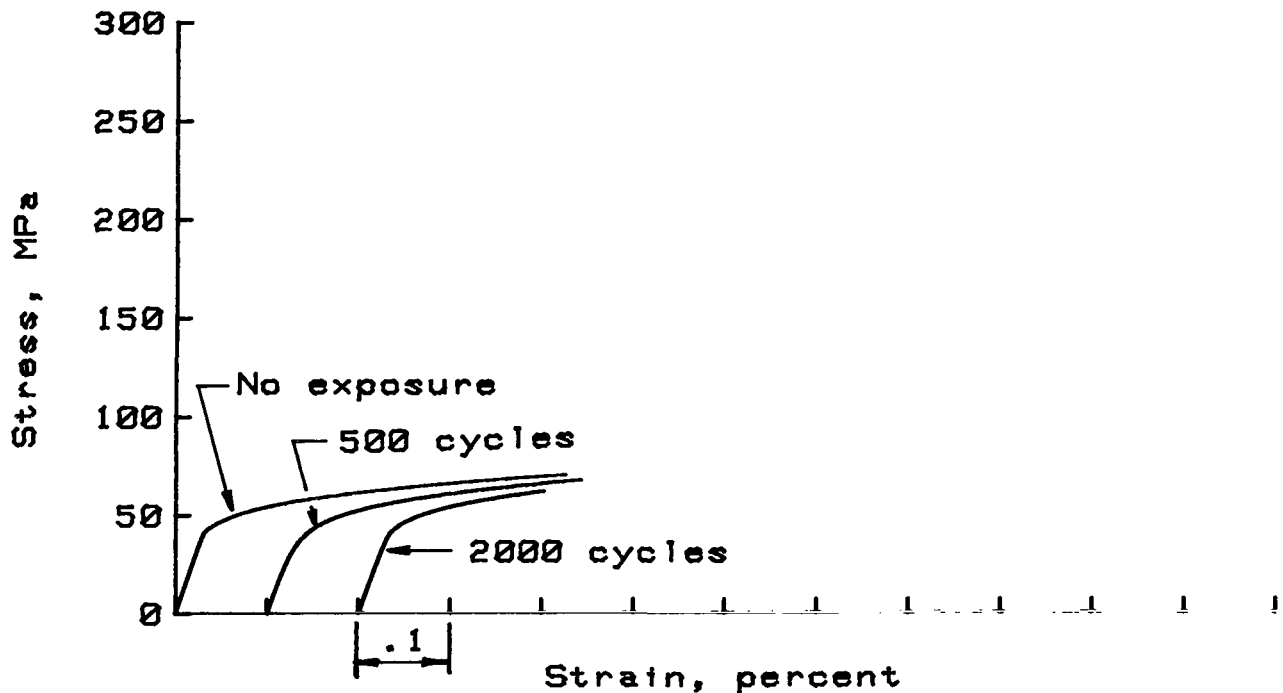
## APPENDIX E

### SPECIMENS THERMALLY CYCLED UP TO 2000 CYCLES BETWEEN 200 K AND 590 K

The mechanical property data for all the B/Al composite tests conducted in this investigation are given in tables V through IX. Typical stress-strain curves for the specimens thermally cycled up to 2000 cycles between 200 K and 590 K and tested at room temperature are presented in appendix E.



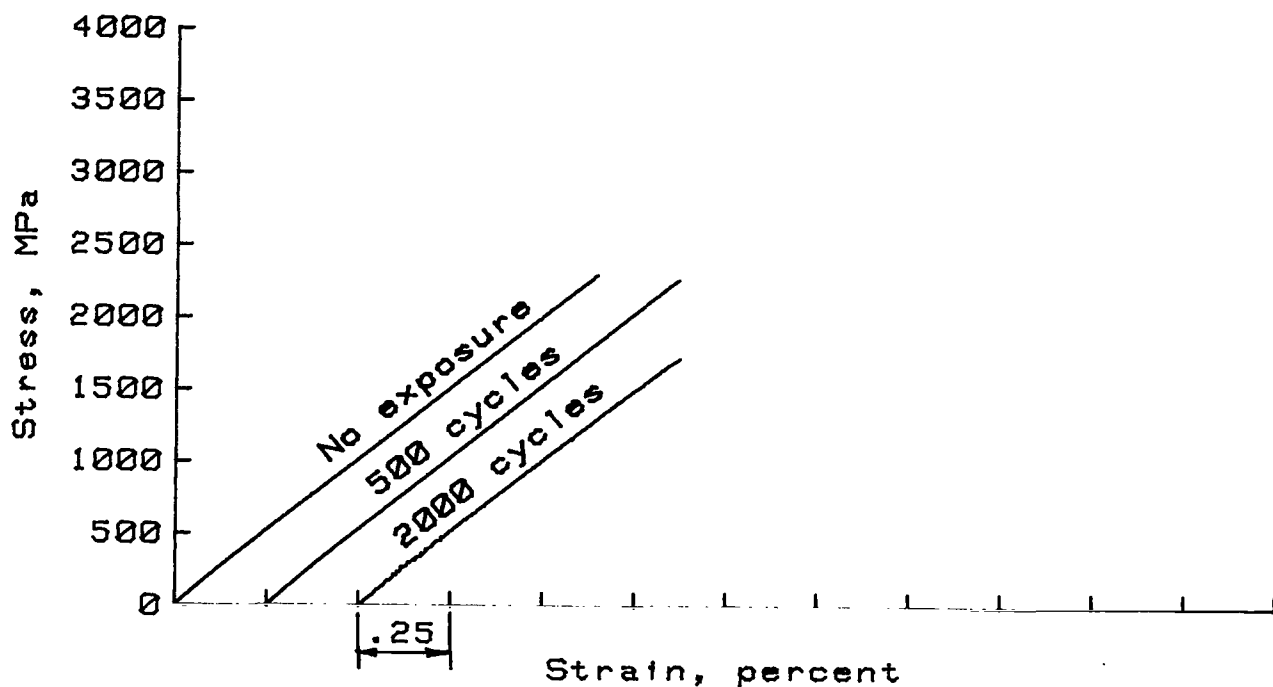
(a) Longitudinal tensile.



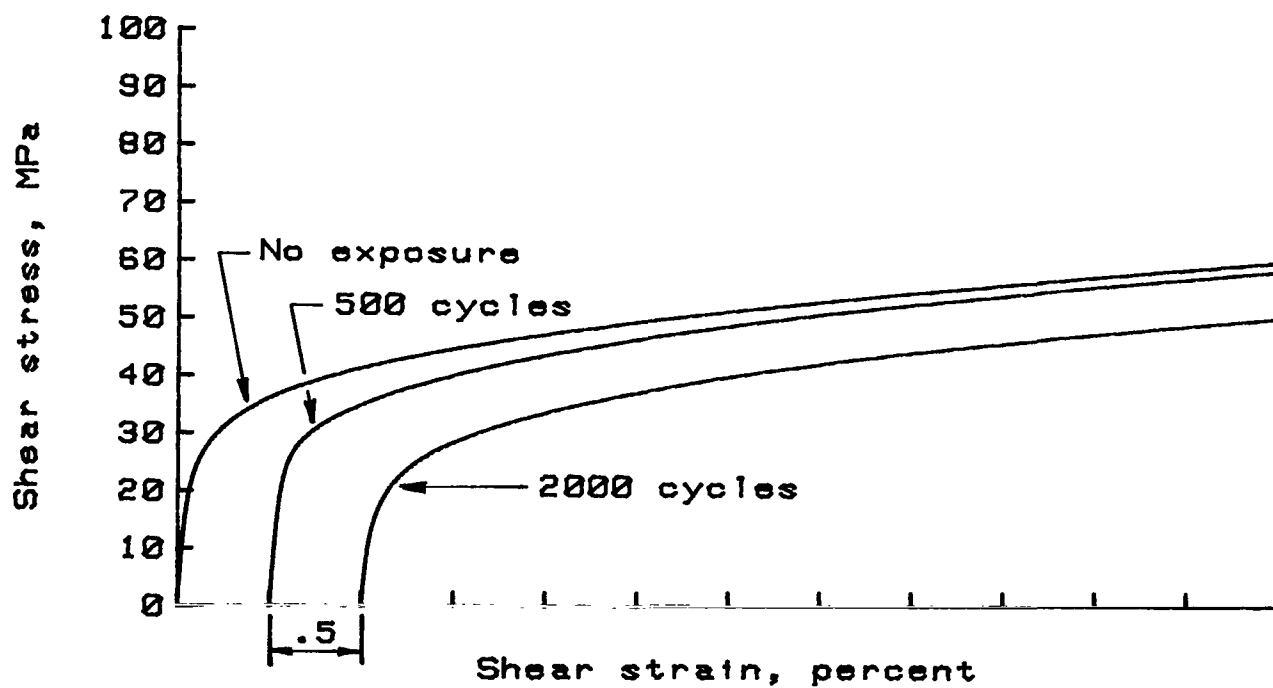
(b) Transverse tensile.

Figure E1.- Typical room-temperature stress-strain curves for B/1100 Al composite material thermally cycled between 200 K and 590 K.

APPENDIX E



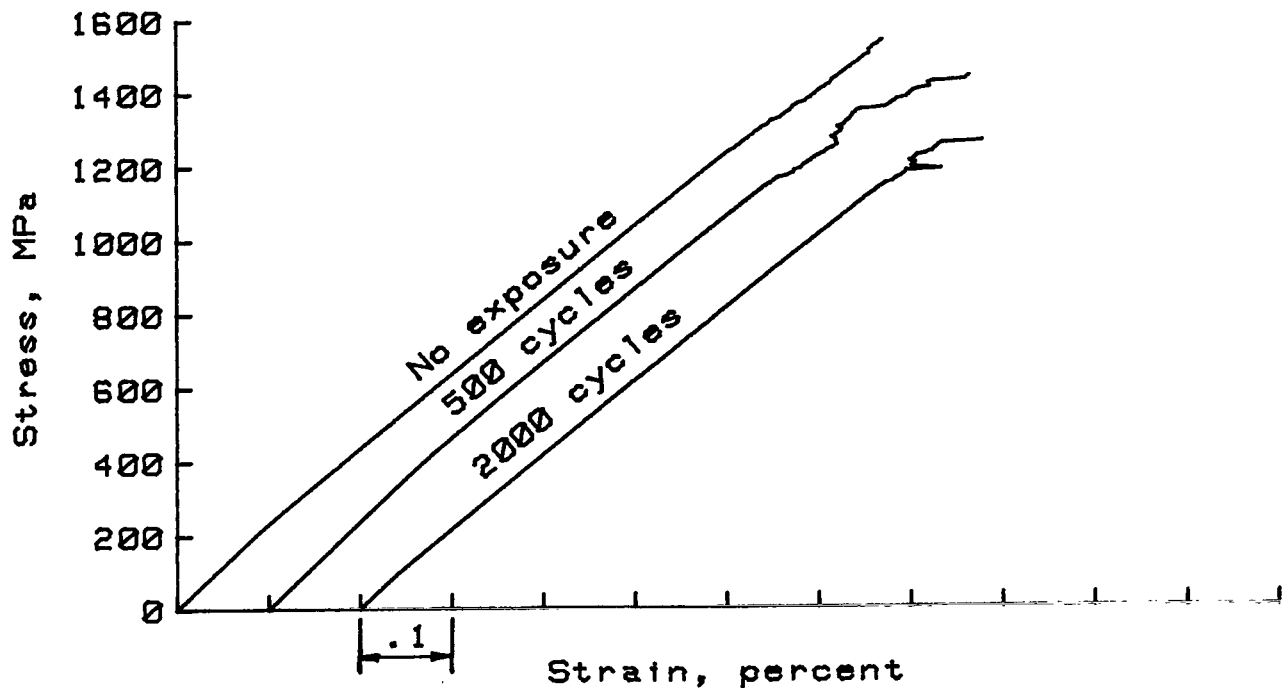
(c) Longitudinal compression.



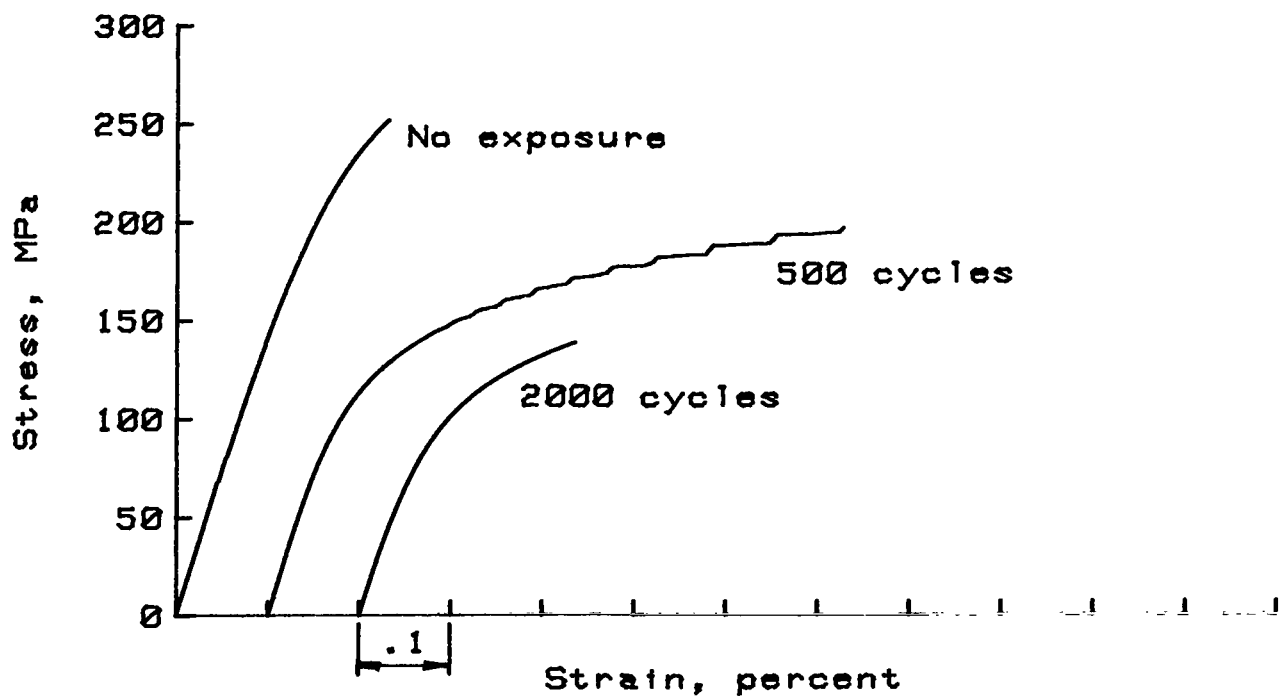
(d) In-plane shear.

Figure E1.- Concluded.

APPENDIX E

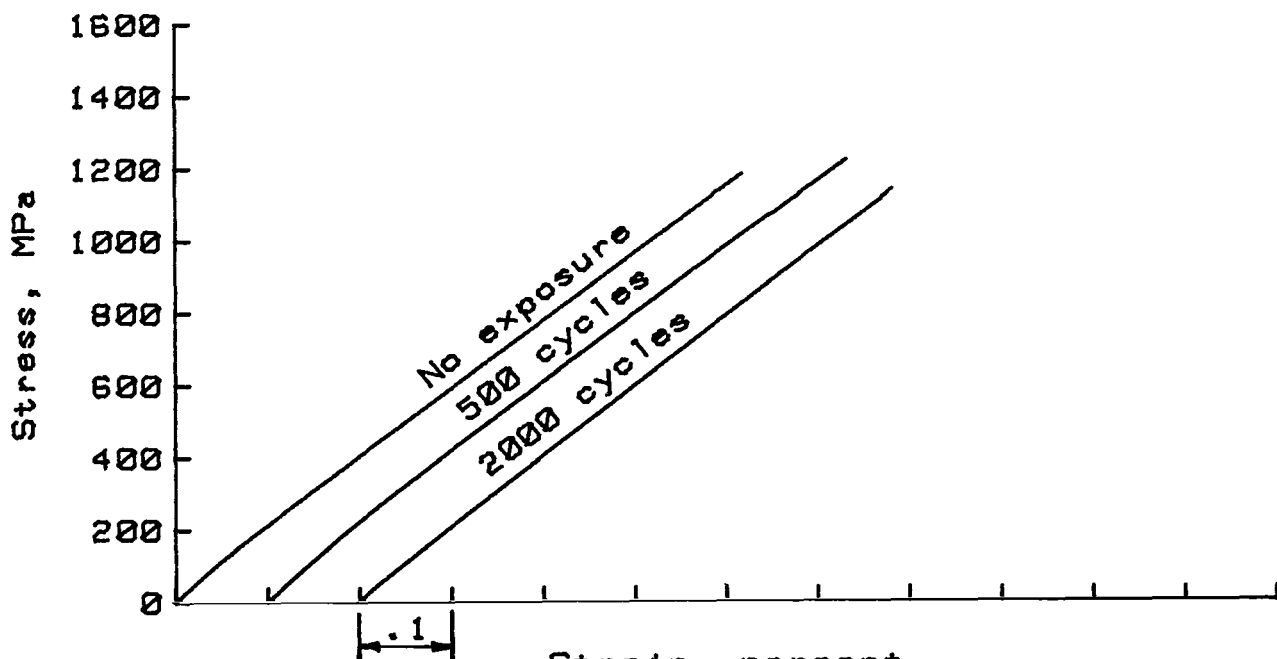


(a) Longitudinal tensile.

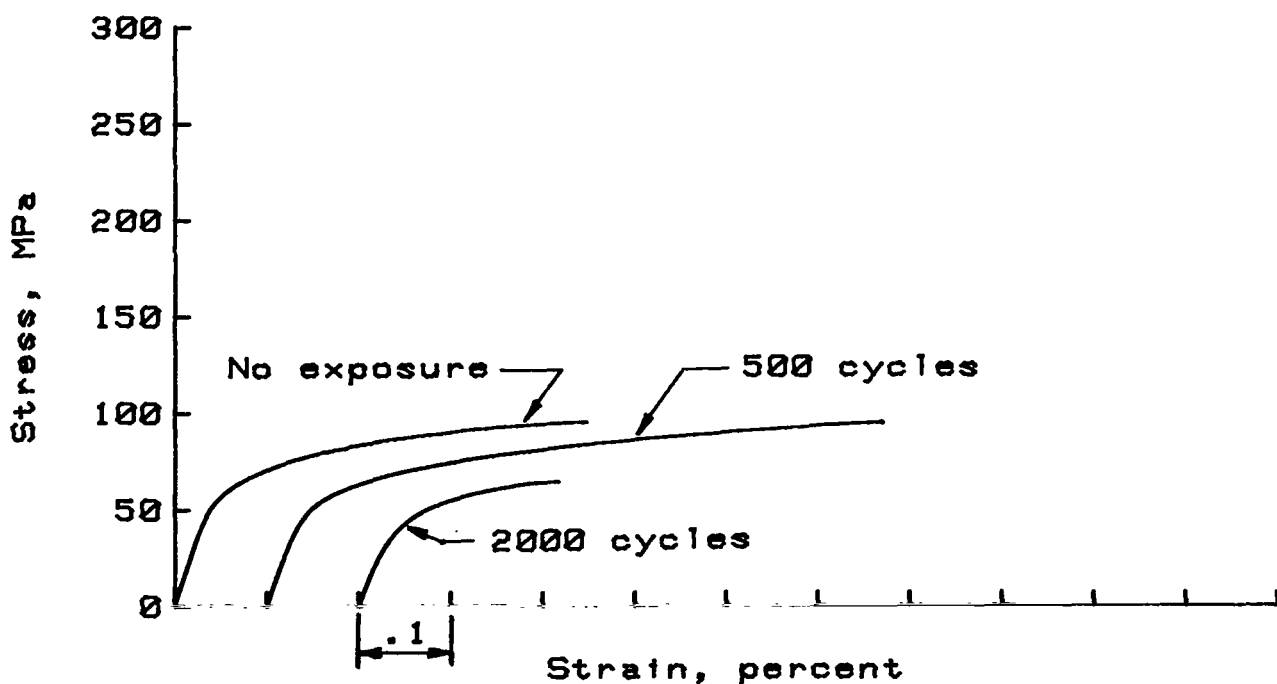


(b) Transverse tensile.

Figure E2.- Typical room-temperature stress-strain curves for B/2024 Al composite material thermally cycled between 200 K and 590 K.



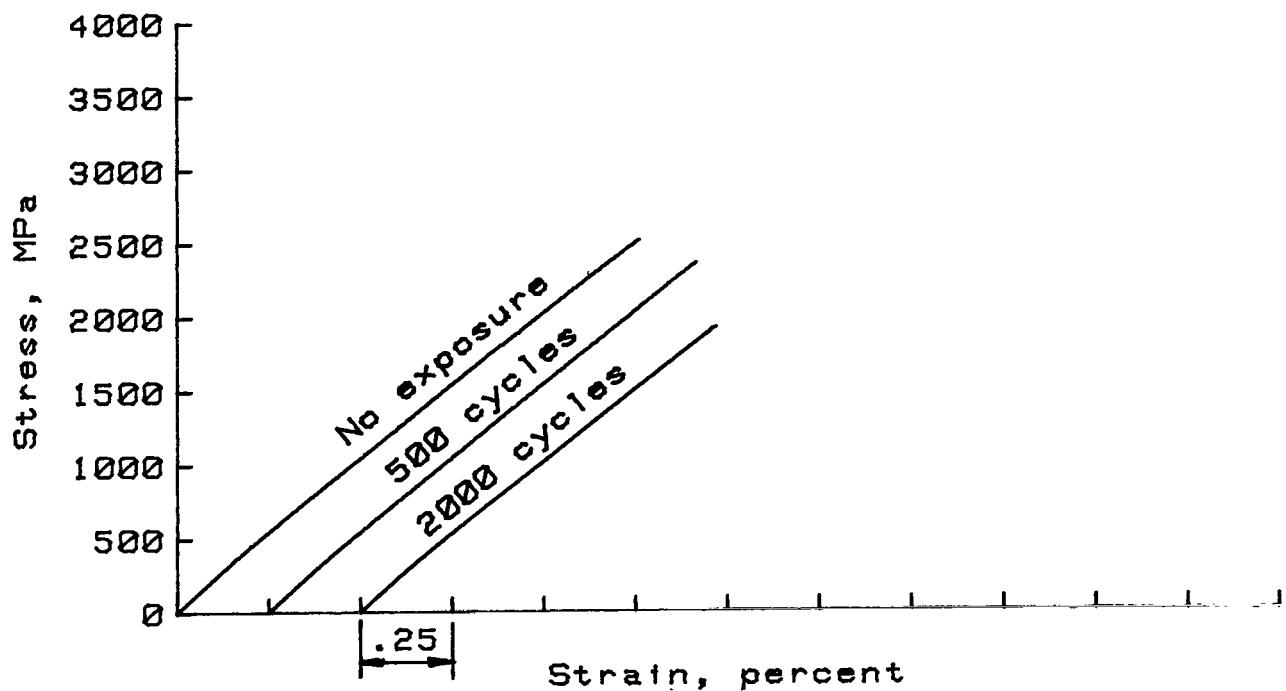
(a) Longitudinal tensile.



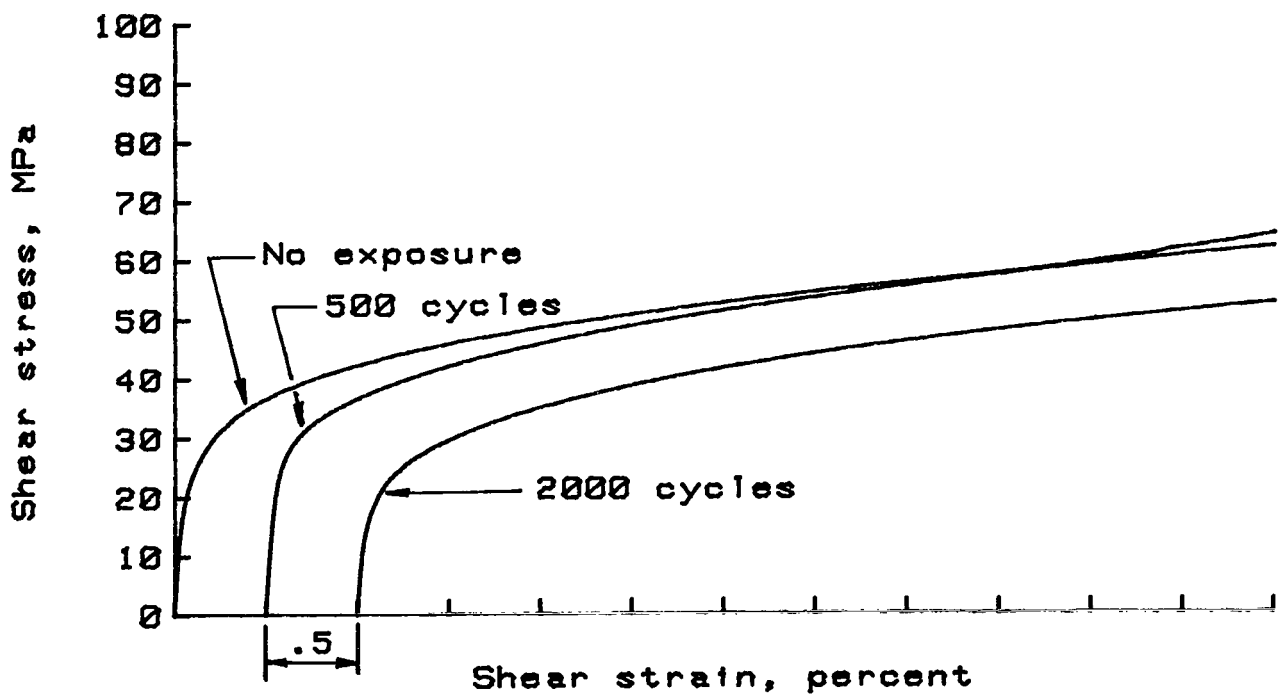
(b) Transverse tensile.

Figure E3.- Typical room-temperature stress-strain curves for B/3003 Al composite material thermally cycled between 200 K and 590 K.

APPENDIX E



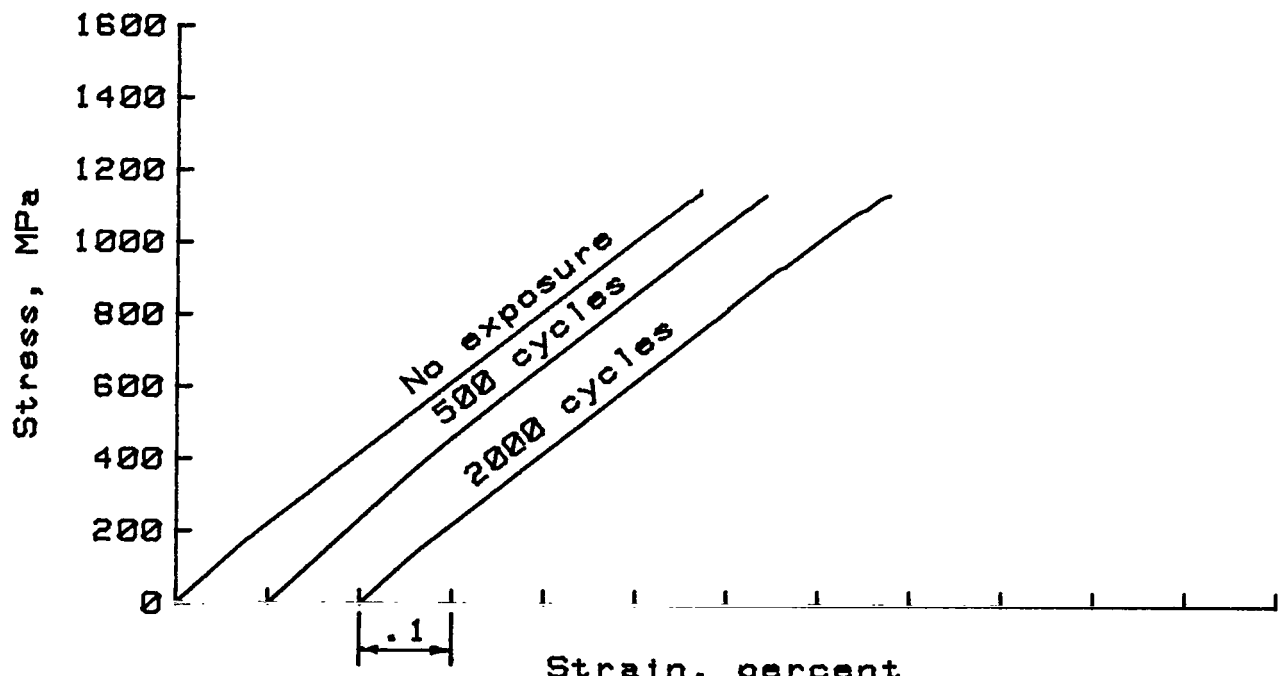
(c) Longitudinal compression.



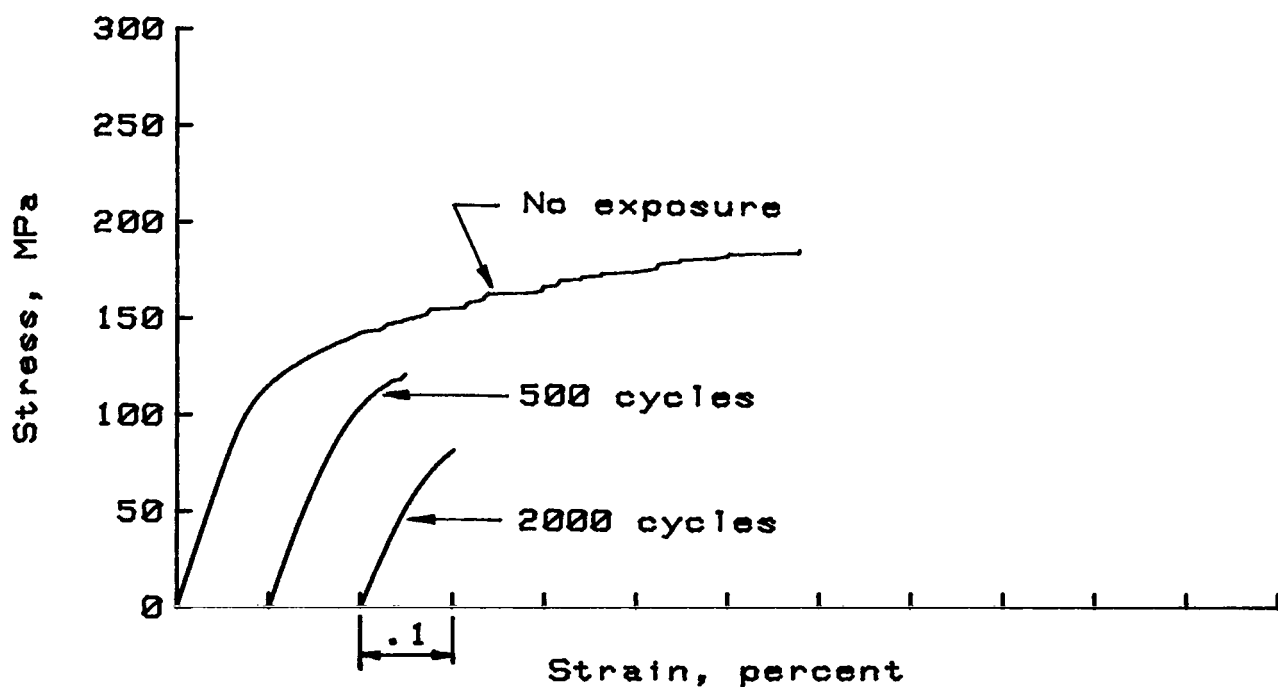
(d) In-plane shear.

Figure E3.- Concluded.

APPENDIX E



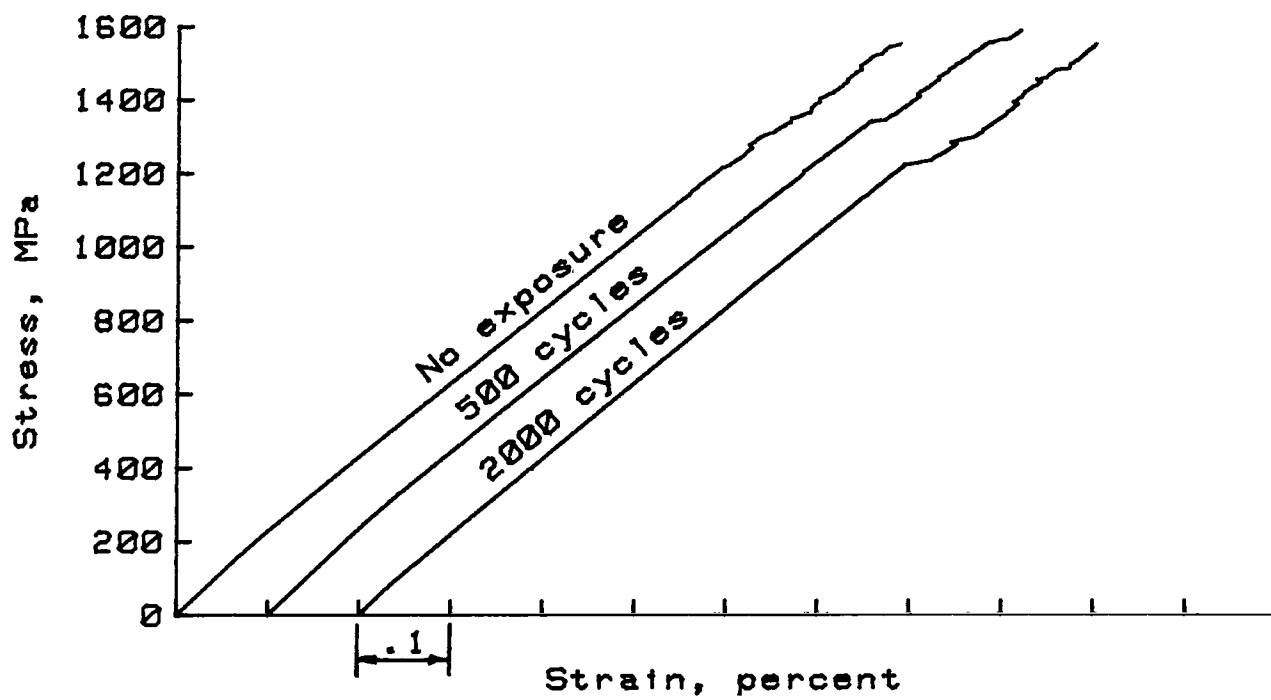
(a) Longitudinal tensile.



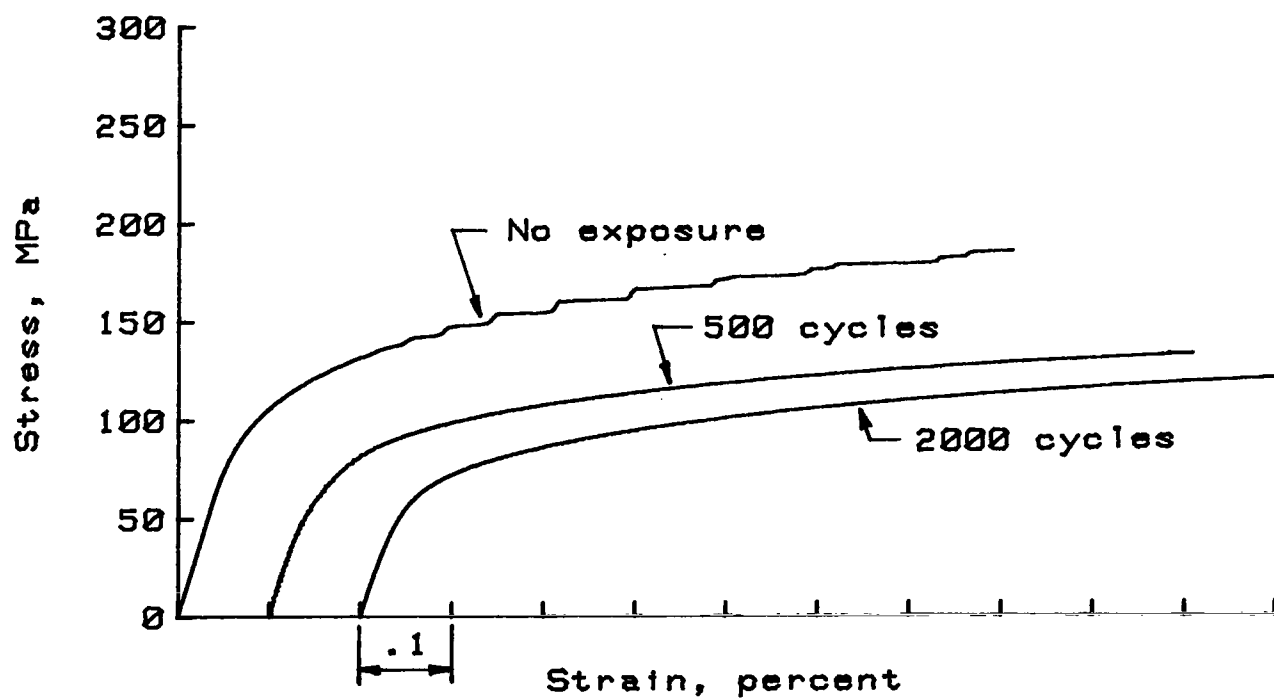
(b) Transverse tensile.

Figure E4.- Typical room-temperature stress-strain curves for B/5052 Al composite material thermally cycled between 200 K and 590 K.

APPENDIX E



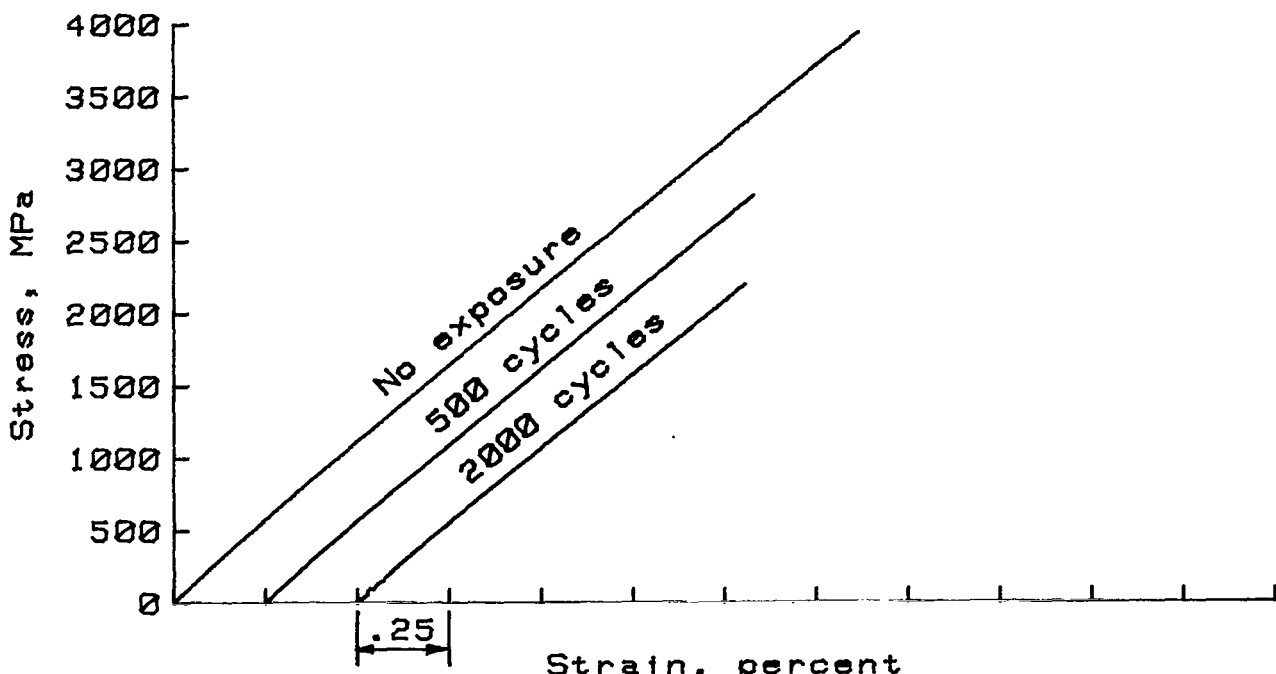
(a) Longitudinal tensile.



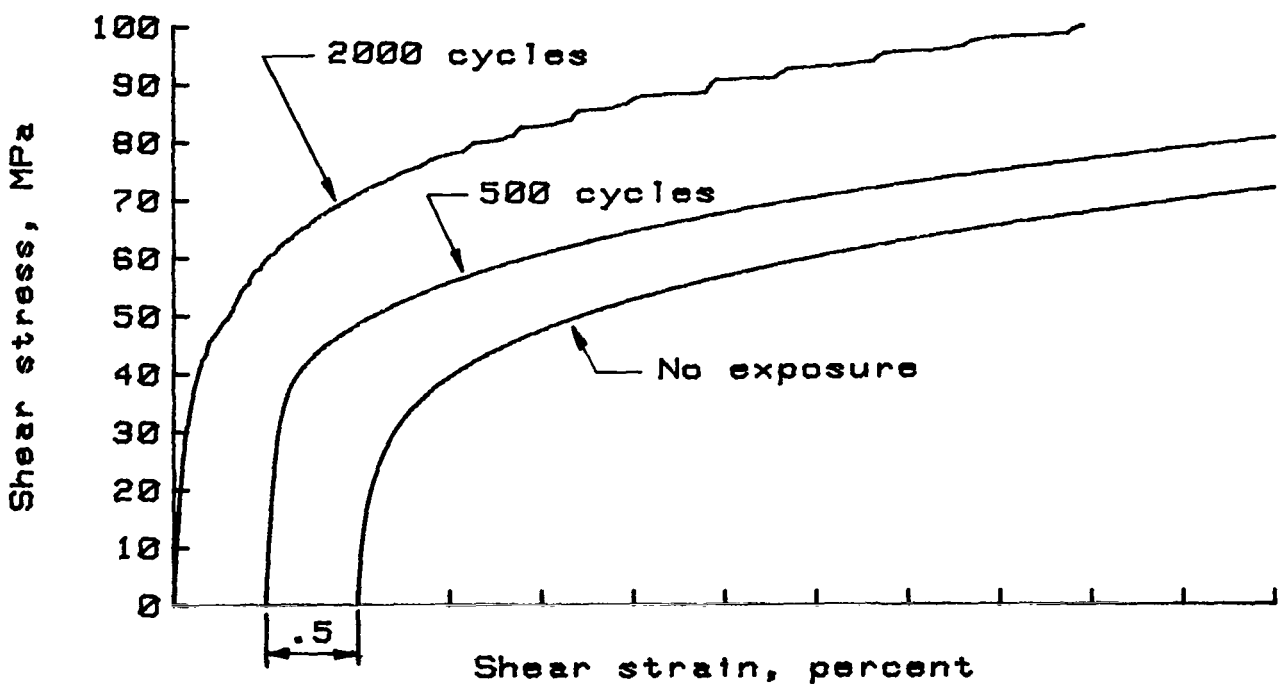
(b) Transverse tensile.

Figure E5.- Typical room-temperature stress-strain curves for B/6061 Al composite material thermally cycled between 200 K and 590 K.

APPENDIX E



(c) Longitudinal compression.



(d) In-plane shear.

Figure E5.- Concluded.

#### REFERENCES

1. Krukonis, V.: I. Chemical Vapor Deposition of Boron Filament. *Boron and Refractory Borides*, V. I. Matkovich, ed., Springer-Verlag, 1977, pp. 517-540.
2. Kreider, Kenneth G.; and Prewo, K. M.: *Boron-Reinforced Aluminum. Metallic Matrix Composites*, Kenneth G. Kreider, ed., Academic Press, Inc., 1974, pp. 399-471.
3. Toth, I. J.; Brentnall, W. D.; and Menke, G. D.: A Survey of Aluminum Matrix Composites. *Composites: State of the Art*, J. W. Weeton and E. Scala, eds., Metall. Soc. AIME, c.1974, pp. 139-207.
4. Lynch, C. T.; and Kershaw, J. P.: *Metal Matrix Composites*. CRC Press, c.1972.
5. Kerr, J. R.; and Haskins, J. F.: Time-Temperature-Stress Capabilities of Composite Materials for Advanced Supersonic Technology Application - Phase I. NASA CR-159267, 1980.
6. Metcalfe, Arthur G.; and Klein, Mark J.: Effect of the Interface on Longitudinal Tensile Properties. *Interfaces in Metal Matrix Composites*, Arthur G. Metcalfe, ed., Academic Press, Inc., 1974, pp. 125-168.
7. Olsen, George C.; and Tompkins, Stephen S.: Effects of Continuous and Cyclic Thermal Exposures on Boron- and Borsic-Reinforced 6061 Aluminum Composites. NASA TP-1063, 1977.
8. Olsen, George C.; and Tompkins, Stephen S.: Continuous and Cyclic Thermal Exposure Induced Degradation in Boron Reinforced 6061 Aluminum Composites. *Failure Modes in Composites IV*, James A. Cornie and Frank W. Crossman, eds., Metall. Soc. AIME, c.1979, pp. 1-21.
9. Shahinian, P.: Thermal Fatigue of Aluminum-Boron Composites. *SAMPE Q.*, vol. 2, no. 1, Oct. 1970, pp. 28-35.
10. Wright, M. A.: The Effect of Thermal Cycling on the Mechanical Properties of Various Aluminum Alloys Reinforced With Unidirectional Boron Fibers. *Metall. Trans.*, vol. 6A, no. 1, Jan. 1975, pp. 129-134.
11. Van Horn, Kent R., ed.: *Aluminum. Volume I. Properties, Physical Metallurgy and Phase Diagrams*. American Soc. Metals, c.1967.
12. Clark, Ronald K.; and Lisagor, W. Barry: Effects of Method of Loading and Specimen Configuration on Compressive Strength of Graphite/Epoxy Composite Materials. NASA TM-81796, 1980.
13. Popov, E. P.: *Mechanics of Materials*. Prentice-Hall Inc., c.1952.
14. Mondolfo, L. F.: *Aluminum Alloys: Structure and Properties*. Butterworth Pub., Inc., 1976.
15. Mettertiers, Earl L.: *The Chemistry of Boron and Its Compounds*. John Wiley & Sons, Inc., c.1967.

16. Thompson, Raymond: The Chemistry of Metal Borides and Related Compounds. Progress in Boron Chemistry, Volume 2, R. J. Brotherton and H. Steinberg, eds., Pergamon Press, Inc., c.1970, pp. 173-230.
17. Dardi, Louis E.; and Kreider, Kenneth G.: Thermal Cycling in Boron-Aluminum Composites. New Horizons in Materials and Processing, Volume 16 of National SAMPE Symposium and Exhibition Soc. Advance. Mater. & Process Eng., Apr. 1973, pp. 125-139.
18. Moorjani, K.; and Feldman, C.: V. Amorphous Boron Films. Boron and Refractory Borides, V. I. Matkovich, ed., Springer-Verlag, 1977, pp. 581-596.
19. Greenwood, N. N.; Parish, R. V.; and Thornton, P.: Metal Borides Q. Rev. (London), vol. 20, no. 3, 1966, pp. 441-464.
20. Hoover, William R.: The Critical Energy Release Rate as a Failure Criterion for B/Al Composites. Failure Modes in Composites III, T. T. Chiao and D. M. Schuster, eds., Metall. Soc. AIME, c.1976, pp. 304-318.
21. Makarenko, G. N.: VII. Borides in the IVb Group, Boron and Refractory Borides, V. I. Matkovich, ed., Springer-Verlag, 1977, pp. 310-330.
22. Gurin, V. N.; and Korsukova, M. M.: VI. Ib and IIb Subgroup Borides. Boron and Refractory Borides, V. I. Matkovich, ed., Springer-Verlag, 1977, pp. 293-309.
23. Perry, A. J.; Nicoll, A. R.; Phillips, K.; and Sahm, P. R.: The Copper-Boron Eutectic - Unidirectionally Solidified. J. Mater. Sci., vol. 8, 1973, pp. 1340-1348.
24. Carlsson, J.-O.; and Lundström, T.: The Solution Hardening of Beta-Rhombohedral Boron. J. Less-Common Met., vol. 22, no. 3, Nov. 1970, pp. 317-320.
25. Chaban, N. F.; and Kuz'ma, Yu. B.: The Ternary Systems Chromium-Aluminum-Boron and Manganese-Aluminum-Boron. Izv. Akad. Nauk SSSR, Neorg. Mater., vol. 9, no. 11, Nov. 1973, pp. 1908-1911.

TABLE I.- ALUMINUM-ALLOY COMPOSITIONS AND ROOM-TEMPERATURE STRENGTHS

Alloy - Temper (Classification)	Nominal Composition, Volume Percent	Ultimate Tensile Strength, MPa	
		Original Temper	Annealed
1100 - H19 (Non-heat-treatable)	99.0 Al (min.) 1.0 impurities <sup>a</sup> (max.)	207	76
2024 - T81 (Heat-treatable)	91.9 Al (min.) 4.5 Cu 0.6 Mn 1.5 Mg 1.5 impurities <sup>a</sup> (max.)	448	186
3003 - H19 (Non-heat-treatable)	97.0 Al (min.) 1.2 Mn 1.8 impurities <sup>a</sup> (max.)	248	110
5052 - H19 (Non-heat-treatable)	96.4 Al (min.) 0.1 Cu 0.1 Mn 2.5 Mg 1.0 impurities <sup>a</sup> (max.)	331	193
6061 - T81 (Heat-treatable)	96.4 Al (min.) 0.6 Si 0.3 Cu 1.0 Mg 0.2 Cr 1.5 impurities <sup>a</sup> (max.)	379	124

<sup>a</sup>Impurities normally are Fe and Si with traces of Ti, Cr, Mn, Cu, and Zn.

TABLE II.- COMPOSITE DIFFUSION BONDING PARAMETERS

Composite System	Temperature, K	Pressure, MPa	Time, min
B/1100	820 to 840	31	40
B/2024	770 to 780	31	30
B/3003	820 to 840	31	40
B/5052	800 to 810	31	30
B/6061	800 to 805	31	30

TABLE III.- SPECIMEN CONFIGURATION

Test Type	Material Tested	Fiber Orientation	Nominal Specimen Dimensions, mm			
			Length	Width	Thickness	Gage Length
Longitudinal Tensile	B/1100 Al	0°	300	25.0	2.0	<sup>a</sup> 100
	B/2024 Al					
	B/3003 Al					
	B/5052 Al					
	B/6061 Al					
	1100 Al	Not Applicable	300	25.0	1.0	<sup>a</sup> 100
	2024 Al					
	3003 Al					
	5052 Al					
	6061 Al					
Transverse Tensile	B/1100 Al	90°	130	25.0	2.0	<sup>a</sup> 50
	B/2024 Al					
	B/3003 Al					
	B/5052 Al					
	B/6061 Al					
Longitudinal Compression	B/1100 Al	0°	150	12.5	2.0	12
	B/3003 Al					
	B/6061 Al					
In-Plane Shear	B/1100 Al	+45°	150	25.0	2.0	<sup>a</sup> 50
	B/3003 Al					
	B/6061 Al					

<sup>a</sup>Distance between grips.

TABLE IV.- MECHANICAL PROPERTY TESTS

Test	Fiber Orientation	Test Standard	Properties Reported (a)	Load Rate, N/sec
Composite Longitudinal Tensile	0°	ASTM D-3552	$\sigma_{1t}$ $E_1$	110
Composite Transverse Tensile	90°	ASTM D-3552	$\sigma_{tt}$ $E_2$	90
Composite Longitudinal Compression	0°	b,c ASTM D-3410	$\sigma_{lc}$	75
Composite In-Plane Shear	+45°	b ASTM D-3518	$\tau_{12}$ $G_{12}$	90
Alloy Tensile	Not Applicable	d ASTM D-3552	$\sigma_t$	15

a $\sigma_{1t}$  - ultimate longitudinal tensile strength

$\sigma_{tt}$  - ultimate transverse tensile strength

$\sigma_{lc}$  - ultimate longitudinal compressive strength

$\sigma_t$  - ultimate tensile strength (alloy only)

$\tau_{12}$  - ultimate in-plane shear stress

$E_1$  - longitudinal elastic modulus

$E_2$  - transverse elastic modulus

$G_{12}$  - in-plane shear modulus

bResin matrix composite standard (no metal matrix standard established).

cIITRI modification of fixture used.

dTested in the same manner as composites.

TABLE V.- B/1100 Al COMPOSITE TENSILE, COMPRESSION, AND SHEAR PROPERTIES

Specimen History	Test Temp., K	Longitudinal Tensile		Transverse Tensile		Ultimate Compression Stress, MPa	Shear	
		Ultimate Stress, MPa	Elastic Modulus, GPa	Ultimate Stress, MPa	Elastic Modulus, GPa		Ultimate Stress, MPa	Elastic Modulus, GPa
As Fabricated	295	1495	231	67	138	2528	141	51
		1538	232	66	137	2294	134	53
		1310	226	70	133	1867	131	50
	500	1333	227	51	---	917	125	49
		1019	231	47	112	1169	134	46
		1284	224	50	118	1251	135	44
	590	1407	189	26	106	474	106	32
		1356	192	26	---	539	111	—
		1024	186	27	111	426	103	35
5000 Hours at 500 K	295	1248	226	79	130	—	—	—
		1194	222	57	124	—	—	—
		1190	224	47	136	—	—	—
10 000 Hours at 500 K	295	1054	223	82	124	—	—	—
		1076	222	61	137	—	—	—
		1261	219	58	136	—	—	—
2500 Hours at 590 K	295	1422	231	91	127	2796	163	54
		1162	226	66	137	2180	129	56
		1289	229	69	---	1949	132	—
5000 Hours at 590 K	295	1488	232	64	133	2407	130	55
		1242	228	68	130	1917	122	52
		1289	226	63	135	2021	131	56
7500 Hours at 590 K	295	1331	225	64	137	1529	125	54
		1120	226	74	131	1638	123	55
		1374	218	63	135	1724	126	54
10 000 Hours at 590 K	295	1334	225	61	139	1274	115	56
		1251	223	72	134	1469	117	52
		1379	218	52	133	1454	125	53
100 Hours at 730 K	295	1318	---	74	140	2169	115	54
		1305	222	76	141	1783	113	53
		1296	224	80	139	—	113	54
300 Hours at 730 K	295	951	223	93	136	2029	100	55
		912	228	85	130	1832	107	53
		968	231	92	132	1982	96	53
500 Hours at 730 K	295	613	230	87	130	2133	105	54
		590	229	77	134	1641	104	53
		824	228	66	132	2347	98	54
500 Cycles 200 K to 590 K	295	1151	233	71	132	2203	137	54
		1254	231	67	120	2234	130	55
		1470	228	45	128	2402	133	52
2000 Cycles 200 K to 590 K	295	1125	214	64	48	1717	110	48
		1030	215	62	127	—	118	49
		1174	216	38	114	1776	127	48

TABLE VI.- B/2024 Al COMPOSITE TENSILE PROPERTIES

Specimen History	Test Temp., K	Longitudinal		Transverse	
		Ultimate Stress, MPa	Elastic Modulus, GPa	Ultimate Stress, MPa	Elastic Modulus, GPa
As Fabricated	295	1537	234	196	149
		1440	236	256	154
		1592	233	251	153
	500	1534	238	177	141
		1439	235	186	136
		1454	233	179	138
	590	1464	212	85	119
		1194	---	86	125
		1389	202	83	111
5000 Hours at 500 K	295	----	---	156	161
		1331	233	159	152
		1369	231	159	152
10 000 Hours at 500 K	295	1369	218	173	151
		1395	227	166	150
		1387	218	175	143
2500 Hours at 590 K	295	1292	231	162	151
		1272	233	194	156
		1322	240	195	151
5000 Hours at 590 K	295	1289	231	182	151
		1279	236	182	149
		1350	239	194	152
7500 Hours at 590 K	295	1263	226	186	152
		1246	228	183	148
		1428	229	191	152
10 000 Hours at 590 K	295	1326	231	179	146
		1307	232	175	144
		1397	230	180	141
100 Hours at 730 K	295	1200	232	256	151
		950*	234	228	155
		1139	234	204	153
300 Hours at 730 K	295	849	234	214	149
		792	234	206	153
		748	234	186	153
500 Hours at 730 K	295	637	231	177	149
		580	232	186	151
		709	232	251	150
500 Cycles 200 K to 590 K	295	1519	230	196	137
		1408	235	201	140
		1437	233	196	145
2000 Cycles 200 K to 590 K	295	1264	227	134	144
		1230	234	138	142
		1324	229	166	146

\*Out-lying data point dropped in regression analysis.

TABLE VII.- B/3003 Al COMPOSITE TENSILE, COMPRESSION, AND SHEAR PROPERTIES

Specimen History	Test Temp., K	Longitudinal Tensile		Transverse Tensile		Ultimate Compression Stress, MPa	Shear	
		Ultimate Stress, MPa	Elastic Modulus, GPa	Ultimate Stress, MPa	Elastic Modulus, GPa		Ultimate Stress, MPa	Elastic Modulus, GPa
As Fabricated	295	1180	225	90	---	2519	134	56
		1214	223	74	140	2154	132	53
		1172	225	95	146	2899	142	55
	500	1149	223	43	116	824	136	45
		1221	221	54	---	928	129	52
		1149	228	55	---	992	128	42
	590	1217	189	35	---	794	112	37
		1199	177	37	100	698	114	—
		1202	183	47	96	864	108	38
5000 Hours at 500 K	295	1057	218	102	145	---	---	---
		---	---	78	---	---	---	---
		1087	219	84	147			
10 000 Hours at 500 K	295	1154	208	108	138	---	---	---
		1101	210	70	145	---	---	---
		1106	220	87	141			
2500 Hours at 590 K	295	1157	223	108	137	2349	135	56
		1025	219	74	146	2772	147	57
		1086	223	90	141	2287	140	56
5000 Hours at 590 K	295	1055	225	66	139	2658	134	56
		1042	218	87	148	3156*	120	58
		1099	225	100	142	2460	129	55
7500 Hours at 590 K	295	1137	220	74	145	2027	124	58
		1025	217	95	145	1891	118	56
		1086	215	100	145	1816	130	56
10 000 Hours at 590 K	295	1029	213	79	137	1640	111	58
		1039	213	90	139	1507	124	56
		1064	210	93	141	---	133	57
100 Hours at 730 K	295	903	223	92	139	2196	119	54
		953	225	92	145	2301	118	55
		958	227	92	141	2917	113	56
300 Hours at 730 K	295	---	---	104	144	2319	107	56
		780	226	99	135	2390	115	54
		874	226	106	145	2941	108	55
500 Hours at 730 K	295	803	223	105	134	2834	103	56
		847	228	103	143	2504	103	55
		766	223	83	135	3107	101	55
500 Cycles 200 K to 590 K	295	1219	233	95	123	2344	130	56
		1201	231	95	128	2669	131	55
		1222	231	68	124	2352	123	56
2000 Cycles 200 K to 590 K	295	1214	225	82	124	---	114	51
		1137	223	99	136	1920	113	51
		1059	227	64	123	1791	109	49

\*Out-lying data point dropped in regression analysis.

TABLE VIII.- B/5052 Al COMPOSITE TENSILE PROPERTIES

Specimen History	Test Temp., K	Longitudinal		Transverse	
		Ultimate Stress, MPa	Elastic Modulus, GPa	Ultimate Stress, MPa	Elastic Modulus, GPa
As Fabricated	295	1197	230	189	146
		1148	230	185	145
		1130	230	169	145
	500	1178	228	115	108
		1174	227	132	114
		1100	230	---	---
	590	1316	199	66	---
		1299	194	66	102
		1217	200	61	92
5000 Hours at 500 K	295	1134	230	140	151
		1151	228	131	148
		1168	233	150	150
10 000 Hours at 500 K	295	1119	233	155	147
		1128	230	155	146
		1183	229	169	144
2500 Hours at 590 K	295	1121	236	162	146
		1094	235	143	139
		1131	236	165	---
5000 Hours at 590 K	295	1072	236	191	143
		1114	235	160	143
		1117	239	151	139
7500 Hours at 590 K	295	1043	231	163	145
		1074	231	160	142
		1092	229	164	138
10 000 Hours at 590 K	295	1046	233	158	139
		1082	234	159	137
		1138	226	133	137
100 Hours at 730 K	295	978	230	181	144
		961	232	190	145
		970	232	138	147
300 Hours at 730 K	295	763	231	180	141
		735	231	162	149
		752	230	147	146
500 Hours at 730 K	295	727	230	178	140
		761	233	132	144
		711	230	145	139
500 Cycles 200 K to 590 K	295	1074	228	165	---
		1133	231	121	134
		1146	234	111	137
2000 Cycles 200 K to 590 K	295	1115	231	112	136
		1137	232	59	119
		1137	232	81	113

TABLE IX.- B/6061 Al COMPOSITE TENSILE, COMPRESSION, AND SHEAR PROPERTIES

Specimen History	Test Temp., K	Longitudinal Tensile		Transverse Tensile		Ultimate Compression Stress, MPa	Shear	
		Ultimate Stress, MPa	Elastic Modulus, GPa	Ultimate Stress, MPa	Elastic Modulus, GPa		Ultimate Stress, MPa	Elastic Modulus, GPa
As Fabricated	295	1685	235	---	---	2960	211	61
		1653	233	182	151	3726	179	54
		1557	232	185	153	3934	214	57
	500	1657	234	121	123	1555	189	49
		1518	233	118	131	1389	202	48
		1612	232	118	125	1191	216	48
	590	1423	210	65	121	818	155	--
		1402	207	63	---	1080	155	42
		1393	---	56	118	762	156	42
5000 Hours at 500 K	295	1388	233	137	150	---	---	---
		1392	233	144	148	---	---	---
		1418	232	144	153	---	---	---
10 000 Hours at 500 K	295	1319	228	126	151	---	---	---
		1346	234	140	153	---	---	---
		1382	233	136	156	---	---	---
2500 Hours at 590 K	295	1277	233	135	144	3356	154	56
		1440	228	141	151	3096	171	57
		1494	227	133	155	2741	147	56
5000 Hours at 590 K	295	1490	236	139	145	3467	145	59
		1429	236	138	153	2831	193	56
		1406	239	133	145	2440	200	57
7500 Hours at 590 K	295	1295	224	136	152	2346	159	58
		1396	229	141	153	2297	218	58
		1509	223	129	146	2482	218	58
10 000 Hours at 590 K	295	1417	224	131	147	2081	217	59
		1520	228	139	151	2250	208	59
		1545	221	128	151	2240	229	57
100 Hours at 730 K	295	1591	229	161	145	2679	205	57
		1474	232	165	141	3379	196	56
		1430	234	160	147	3072	173	60
300 Hours at 730 K	295	1178	234	165	150	3006	152	57
		1111	231	164	144	2950	138	59
		1138	233	168	146	2771	151	58
500 Hours at 730 K	295	911	230	162	144	3582	119	58
		907	227	160	142	3397	132	56
		889	229	169	145	3002	108	57
500 Cycles 200 K to 590 K	295	1585	233	132	152	3453	219	57
		1507	234	127	136	2890	218	58
		1671	235	138	139	2808	213	56
2000 Cycles 200 K to 590 K	295	1539	233	125	136	2291	196	54
		1567	233	119	136	2028	206	52
		1545	232	126	134	2193	153	53

TABLE X.- TENSILE STRENGTHS OF DIFFUSION BONDED ALUMINUM ALLOYS

[The mean room-temperature elastic modulus of all the alloys was 7.29 GPa]

Specimen History	Test Temp., K	Ultimate Tensile Stress, MPa				
		1100	2024	3003	5052	6061
As Fabricated	295	75	377	113	219	249
		65	365	112	225	255
		70	362	112	208	255
	500	34	202	56	121	166
		33	189	57	128	176
		35	190	46	125	185
	590	21	65	31	55	65
		22	67	31	54	60
		18	66	30	52	---
	5000 Hours at 500 K	73	200	109	188	146
		72	195	110	189	145
		70	193	110	189	146
	10 000 Hours at 500 K	71	193	110	194	128
		72	191	111	189	129
		71	191	109	189	128
	2500 Hours at 590 K	67	188	105	183	113
		71	188	105	184	113
		70	185	105	184	113
	5000 Hours at 590 K	68	182	106	184	112
		70	183	105	183	113
		69	184	106	183	114
	7500 Hours at 590 K	71	182	107	183	113
		70	182	107	183	113
		72	182	106	184	114
	10 000 Hours at 590 K	69	175	108	182	114
		71	174	106	183	115
		69	175	106	186	116
	100 Hours at 730 K	72	357	108	189	146
		69	357	110	185	155
		68	357	108	187	147
	300 Hours at 730 K	73	368	108	189	161
		72	377	109	186	159
		68	368	106	191	162
	500 Hours at 730 K	69	365	107	187	159
		75	366	107	187	164
		67	364	106	189	161
	500 Cycles 200 K to 590 K	72	208	108	186	122
		70	213	108	188	129
	2000 Cycles 200 K to 590 K	69	195	111	192	122
		72	196	110	192	122

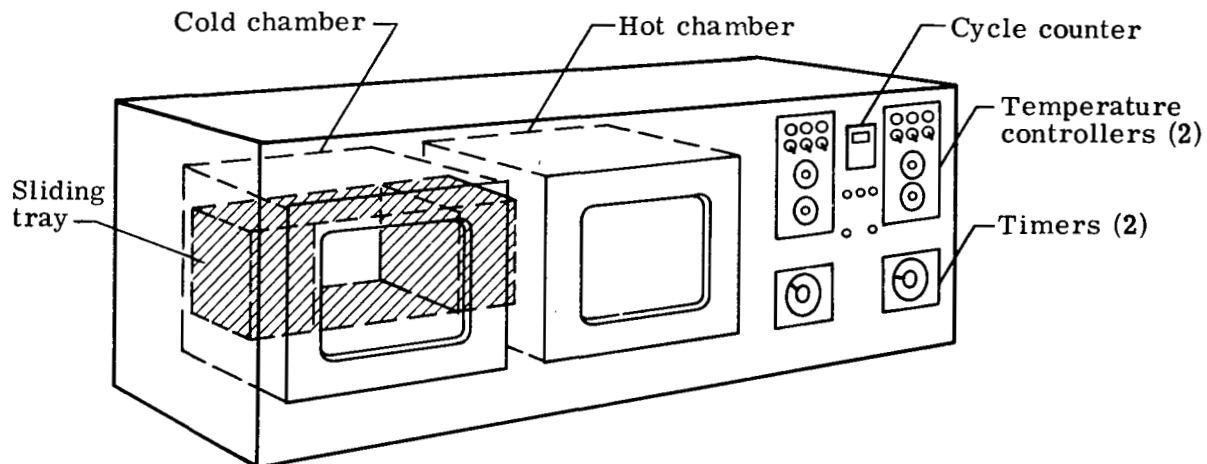
TABLE XI.- MECHANICAL PROPERTIES OF AS-FABRICATED UNIDIRECTIONAL B/Al  
COMPOSITES AT ROOM TEMPERATURE

[Quantity in parentheses indicates percentage difference  
when compared with B/6061 Al property]

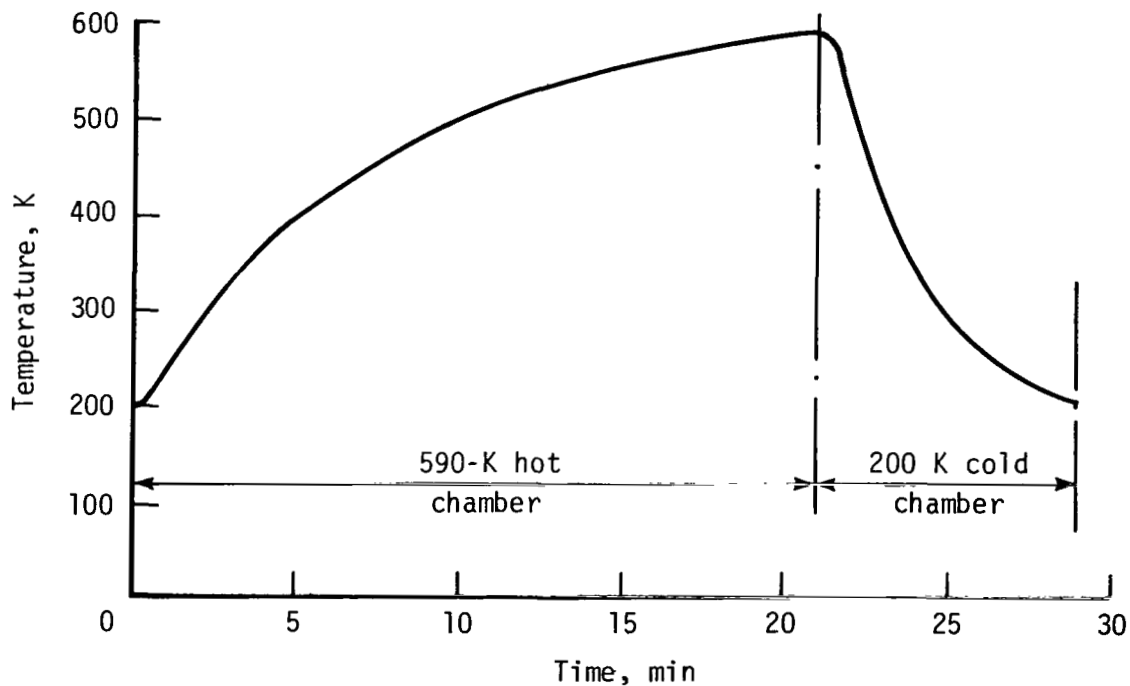
MECHANICAL PROPERTY	Composite System				
	B/1100 Al	B/2024 Al	B/3003 Al	B/5052 Al	B/6061 Al
Longitudinal Tensile Strength, $\sigma_{lt}$ , MPa	1448 (-11%)	1523 (-7%)	1189 (-27%)	1158 (-29%)	1632
Longitudinal Elastic Modulus, $E_1$ , GPa	230 (-1%)	234 (0%)	225 (-3%)	230 (-1%)	233
Transverse Tensile Strength, $\sigma_{tt}$ , MPa	68 (-63%)	234 (+27%)	86 (-53%)	181 (-2%)	184
Transverse Elastic Modulus, $E_2$ , GPa	136 (-11%)	152 (0%)	143 (-6%)	145 (-5%)	152
Longitudinal Compressive Strength, $\sigma_{lc}$ , MPa	2230 (-37%)	----	2524 (-29%)	----	3540
In-plane Shear Stress, $\tau$ , GPa	135 (-33%)	----	136 (-32%)	----	201
In-plane Shear Elastic Modulus, $G_{12}$ , MPa	51 (-11%)	----	54 (-5%)	----	57

TABLE XII.- B/AL COMPOSITE PROPERTY DEGRADATION AFTER 10 000 HOURS  
EXPOSURE AT 500 K AND 590 K

B/Al Composite System	Mechanical Property Degradation			
	Transverse Tensile Strength	Longitudinal Tensile Strength	Longitudinal Compression Strength	In-Plane Shear Strength
B/1100 Al	None	22% (Occurred at 500 K worse condition may exist)	38%	12%
B2024/Al	15% (all due to matrix annealing)	14% (includes 6% attributed to matrix annealing)	----	----
B/3003 Al	None	10%	38%	10%
B/5052 Al	10% (all due to matrix annealing)	8% (includes 1% attributed to matrix annealing)	----	----
B/6061 Al	28% (all due to matrix annealing)	17% (occurred at 500 K worse condition may exist) (includes 4% attributed to matrix annealing)	38%	22% (all due to matrix annealing)



(a) Thermal cycling apparatus.



(b) Typical specimen temperature history for one cycle.

Figure 1.- Thermal cycling exposure.

**Test Fixture Key**

Fiber breaks on mandrel no.	Strength range of 203- $\mu$ m diam. boron fiber, GPa
1	Less than 1.80
2	1.80 to 2.00
3	2.00 to 2.20
4	2.20 to 2.40
5	2.40 to 2.60
6	2.60 to 2.80
7	2.80 to 3.00
8	3.00 to 3.20
9	3.20 to 3.40
10	3.40 to 3.60
11	3.60 to 3.80
12	3.80 to 4.00
13	4.00 to 4.27
14	4.27 to 4.65
15	4.65 to 5.12
16	5.12 to 5.67
Fiber does not break	
	Greater than 5.67

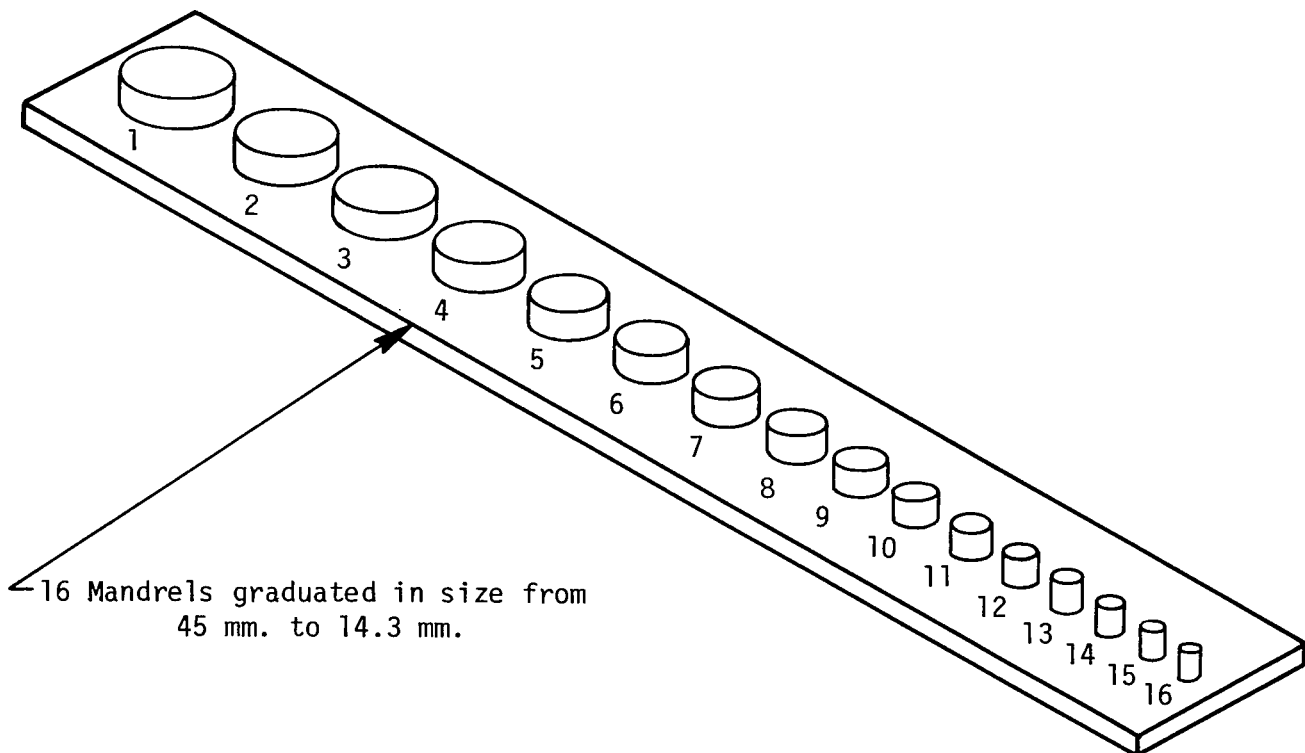


Figure 2.- Schematic of fiber bend-test fixture.

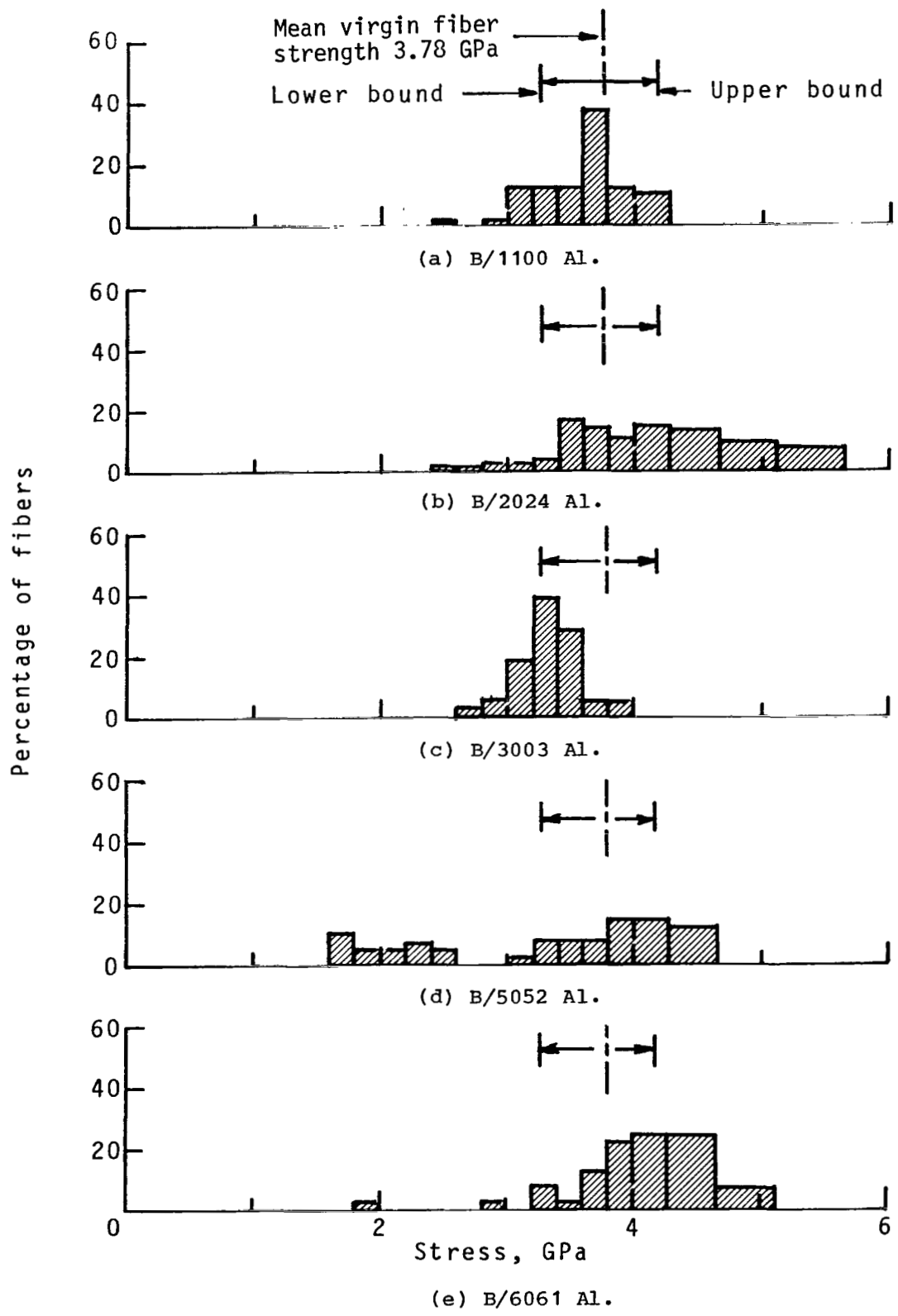
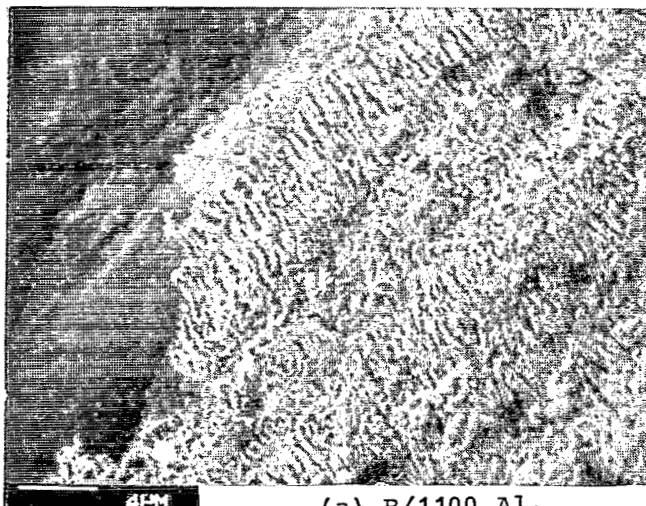
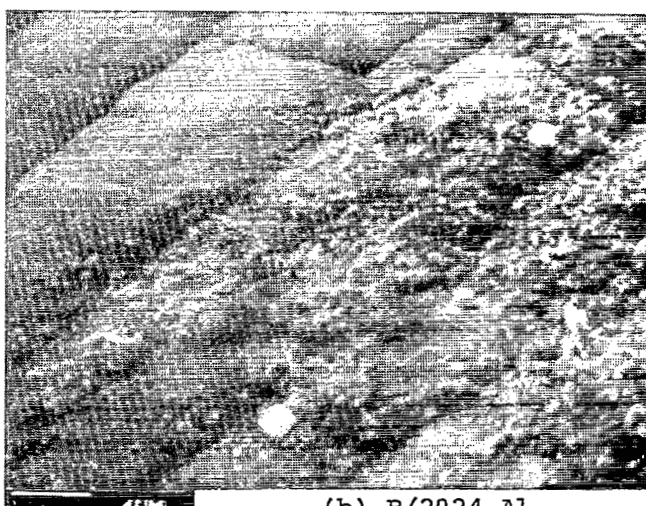


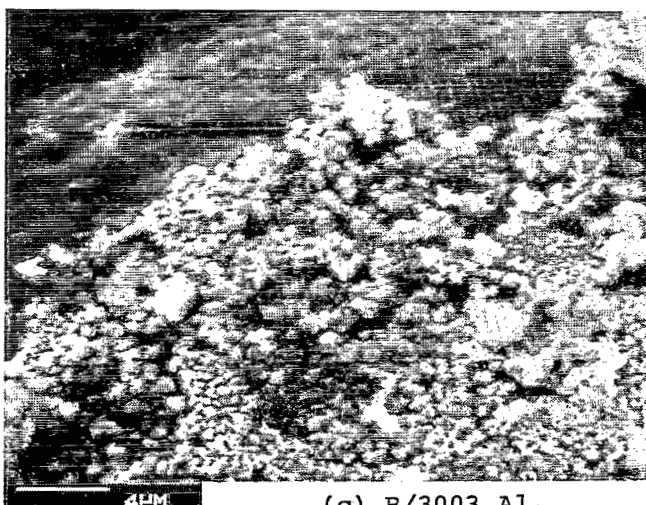
Figure 3.- Fiber strength distributions for as-fabricated composites.



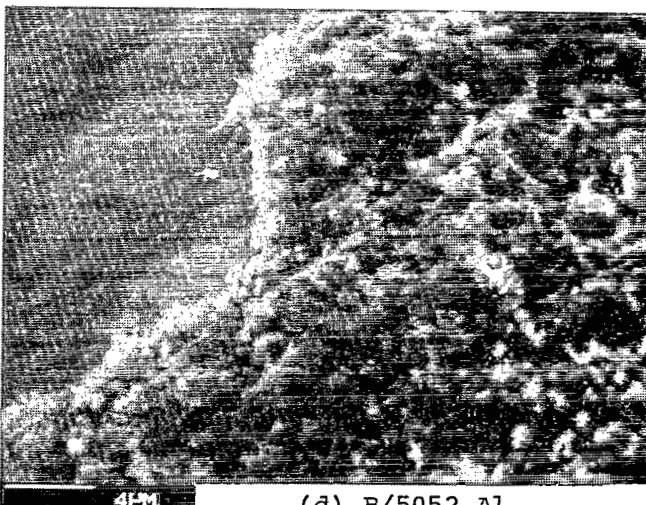
(a) B/1100 Al.



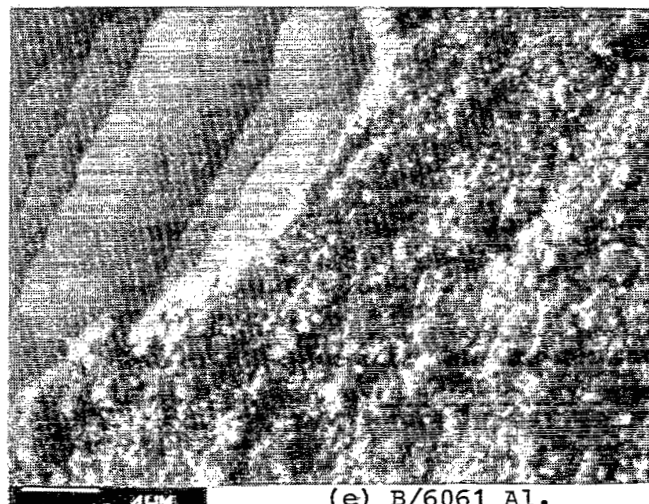
(b) B/2024 Al.



(c) B/3003 Al.



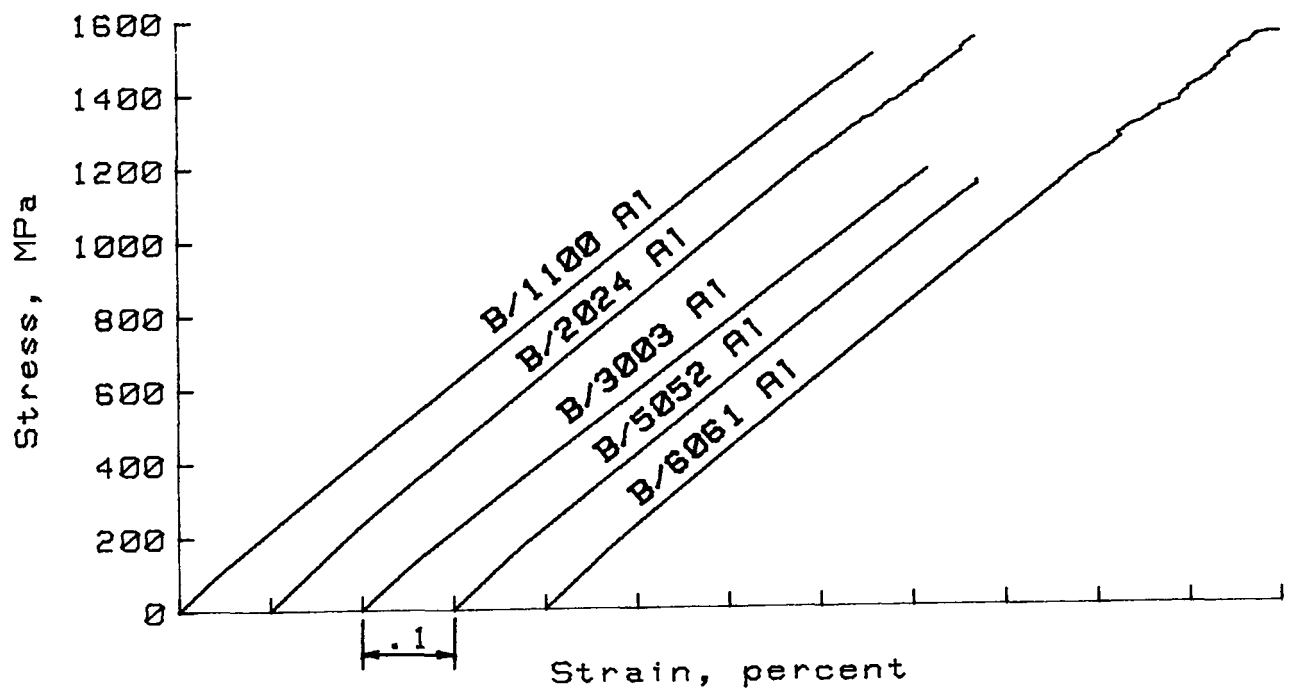
(d) B/5052 Al.



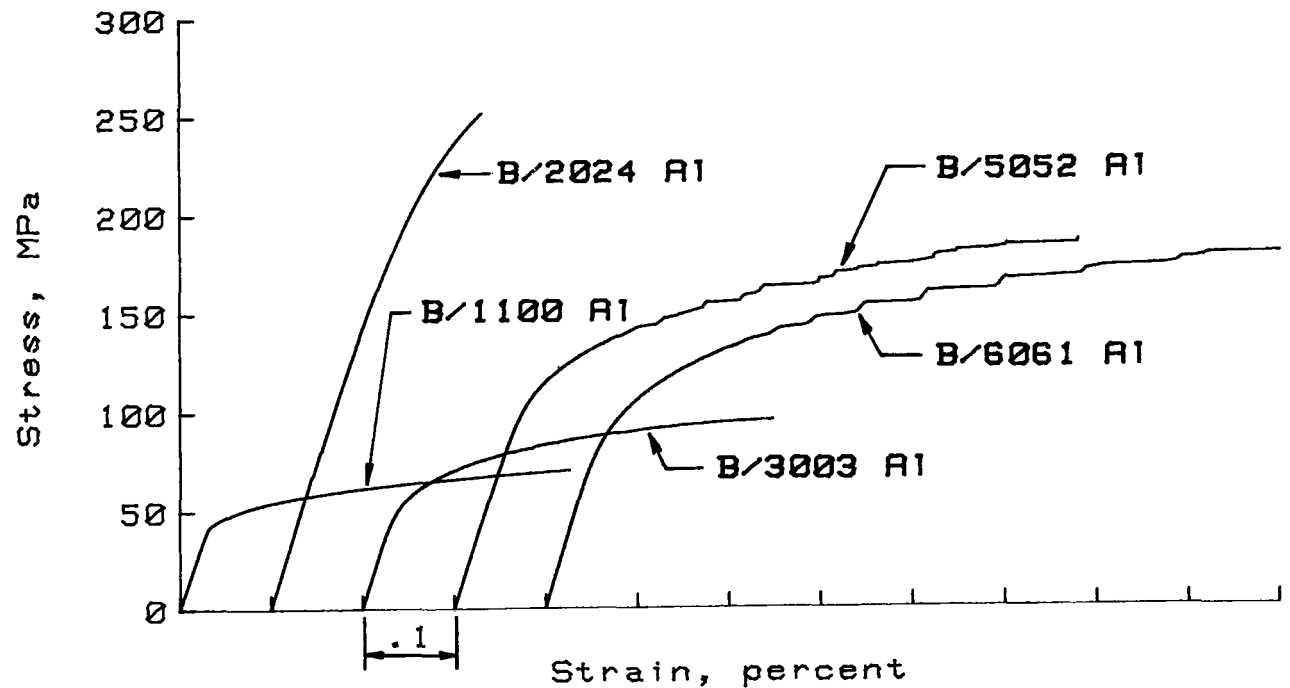
(e) B/6061 Al.

L-81-101

Figure 4.- Reaction layers on fibers removed from as-fabricated composite specimens.

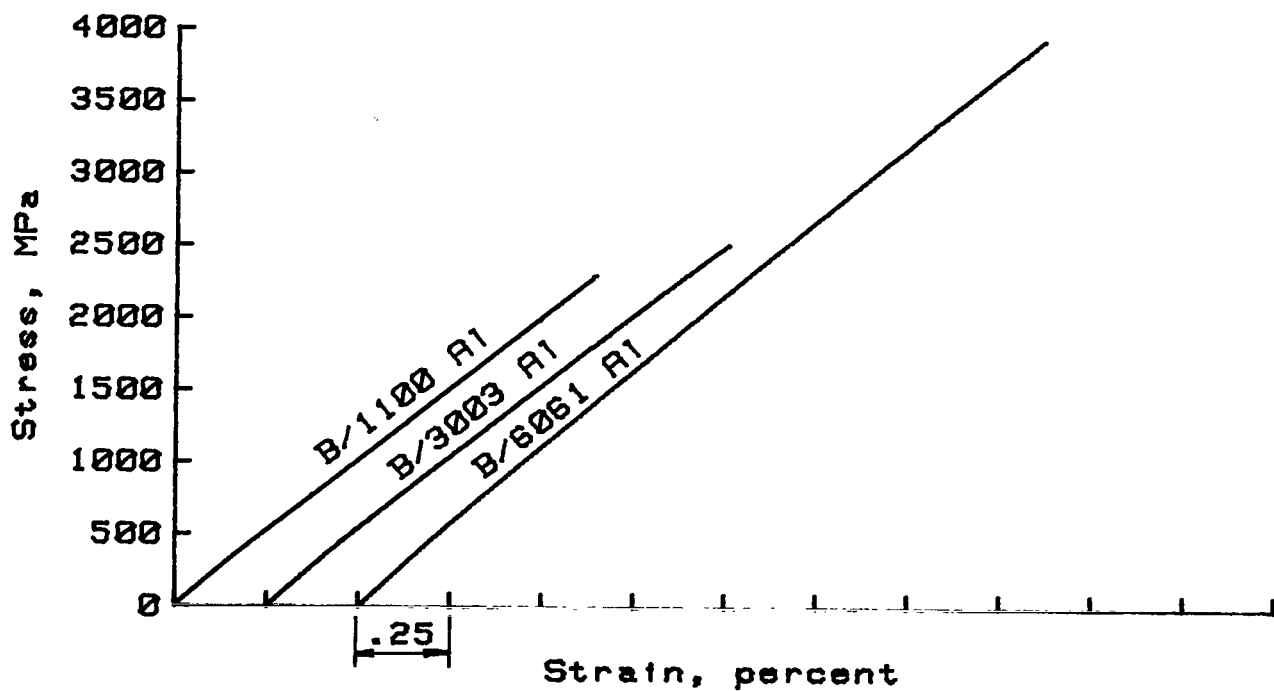


(a) Longitudinal tensile.

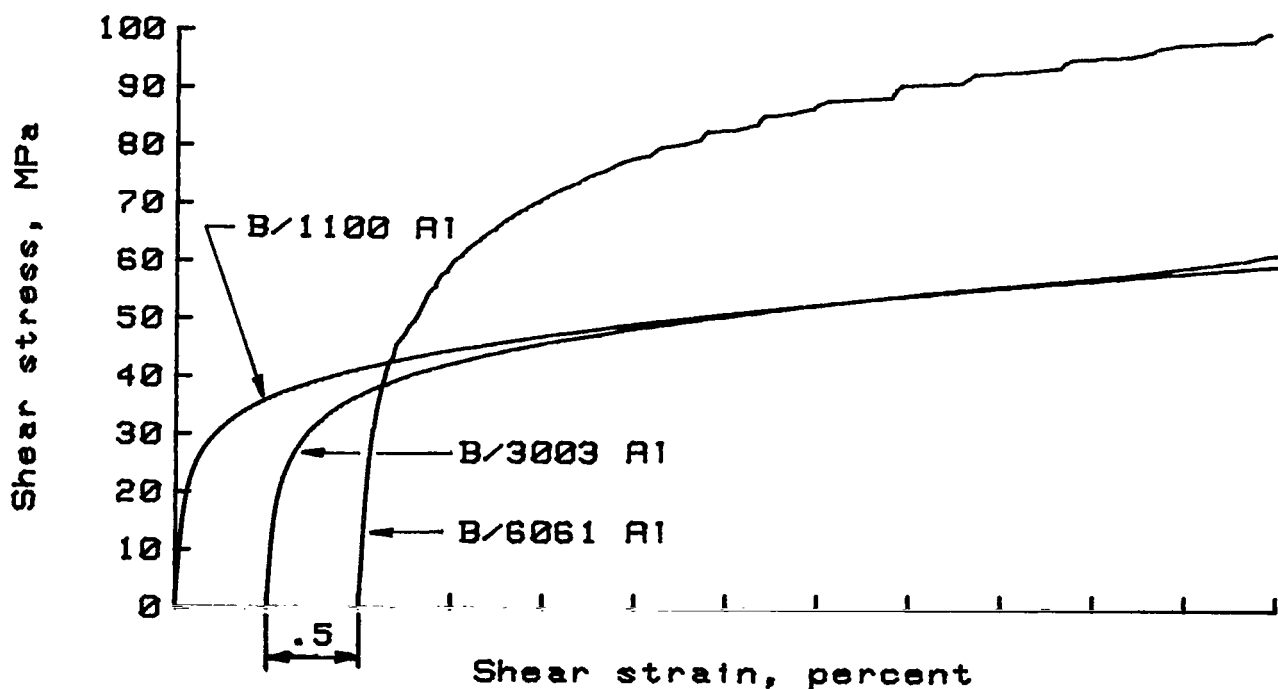


(b) Transverse tensile.

Figure 5.- Typical room-temperature stress-strain curves for as-fabricated B/Al composites.

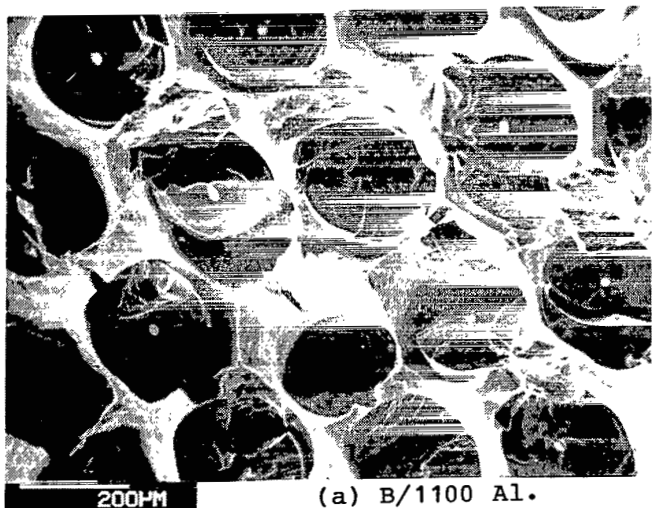


(c) Longitudinal compression.

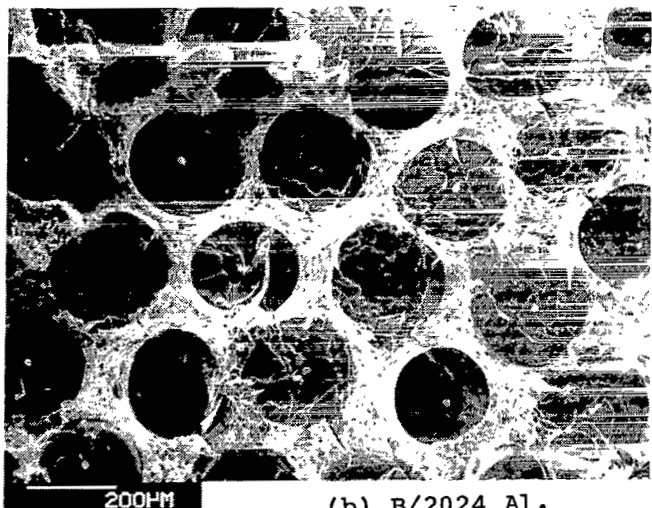


(d) In-plane shear.

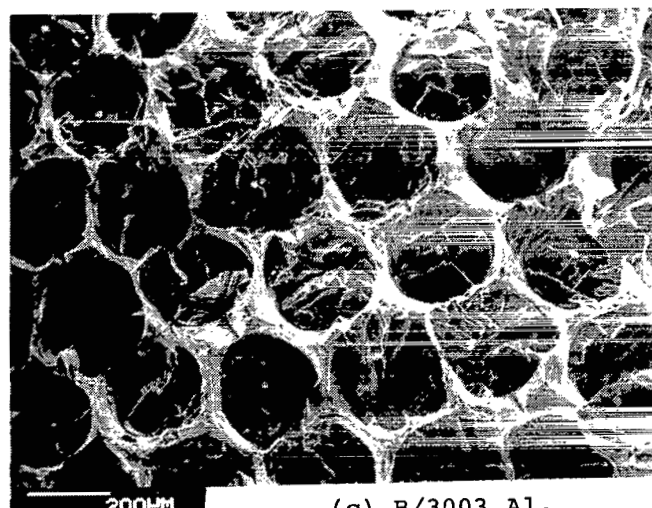
Figure 5.- Concluded.



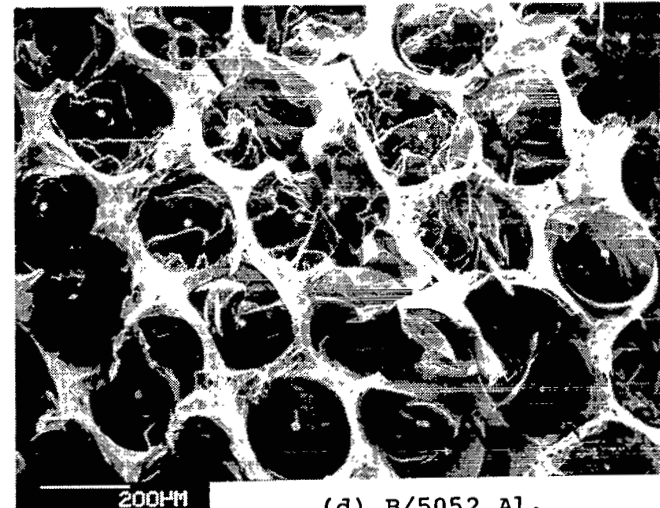
(a) B/1100 Al.



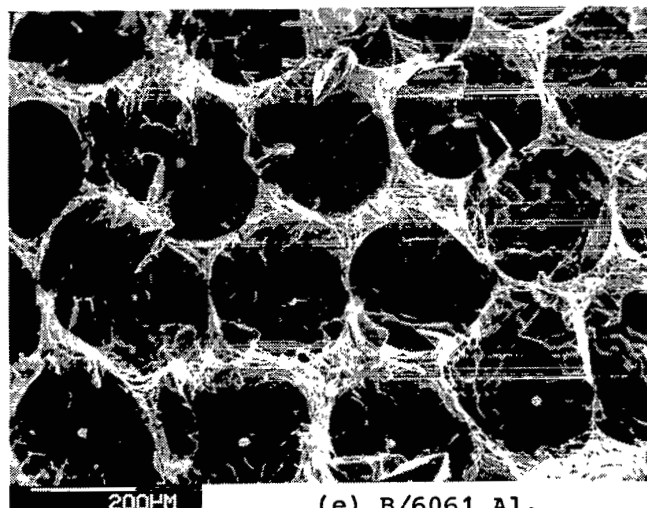
(b) B/2024 Al.



(c) B/3003 Al.



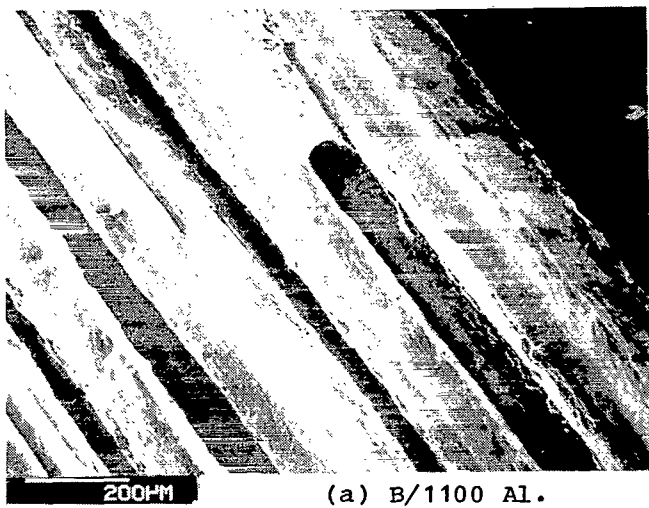
(d) B/5052 Al.



(e) B/6061 Al.

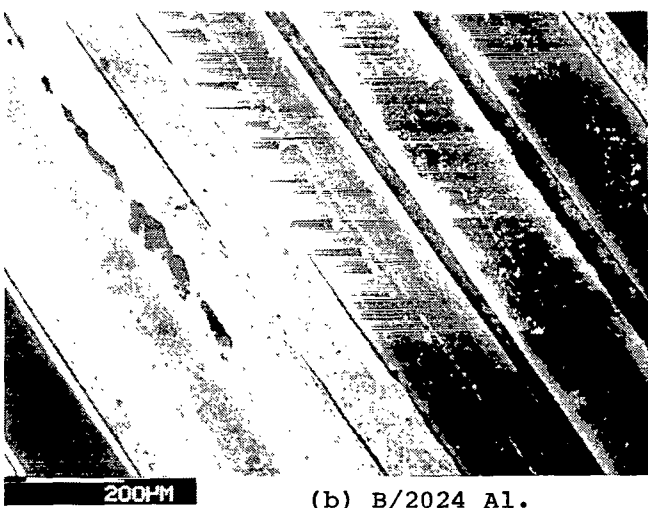
L-82-102

Figure 6.- Longitudinal fracture surfaces of as-fabricated specimens.



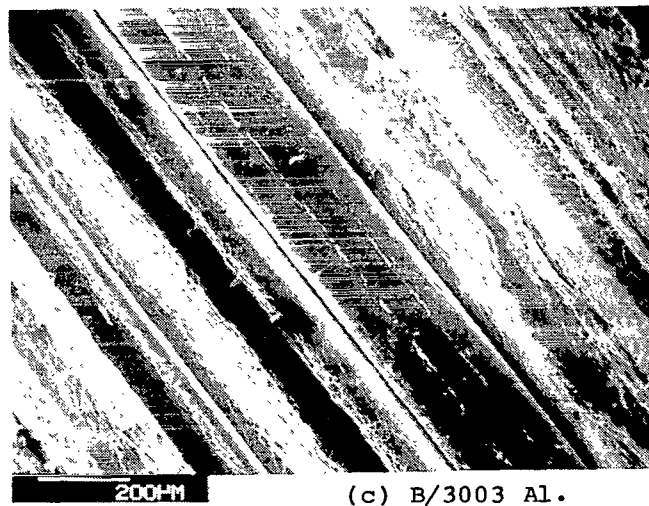
200HM

(a) B/1100 Al.



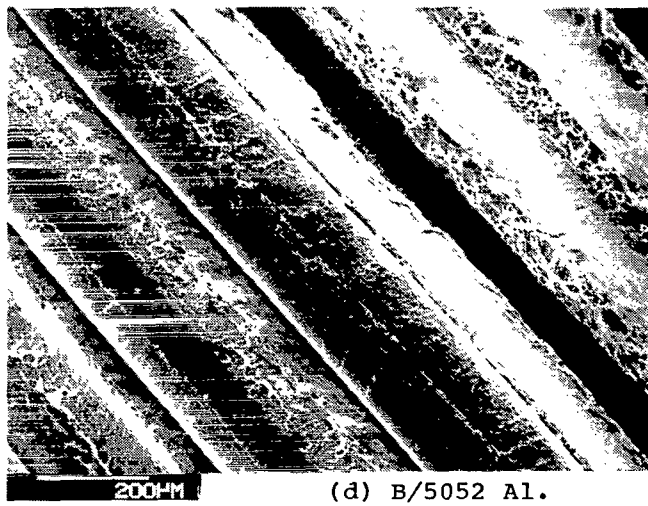
200HM

(b) B/2024 Al.



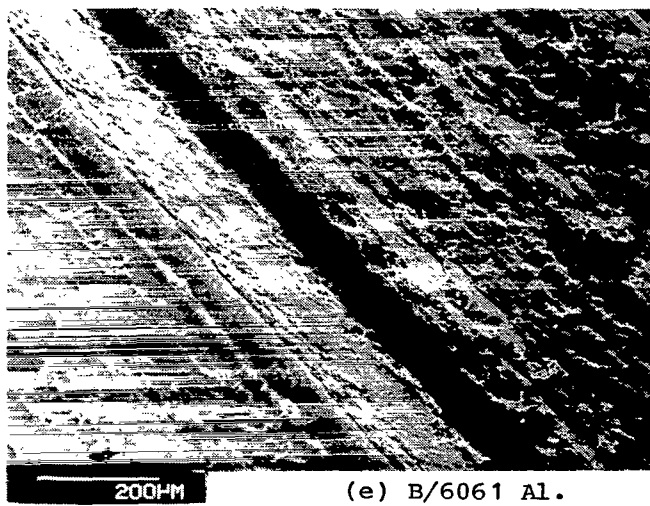
200HM

(c) B/3003 Al.



200HM

(d) B/5052 Al.



200HM

(e) B/6061 Al.

L-82-103

Figure 7.- Transverse fracture surfaces of as-fabricated specimens.

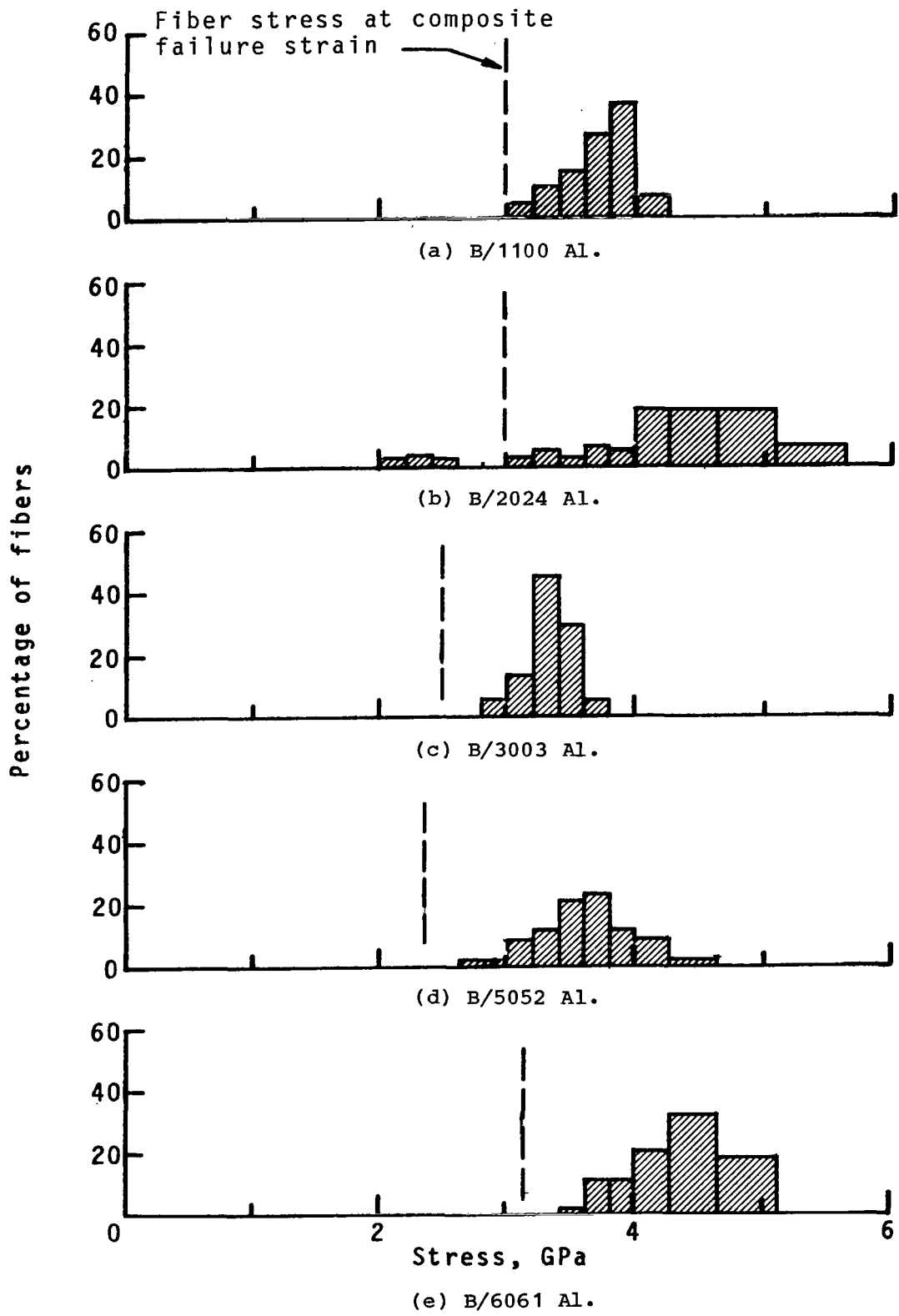


Figure 8.- Residual fiber strength distribution for as-fabricated composites after tensile testing.

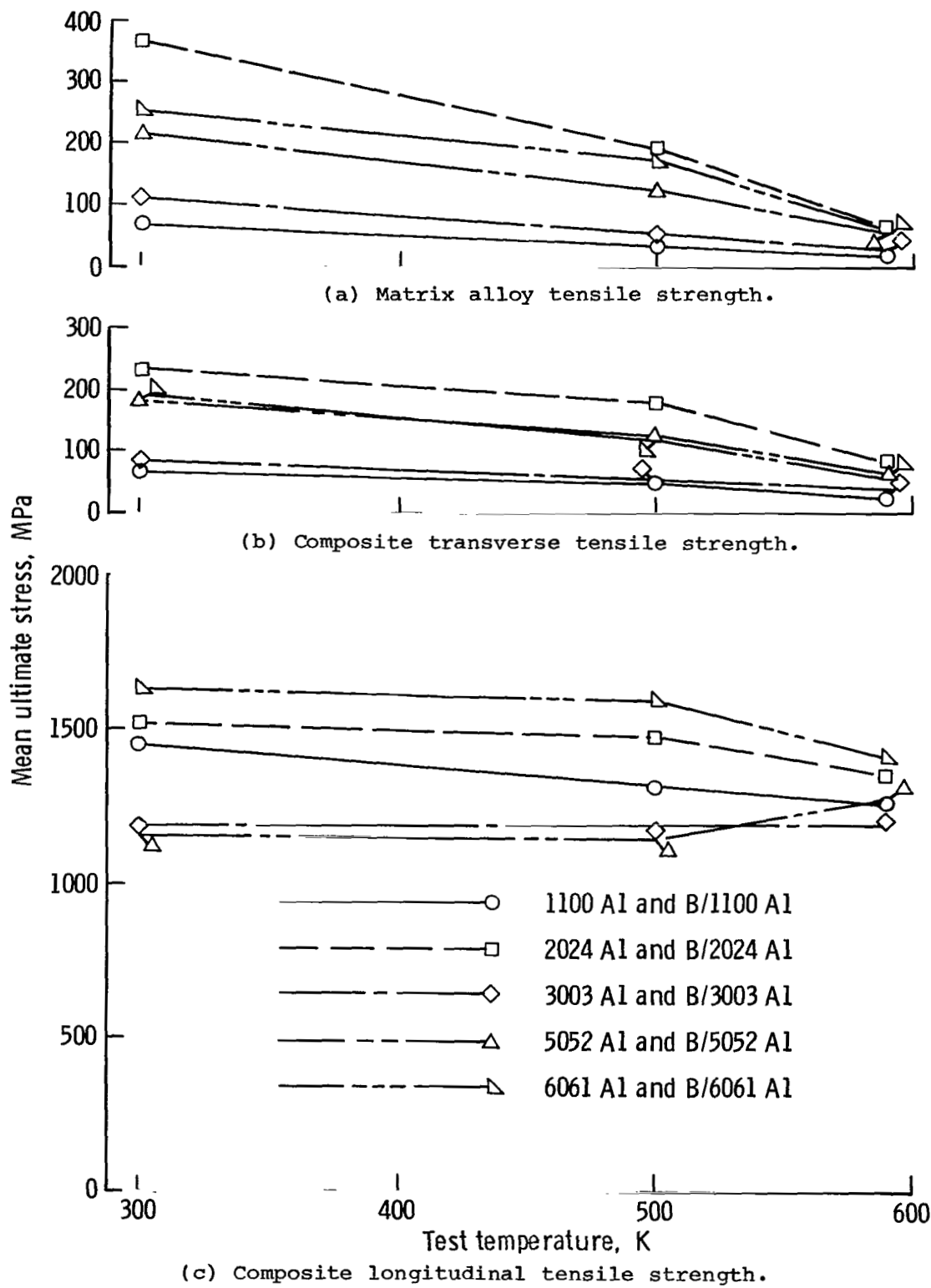


Figure 9.- Effect of elevated test temperature on mean ultimate strengths of B/Al composites.

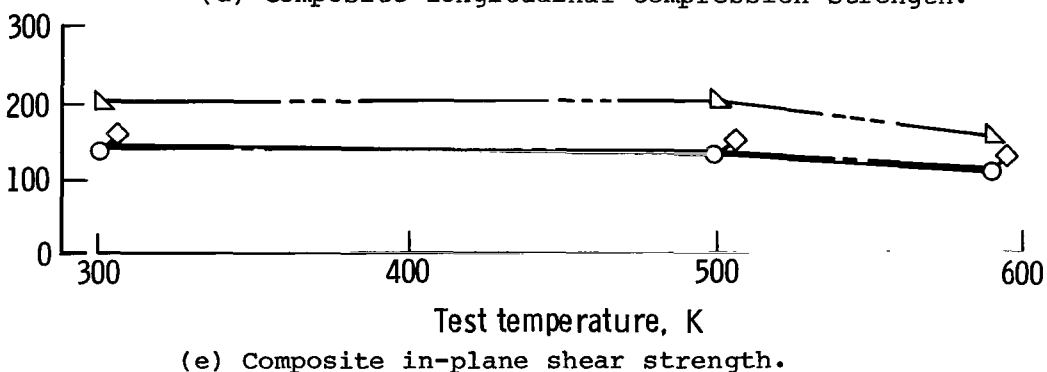
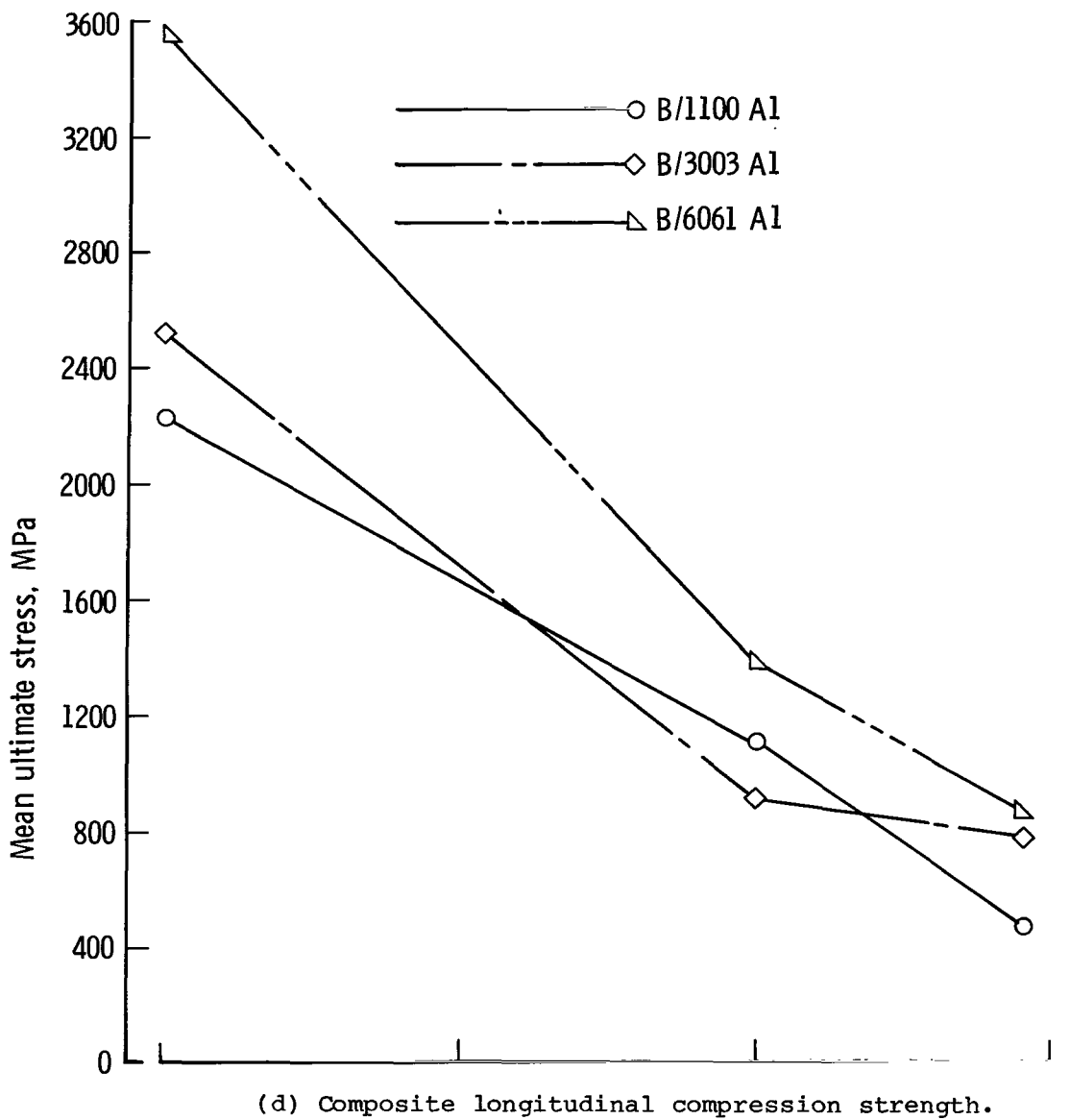


Figure 9.- Concluded.

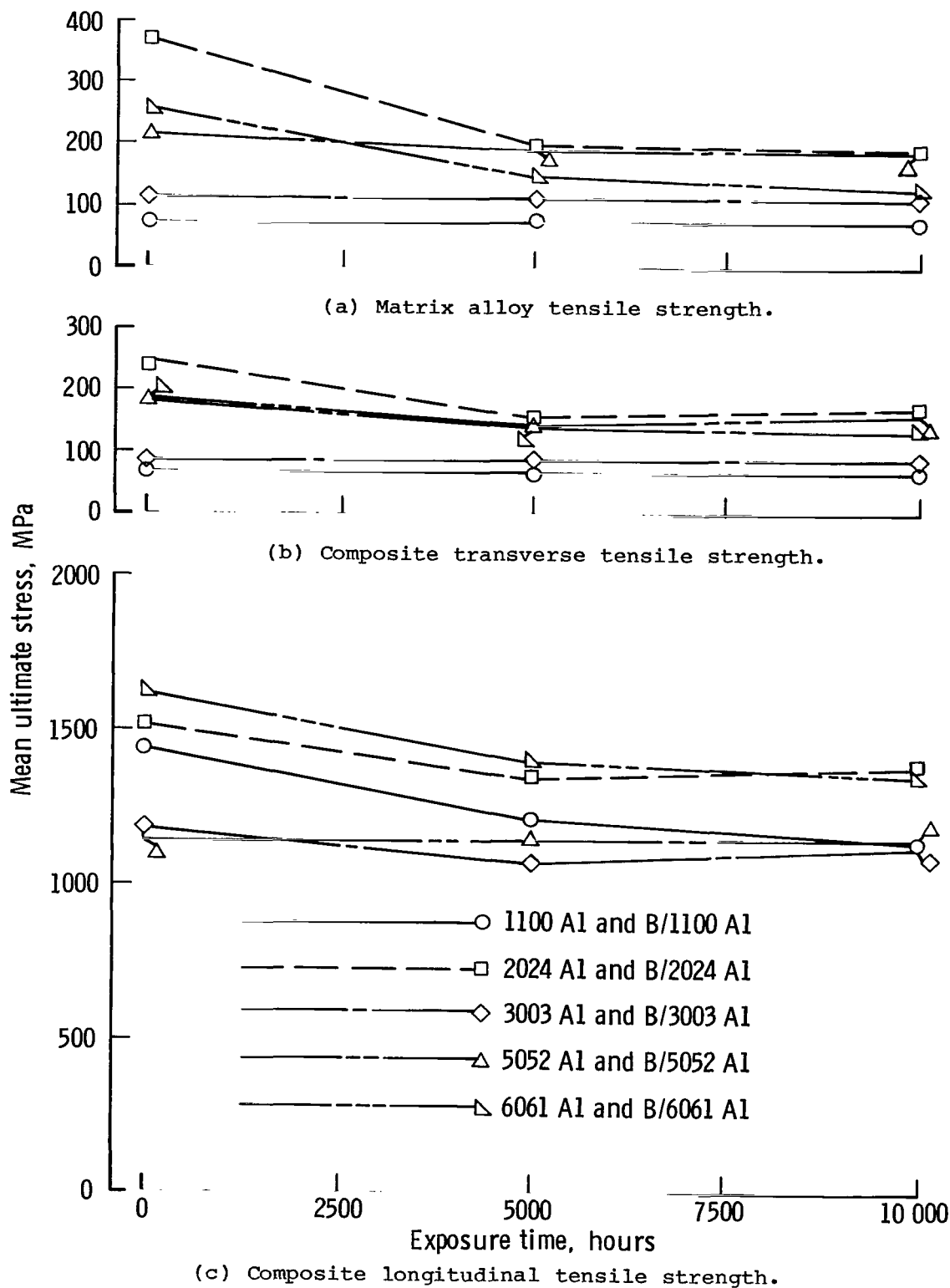


Figure 10.- Effect of isothermal exposure at 500 K on ultimate stress of B/Al composites and their matrix alloys.

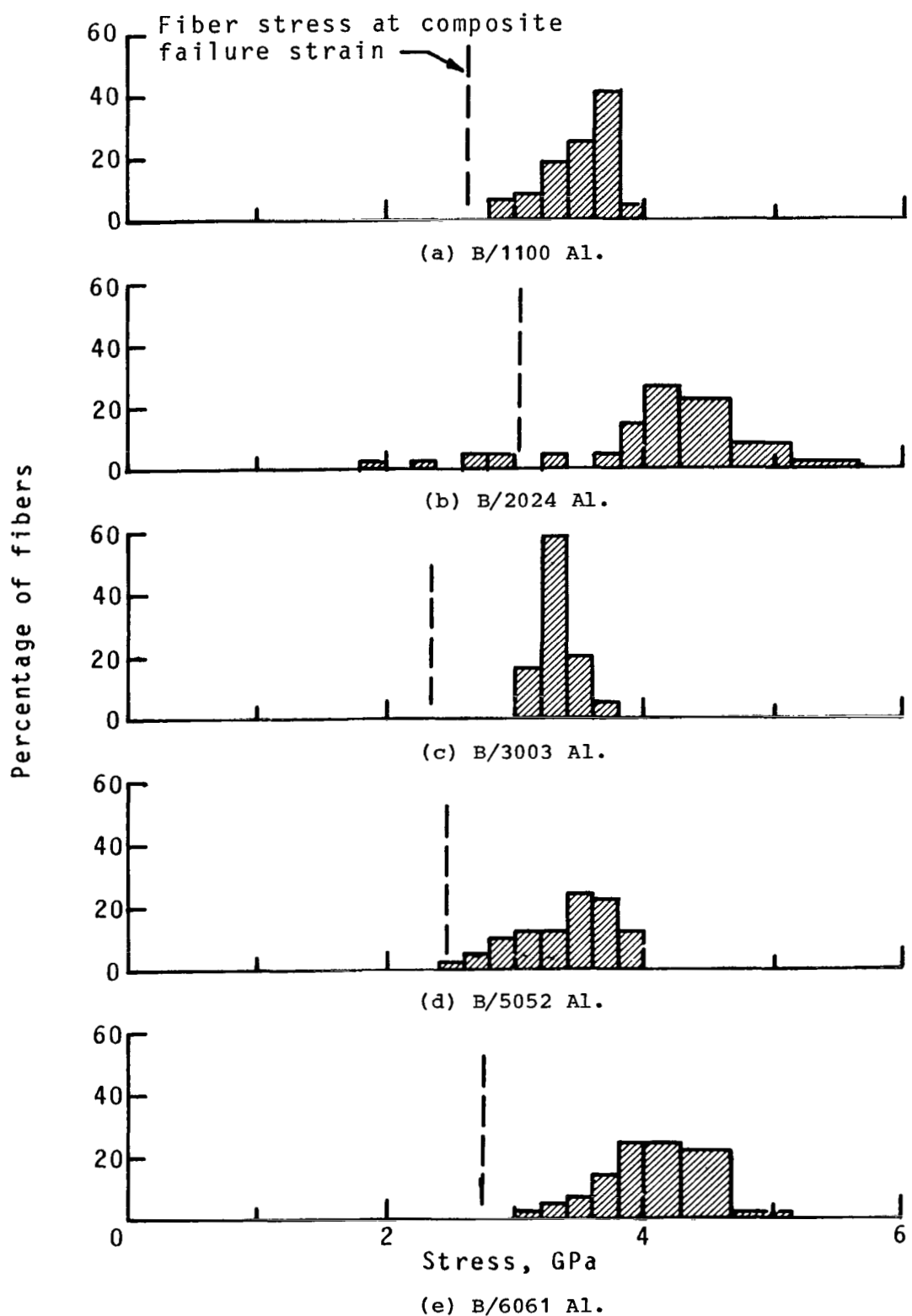


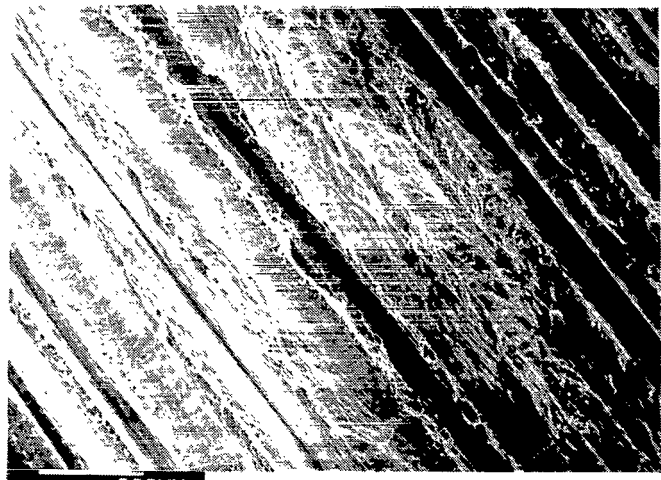
Figure 11.- Residual fiber strength distributions for composites after 10 000 hours exposure at 500 K and tensile testing.



(a) B/1100 Al.



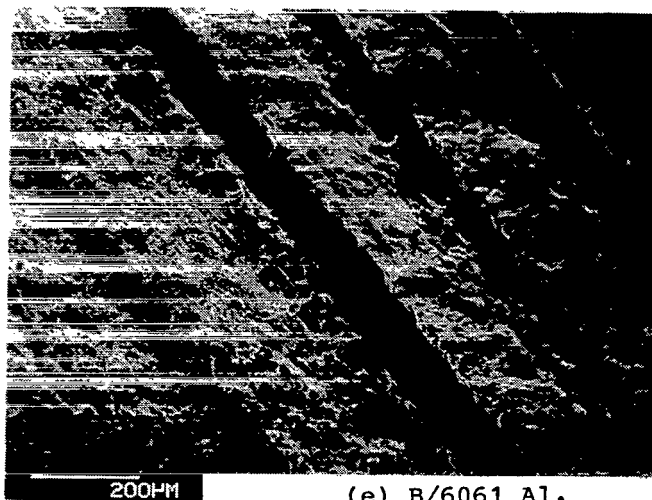
(b) B/2024 Al.



(c) B/3003 Al.



(d) B/5052 Al.



(e) B/6061 Al.

L-82-104

Figure 12.- Transverse fracture surfaces of specimens isothermally exposed for 10 000 hours at 500 K.

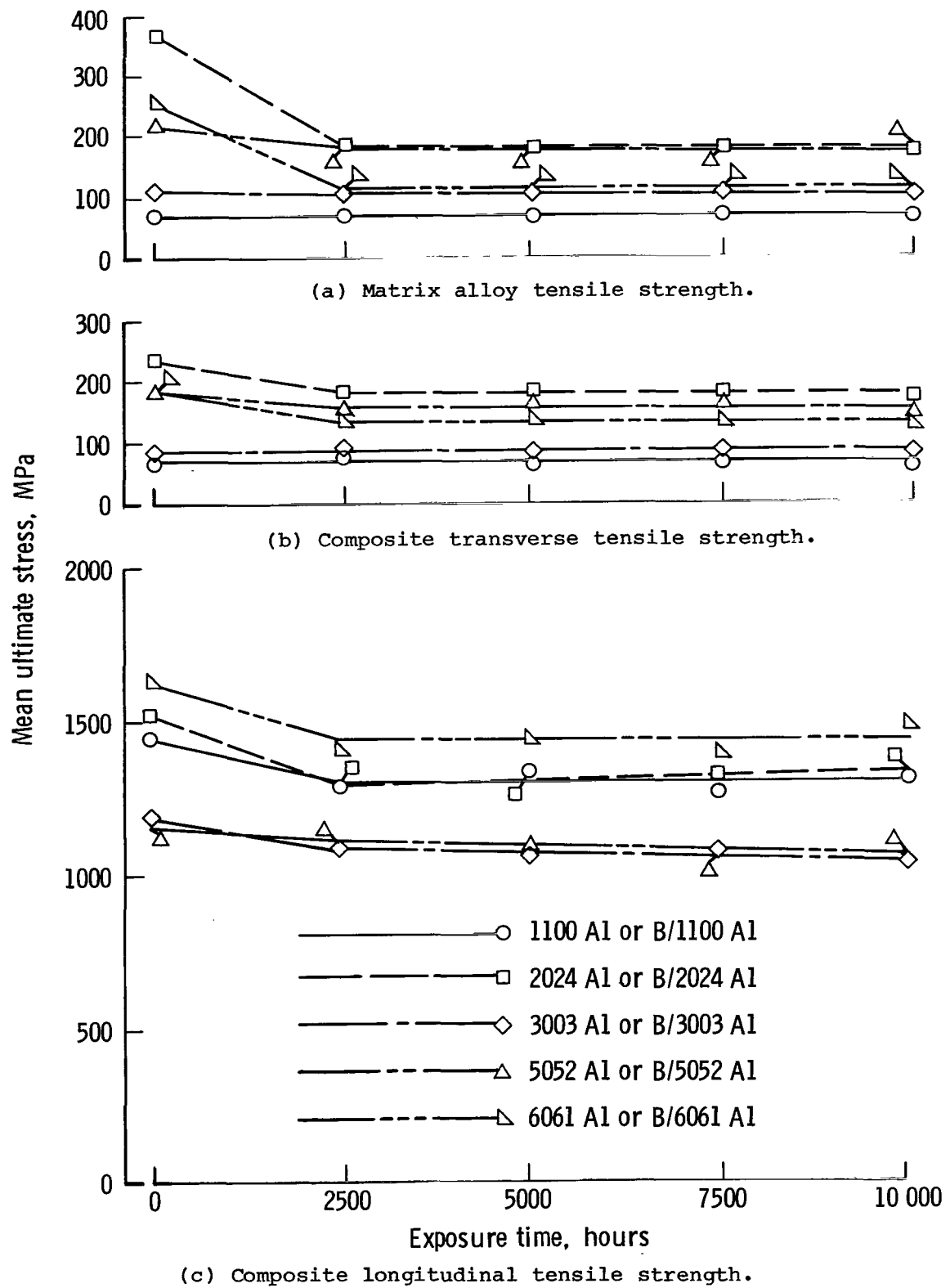


Figure 13.— Effect of isothermal exposure at 590 K on ultimate stress of B/Al composites and their matrix alloys.

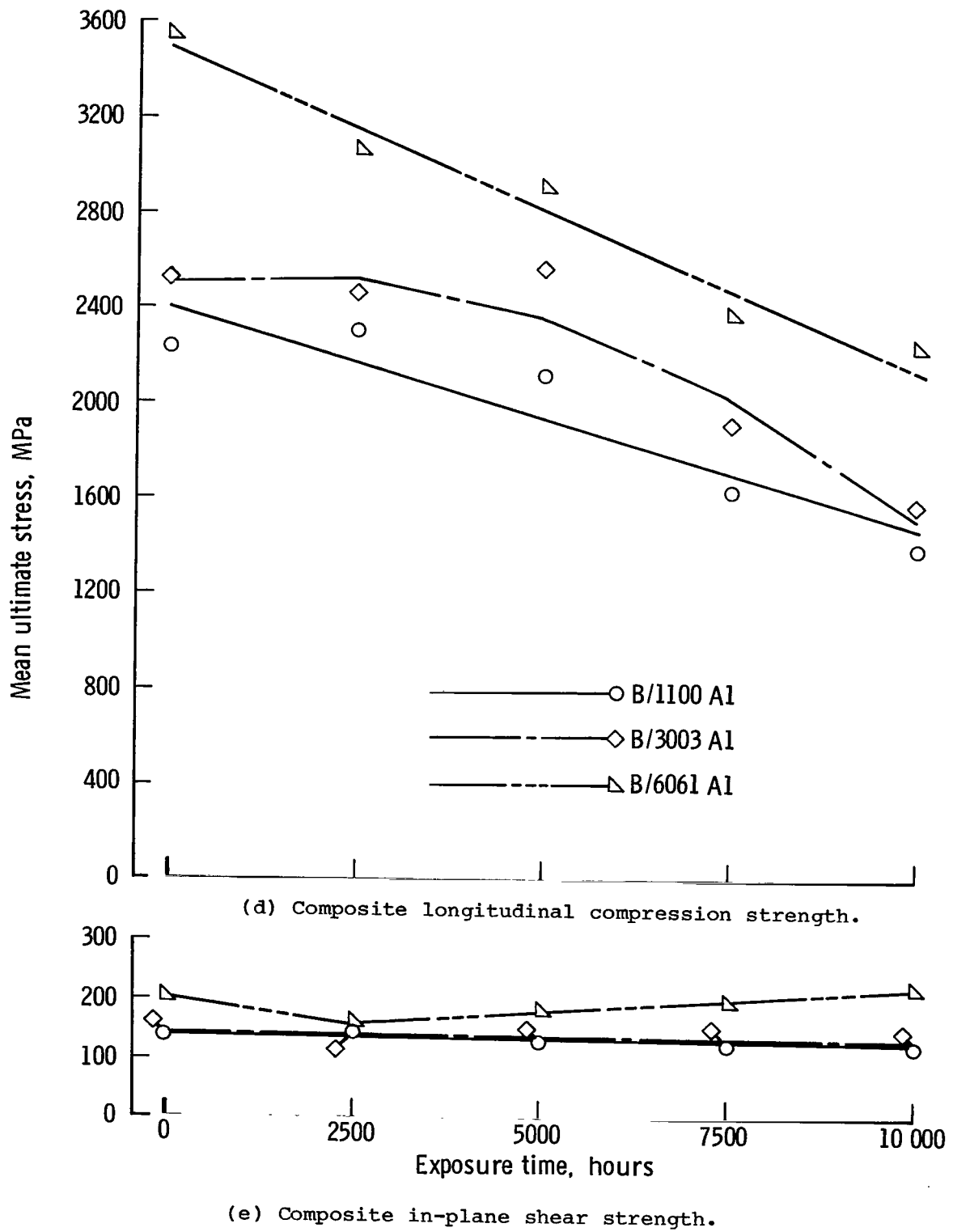
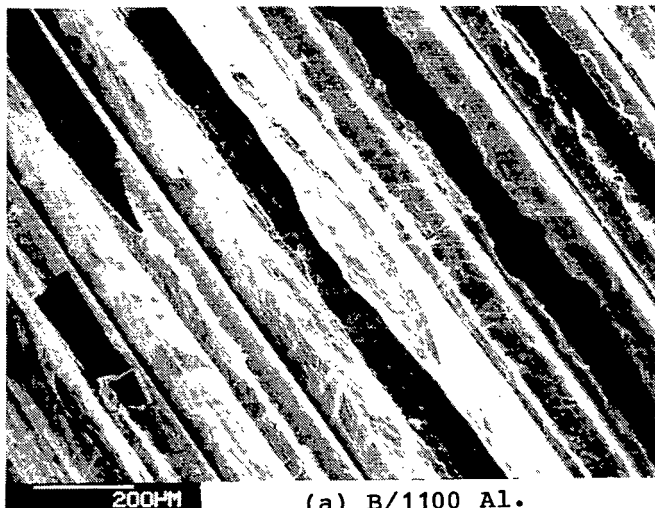
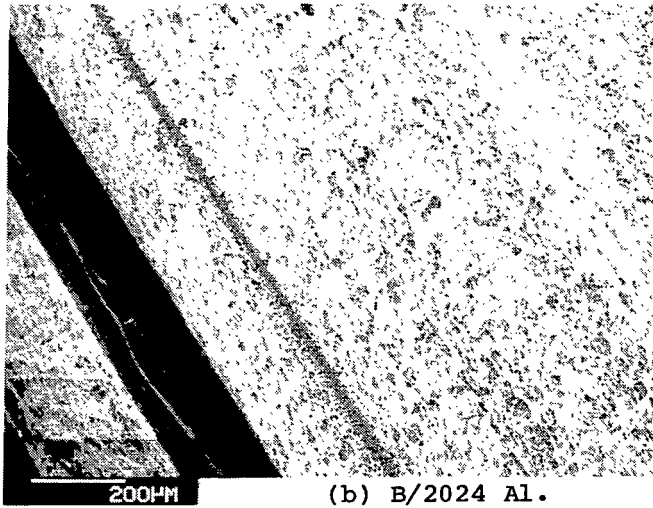


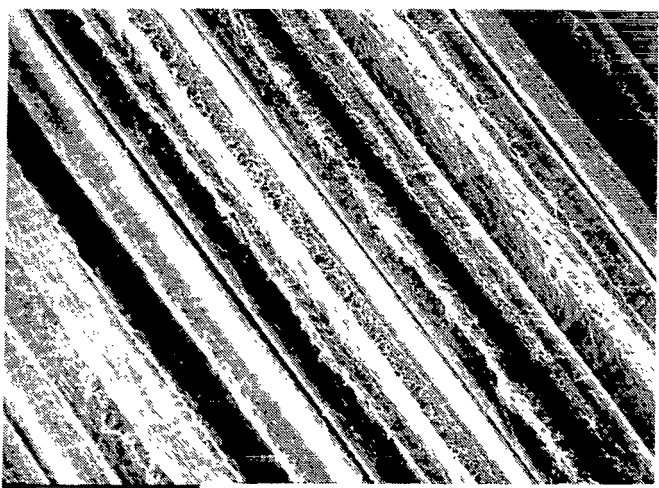
Figure 13.- Concluded.



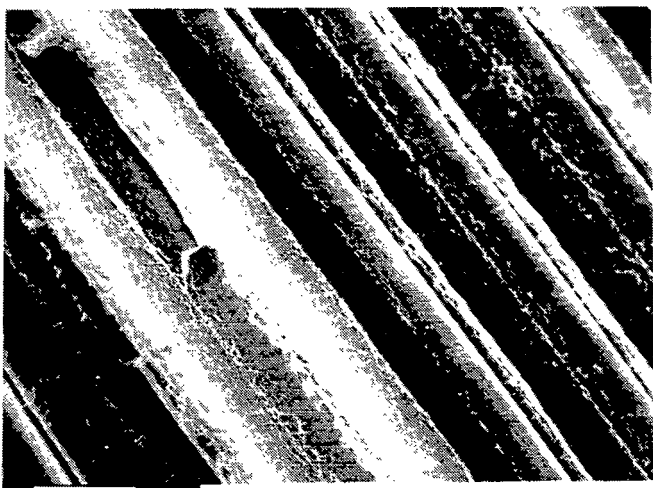
(a) B/1100 Al.



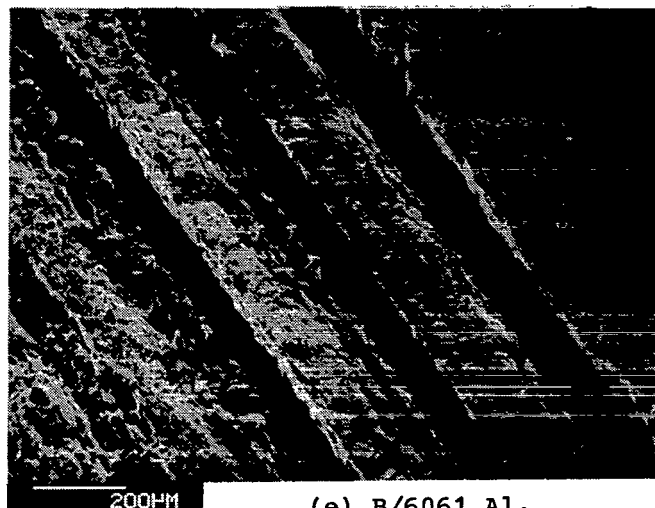
(b) B/2024 Al.



(c) B/3003 Al.



(d) B/5052 Al.



(e) B/6061 Al.

L-82-105

Figure 14.- Transverse fracture surfaces of specimens isothermally exposed for 10 000 hours at 590 K.

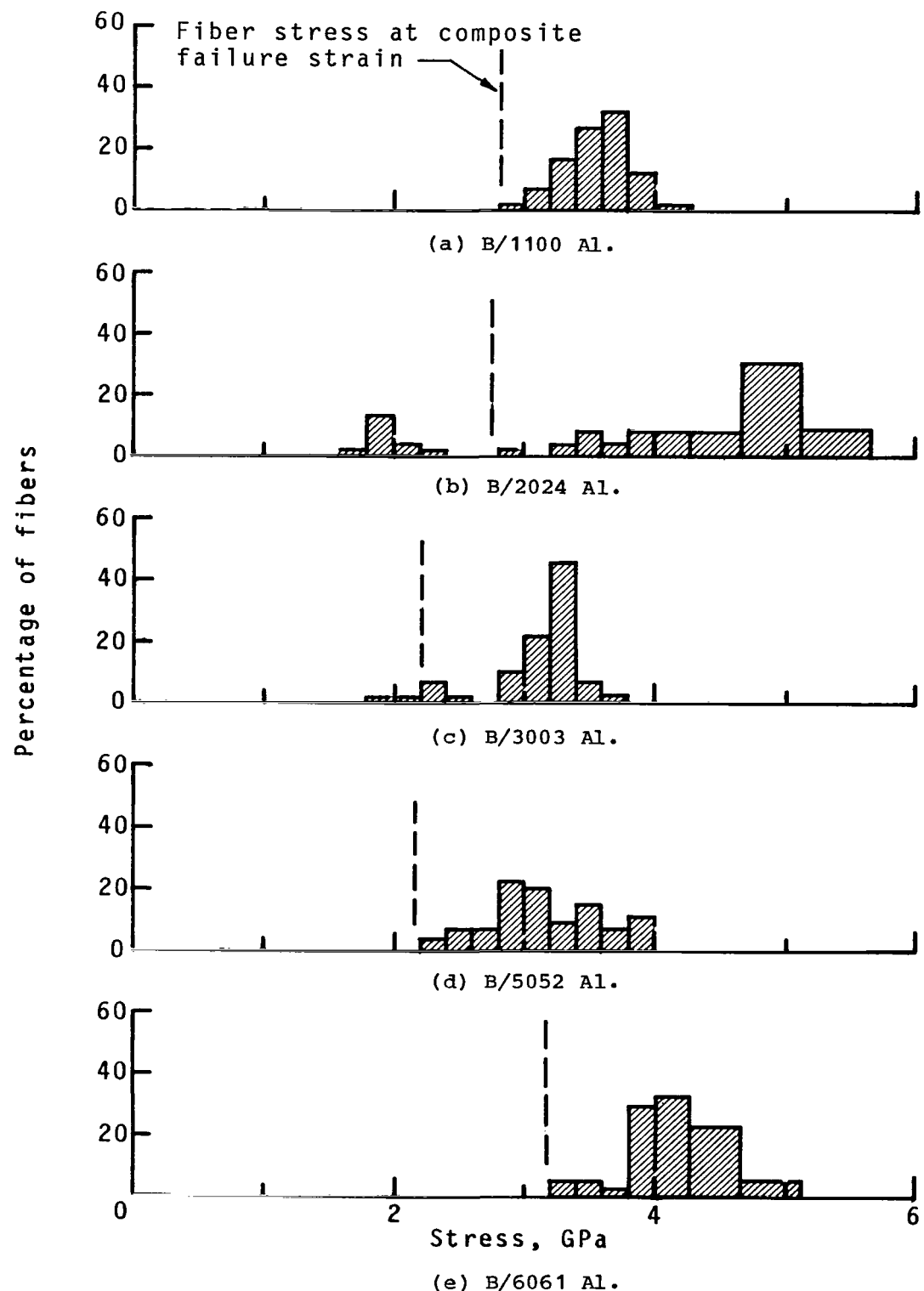
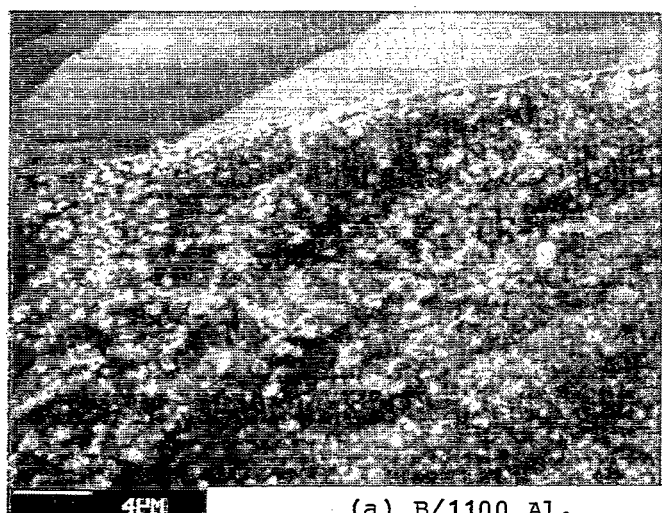
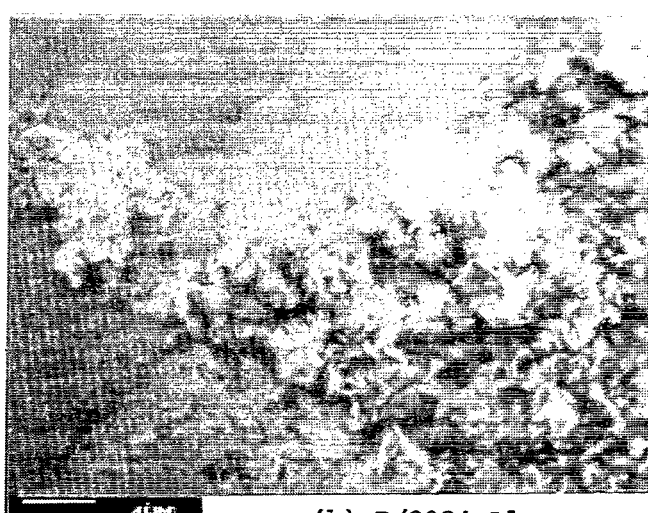


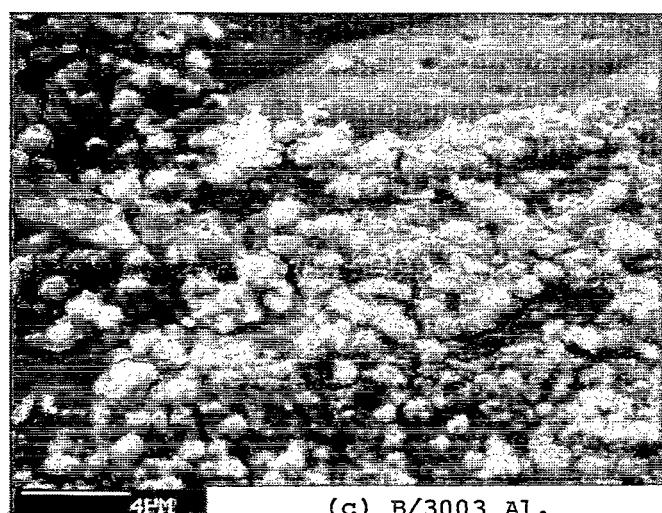
Figure 15.- Residual fiber strength distributions for composites after 10 000 hours exposure at 590 K and tensile testing.



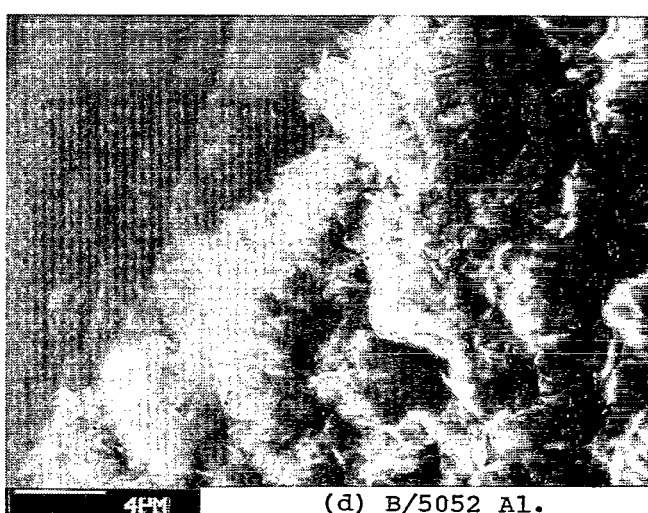
(a) B/1100 Al.



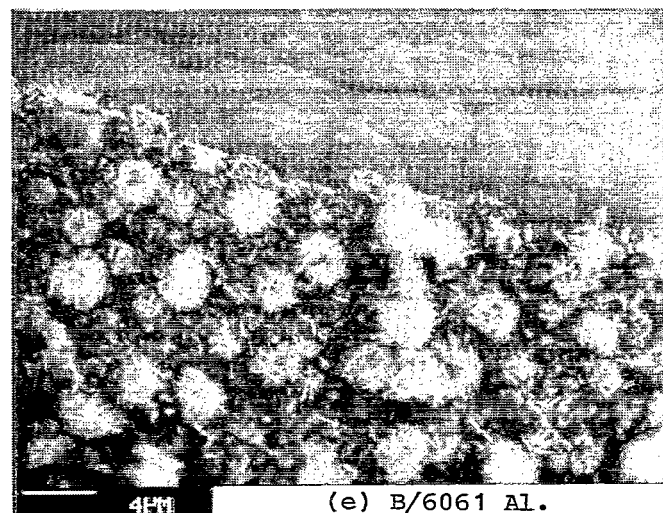
(b) B/2024 Al.



(c) B/3003 Al.



(d) B/5052 Al.



(e) B/6061 Al.

L-82-106

Figure 16.- Reaction layers on fibers removed from composite specimens after 10 000 hours exposure at 590 K.

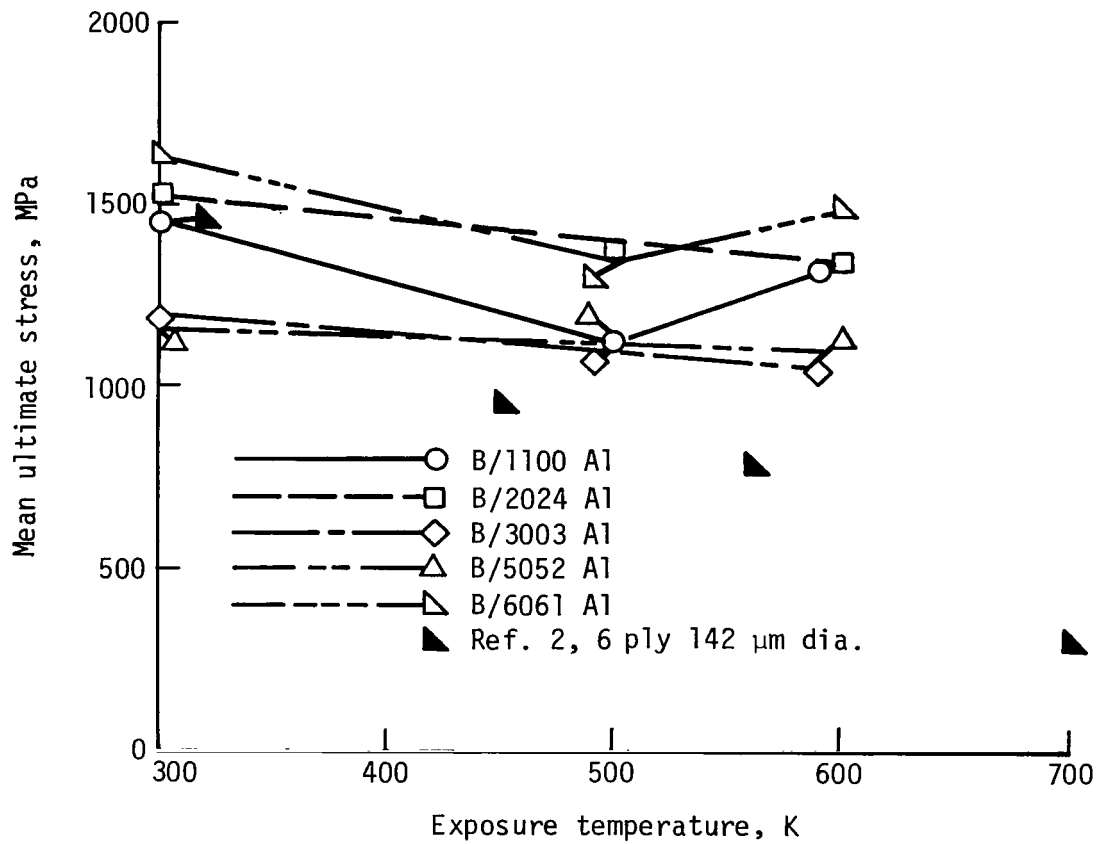


Figure 17.- Longitudinal tensile strength as function of 10 000 hours exposure at elevated temperature.

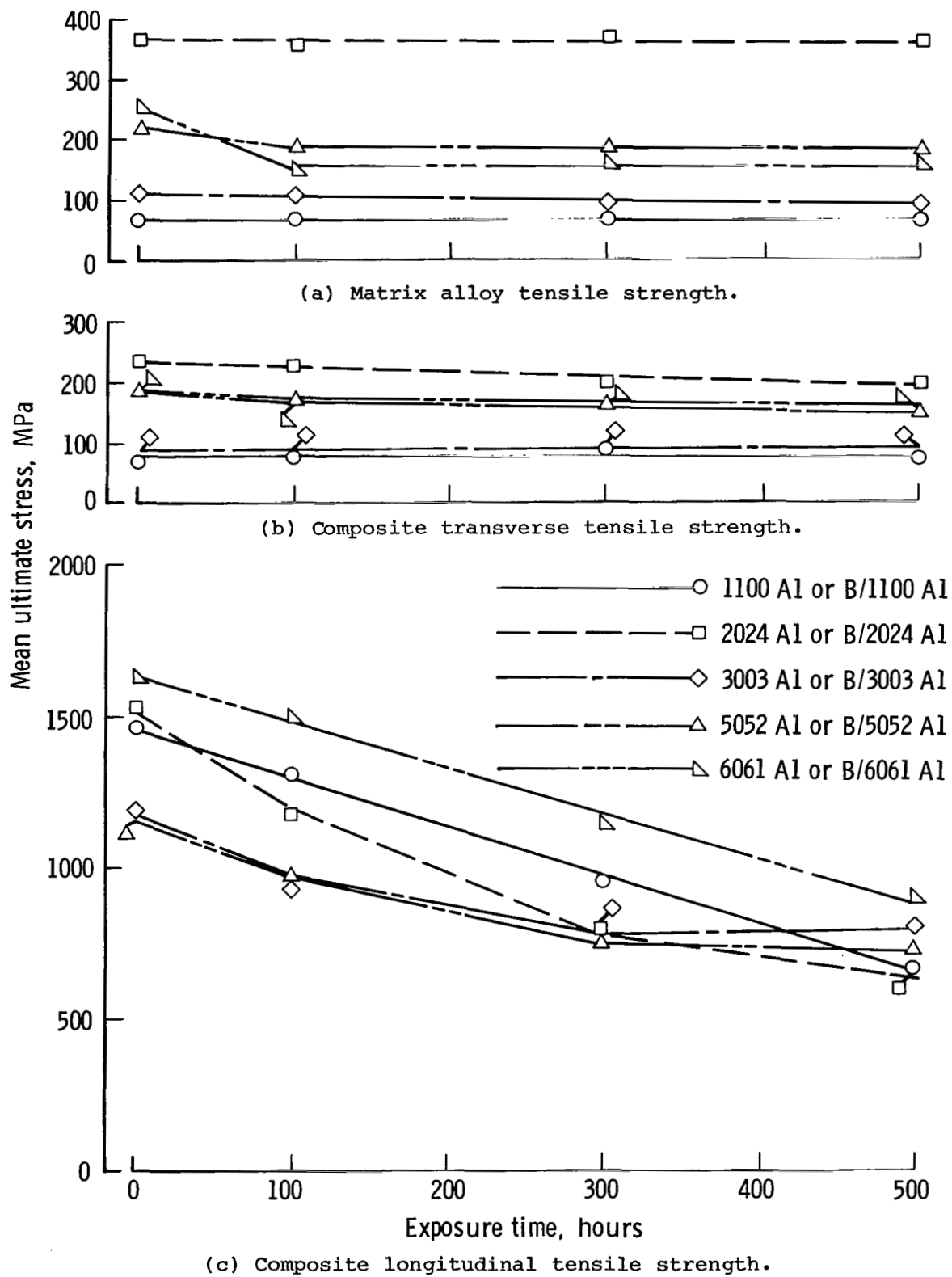
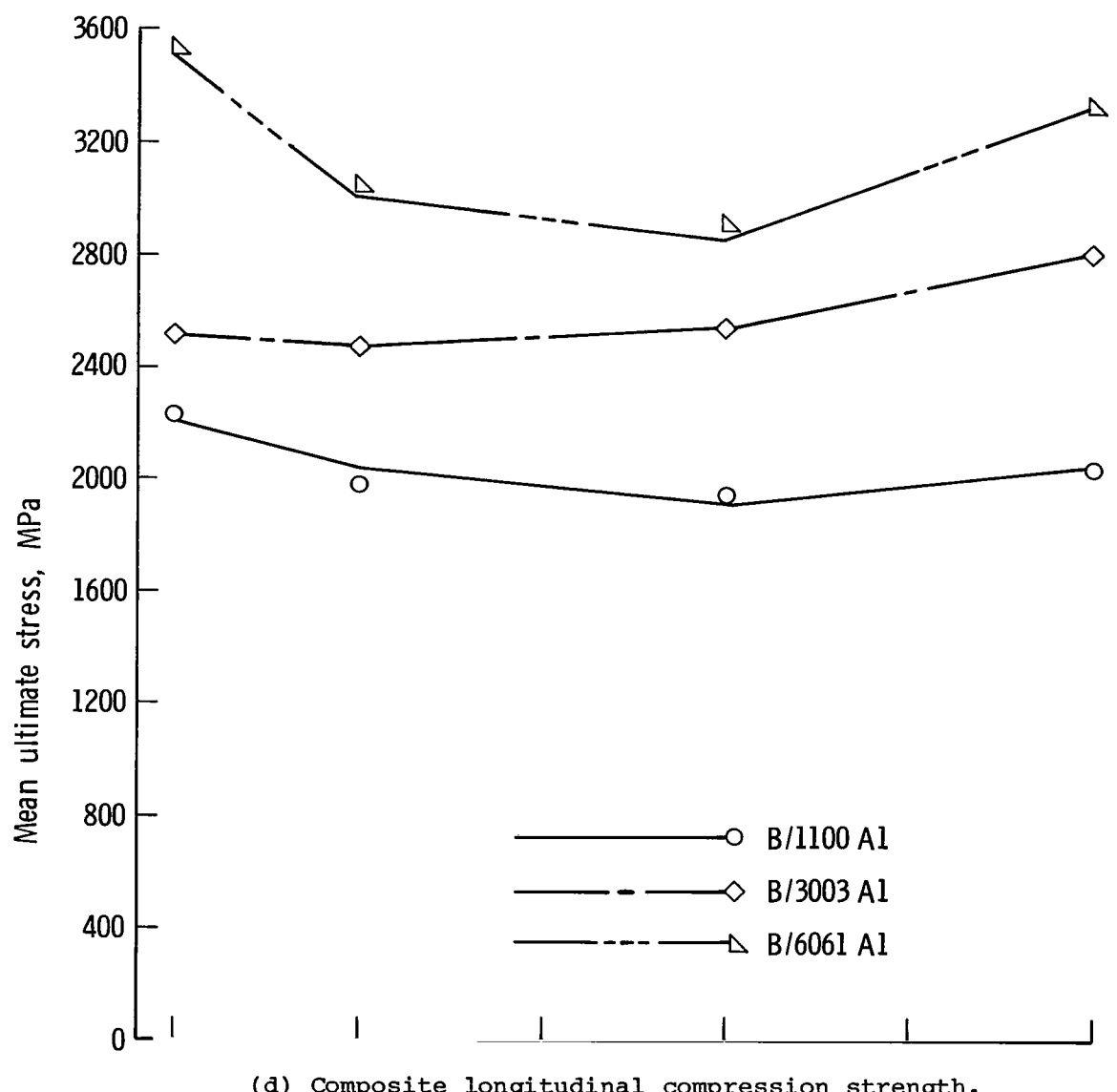


Figure 18.- Effect of isothermal exposure at 730 K on ultimate stress of B/Al composites and their matrix alloys.



(d) Composite longitudinal compression strength.

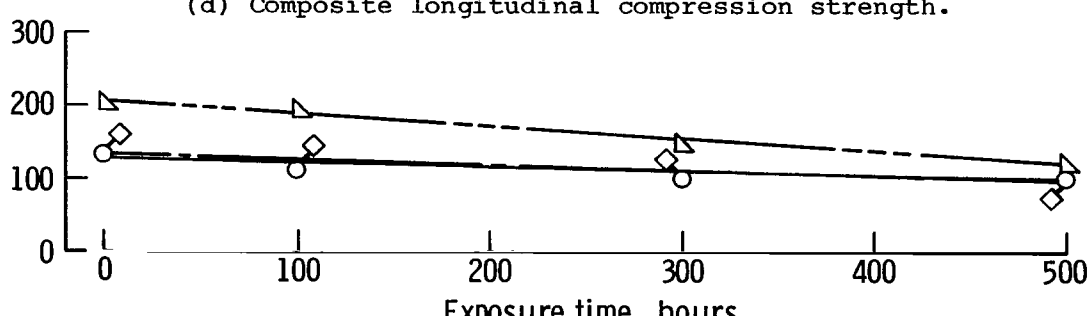
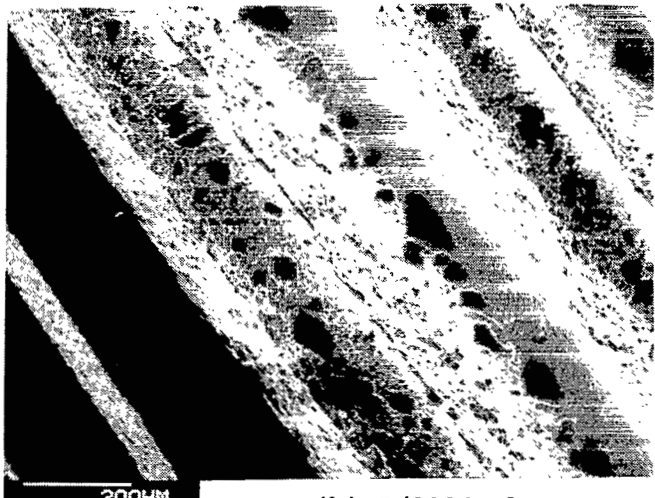


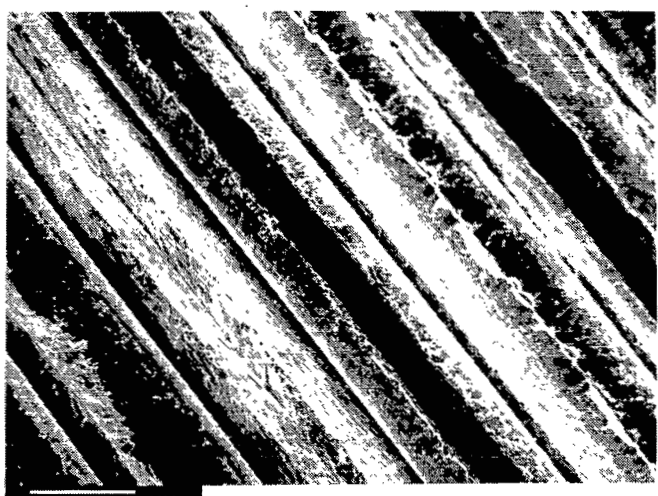
Figure 18.- Concluded.



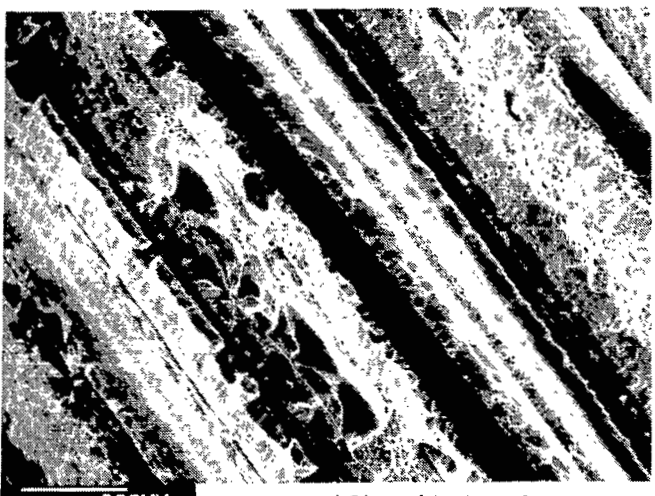
(a) B/1100 Al.



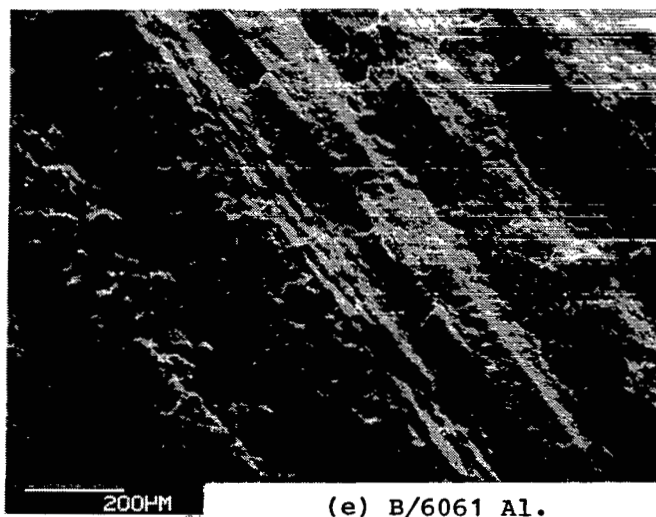
(b) B/2024 Al.



(c) B/3003 Al.



(d) B/5052 Al.



(e) B/6061 Al.

L-82-107

Figure 19.- Transverse fracture surfaces of specimens isothermally exposed for 500 hours at 730 K.

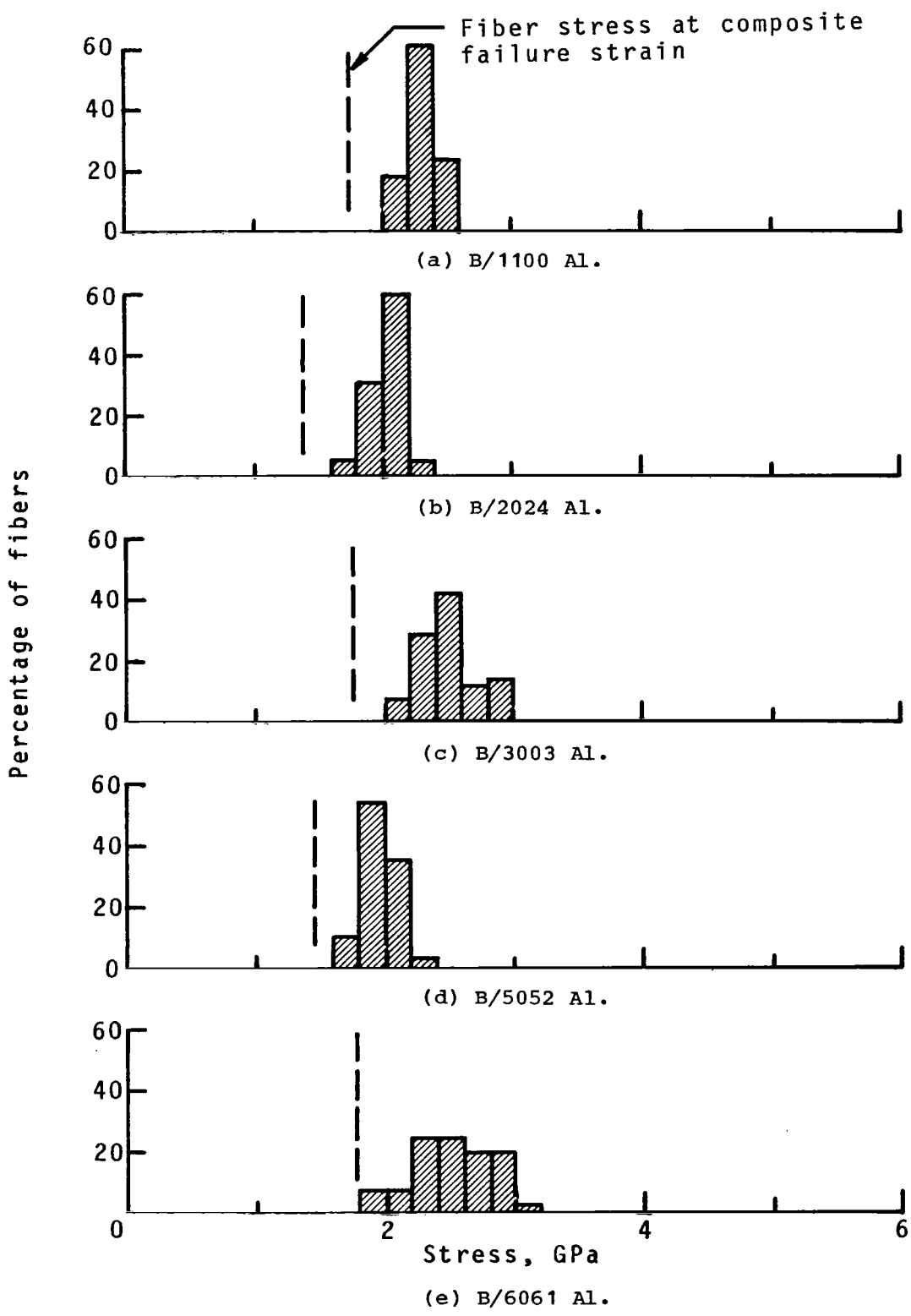
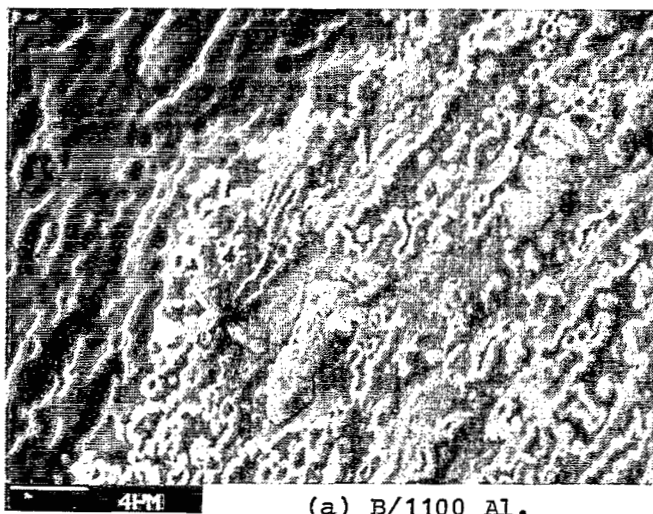
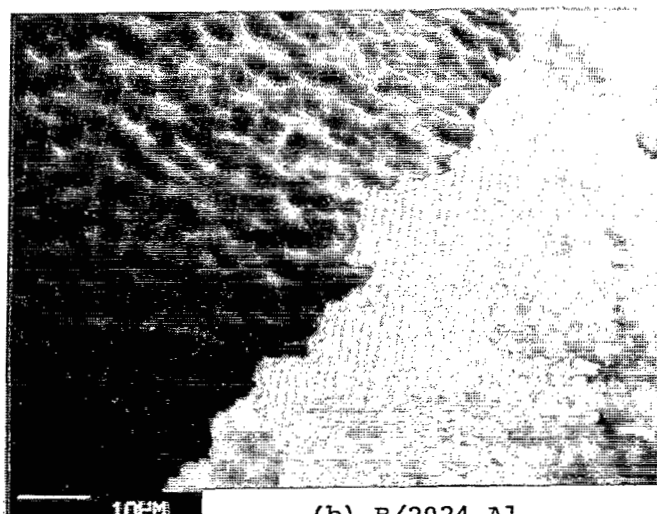


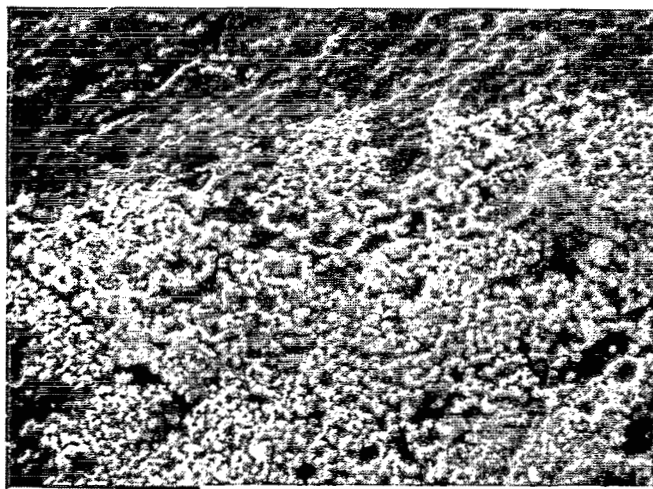
Figure 20.- Residual fiber strength distributions for composites after 500 hours exposure at 730 K and tensile testing.



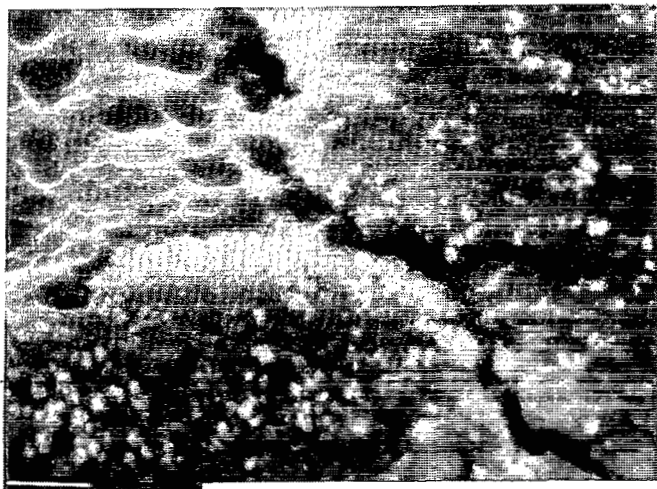
(a) B/1100 Al.



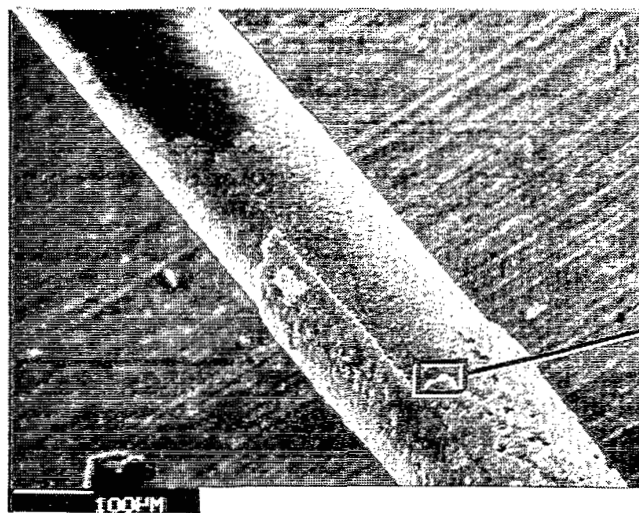
(b) B/2024 Al.



(c) B/3003 Al.



(d) B/5052 Al.



(e) B/6061 Al.

L-82-108

Figure 21.- Reaction layers on fibers removed from composite specimens after 500 hours exposure at 730 K.

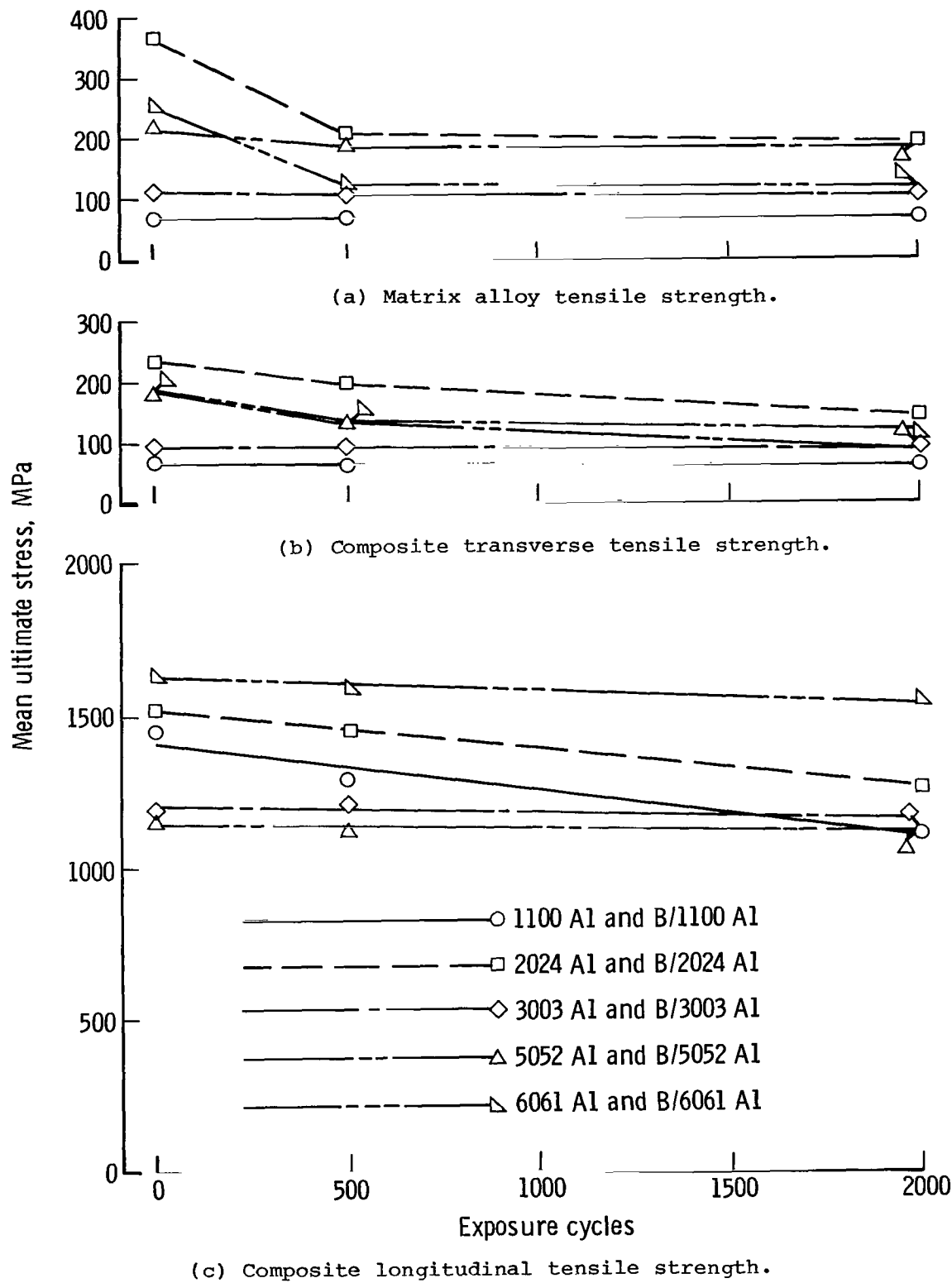


Figure 22.- Effect of thermal cycling between 200 K and 590 K on ultimate stress of B/Al composites and their matrix alloys.

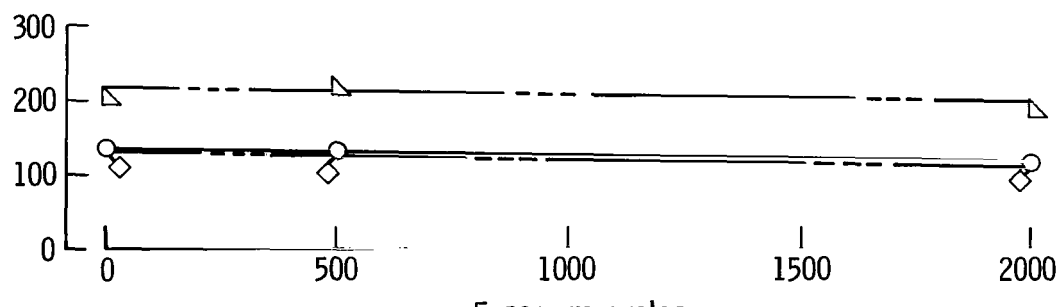
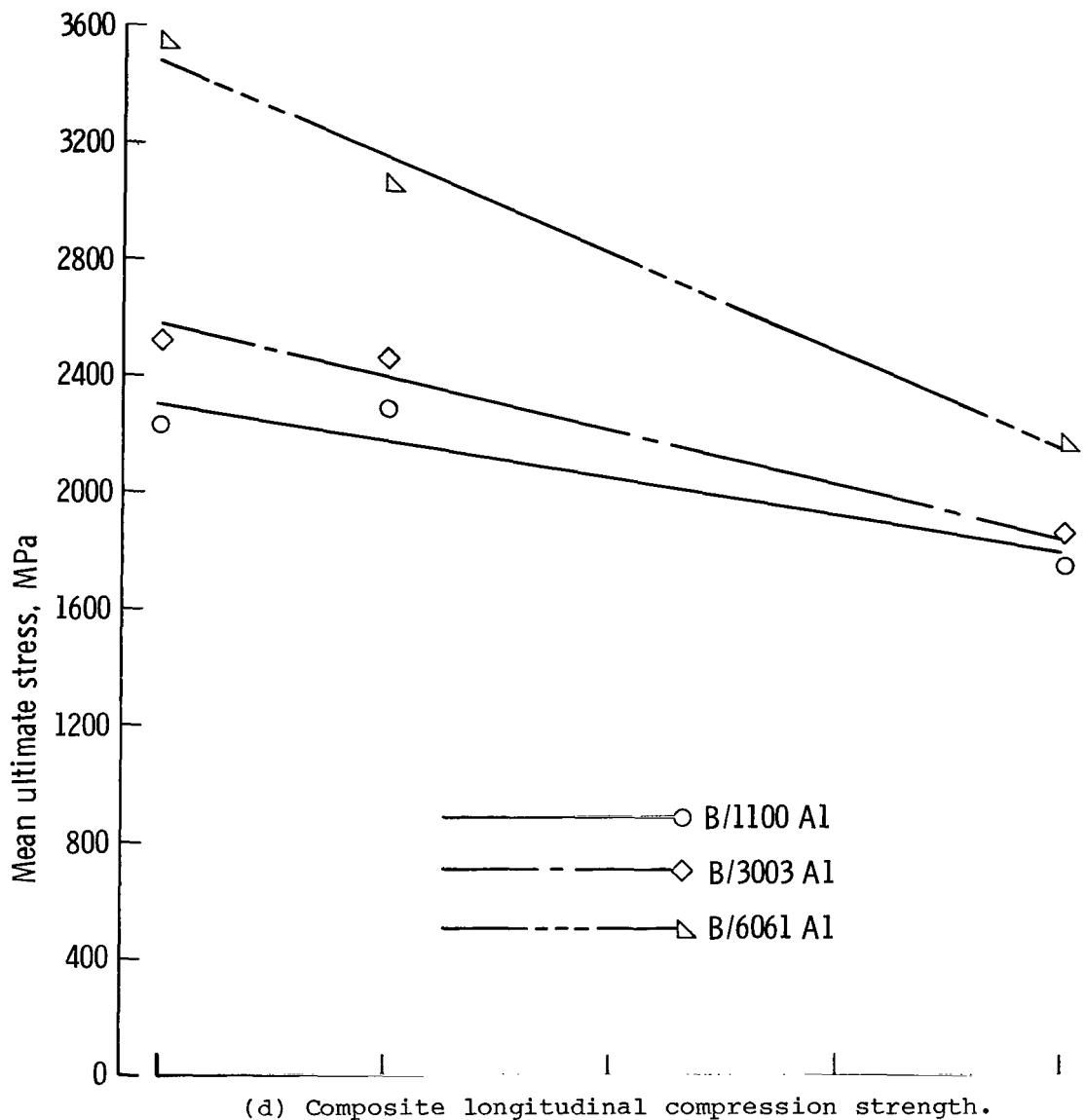


Figure 22.- Concluded.



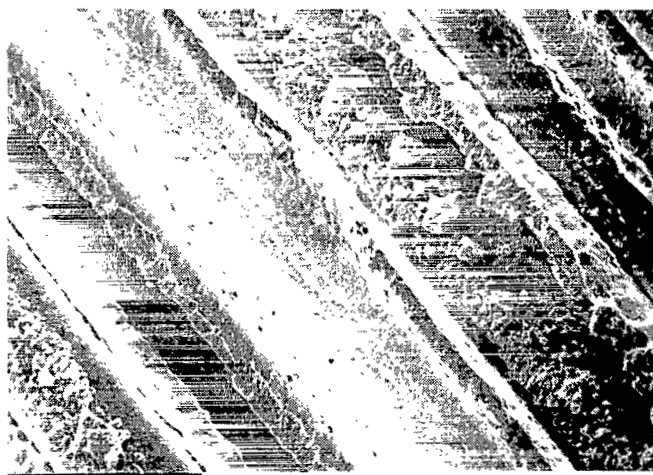
(a) B/1100 Al.



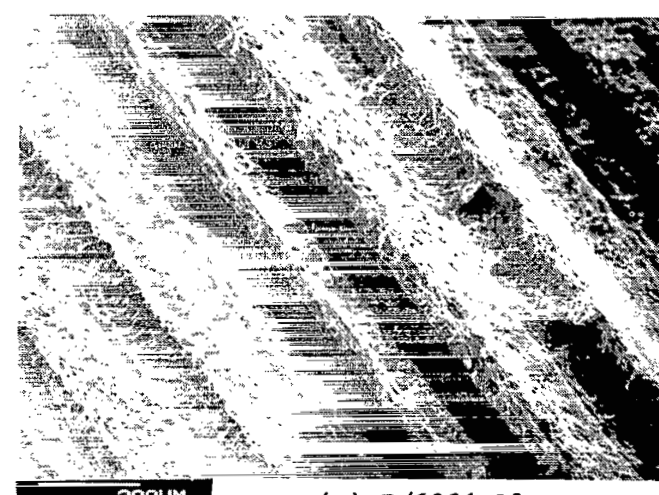
(b) B/2024 Al.



(c) B/3003 Al.



(d) B/5052 Al.



(e) B/6061 Al.

L-82-109

Figure 23.- Transverse fracture surfaces of specimens thermally cycled 2000 times between 200 K and 590 K.

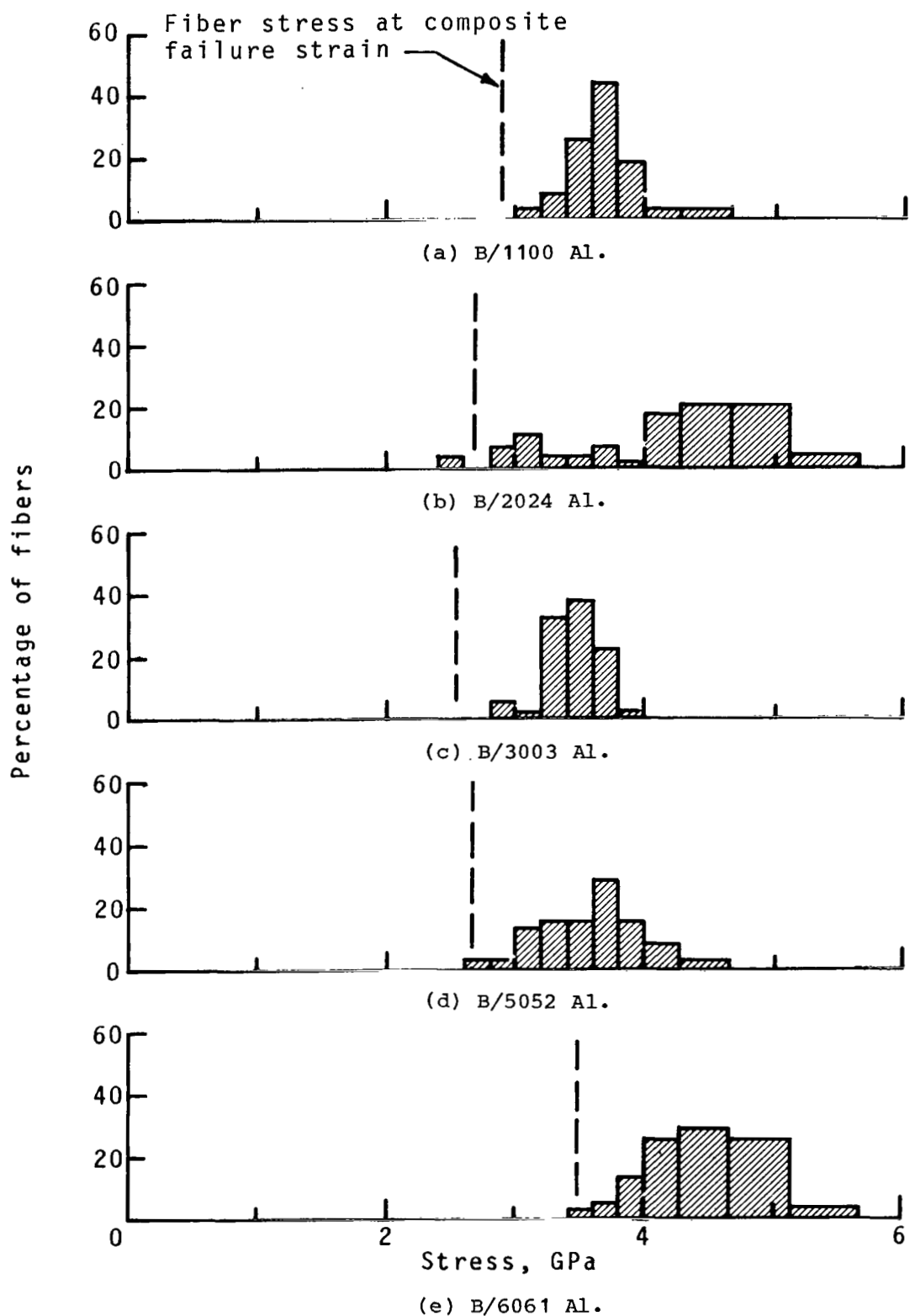


Figure 24.- Residual fiber strength distributions for composites after 2000 thermal cycles between 200 K and 590 K.

1. Report No. NASA TP-1977	2. Government Accession No.	3. Recipient's Catalog No.	
4. Title and Subtitle  LONG-TERM THERMAL DEGRADATION AND ALLOYING CONSTITUENT EFFECTS ON FIVE BORON/ALUMINUM COMPOSITES		5. Report Date April 1982	
7. Author(s)  George C. Olsen		6. Performing Organization Code L-14779	
9. Performing Organization Name and Address  NASA Langley Research Center Hampton, VA 23665		8. Performing Organization Report No. 506-53-23-01	
12. Sponsoring Agency Name and Address  National Aeronautics and Space Administration Washington, DC 20546		10. Work Unit No.  11. Contract or Grant No.	
15. Supplementary Notes		13. Type of Report and Period Covered Technical Paper	
		14. Sponsoring Agency Code	
16. Abstract  Thermal exposure effects on the properties of five boron/aluminum composite systems were experimentally investigated. The composite systems were 49 volume percent boron fibers (203 µm diameter) in aluminum-alloy matrices 1100 Al, 2024 Al, 3003 Al, 5052 Al, and 6061 Al. Specimens were thermally exposed up to 10 000 hours at 500 K and 590 K, up to 500 hours at 730 K, and up to 2000 thermal cycles between 200 K and 590 K. Composite longitudinal and transverse tensile strengths, longitudinal compression strength, and in-plane shear strength were determined. None of the systems was severely degraded by exposure at 590 K. The best performing system was B/2024 Al. Effects of matrix alloys on degradation mechanisms were experimentally investigated. Composite specimens and individual fibers were metallurgically analyzed with a scanning electron microscope and an electron microprobe to determine failure characteristics, chemical element distribution, and reaction layer morphology. Alloying constituents were found to affect the composite degradation mechanisms as follows: alloys containing iron, but without manganese as a stabilizer, caused increased low-temperature degradation; alloys containing magnesium, iron, or manganese caused increased degradation; and alloys containing copper caused increased fiber strength.			
17. Key Words (Suggested by Author(s))  Metal matrix composite Boron/aluminum Thermal degradation Thermal fatigue	18. Distribution Statement  Unclassified - Unlimited	Subject Category 24	
19. Security Classif. (of this report) Unclassified	20. Security Classif. (of this page) Unclassified	21. No. of Pages 105	22. Price A06

National Aeronautics and  
Space Administration

Washington, D.C.  
20546

Official Business

Penalty for Private Use, \$300

THIRD-CLASS BULK RATE

Postage and Fees Paid  
National Aeronautics and  
Space Administration  
NASA-451



U.S. AIR FORCE  
AERONAUTICAL LABORATORY  
TECHNICAL LIBRARY (SAC)  
DAFFL-AFRL-37117

NASA

POSTMASTER: If Undeliverable (Section 158  
Postal Manual) Do Not Return